National Library of Canada
Bibliothèque nationale du Canada

Canadian Theses Service
Service des thèses canadiennes

Ottawa, Canada
K1A 0N4

NOTICE

The quality of this microform is heavily dependent upon the quality of the original thesis submitted for microfilming. Every effort has been made to ensure the highest quality of reproduction possible.

If pages are missing, contact the university which granted the degree.

Some pages may have indistinct print especially if the original pages were typed with a poor typewriter ribbon or if the university sent us an inferior photocopy.

Reproduction in full or in part of this microform is governed by the Canadian Copyright Act, R.S.C. 1970, c. C-30, and subsequent amendments.

AVIS

La qualité de cette microforme dépend grandement de la qualité de la thèse soumise au microfilmage. Nous avons tout fait pour assurer une qualité supérieure de reproduction.

S'il manque des pages, veuillez communiquer avec l'université qui a conféré le grade.

La qualité d'impression de certaines pages peut laisser à désirer, surtout si les pages originales ont été dactylographiées à l'aide d'un ruban usé ou si l'université nous a fait parvenir une photocopie de qualité inférieure.

La reproduction, même partielle, de cette microforme est soumise à la Loi canadienne sur le droit d'auteur, SRC 1970, c. C-30, et ses amendements subséquents.

NL-339 (r. 88/04) c

Canada

UNIVERSITY OF ALBERTA

STUDIES ON THE DESORPTION IONIZATION MECHANISM IN FAST ATOM BOMBARDMENT MASS SPECTROMETRY

BY

ANGELINA MORALES

(C)

A THESIS SUBMITTED TO THE FACULTY OF GRADUATE STUDIES AND RESEARCH IN PARTIAL FULFILLMENT OF THE REQUIREMENTS FOR THE DEGREE OF DOCTOR OF PHILOSOPHY

DEPARTMENT OF CHEMISTRY

EDMONTON, ALBERTA

FALL, 1990

National Library of Canada
Bibliothèque nationale du Canada

Canadian Theses Service
Service des thèses canadiennes

Ottawa, Canada
K1A 0N4

The author has granted an irrevocable non-exclusive licence allowing the National Library of Canada to reproduce, loan, distribute or sell copies of his/her thesis by any means and in any form or format, making this thesis available to interested persons.

The author retains ownership of the copyright in his/her thesis. Neither the thesis nor substantial extracts from it may be printed or otherwise reproduced without his/her permission.

L'auteur a accordé une licence irrévocable et non exclusive permettant à la Bibliothèque nationale du Canada de reproduire, prêter, distribuer ou vendre des copies de sa thèse de quelque manière et sous quelque forme que ce soit pour mettre des exemplaires de cette thèse à la disposition des personnes intéressées.

L'auteur conserve la propriété du droit d'auteur qui protège sa thèse. Ni la thèse ni des extraits substantiels de celle-ci ne doivent être imprimés ou autrement reproduits sans son autorisation.

ISBN 0-315-65041-9

UNIVERSITY OF ALBERTA

RELEASE FORM

NAME OF THE AUTHOR: ANGELINA MORALES.

TITLE OF THESIS: STUDIES ON THE DESORPTION IONIZATION MECHANISM IN FAST ATOM BOMBARDMENT MASS SPECTROMETRY.

DEGREE: Ph. D.

YEAR THIS DEGREE GRANTED: 1990.

Permission is hereby granted to the University of Alberta Library to reproduce single copies of this thesis and to lend or sell such copies for private, scholarly or scientific research purposes only.

The author reserves other publications rights and neither the thesis nor extensive extracts from it may be printed or otherwise reproduced without the author's written permission.

Angelina Morales

Permanent Address: Urb. San Luis, Av. Principal, Res. Tiuna A, # 51, Caracas, 1061. Venezuela.

May 30, 1990.

UNIVERSITY OF ALBERTA

FACULTY OF GRADUATE STUDIES AND RESEARCH

The undersigned certify that they have read and recommend to the Faculty of Graduate Studies and Research for acceptance, a thesis entitled "Studies on the Desorption Ionization Mechanism in Fast Atom Bombardment Mass Spectrometry", submitted by Angelina Morales in partial fulfillment of the requirements for the degree of Doctor of Philosophy.

Supervisor: Dr. P. Kebarle

Dr. N. Dovichi

Dr. H. B. Dunford

Dr. B. Kratochvil

Dr. R. T. Coutts

External Examiner: Dr. E. P. Grimsrud

May 18, 1990.

ABSTRACT

Systematic variations of certain conditions of the FAB experiments were carried out in the present work, in order to determine the importance of Gas Phase Chemistry in the phenomena operating in the production of the FAB spectra.

The effect of the basicity of the analyte was studied. FAB spectra were obtained for glycerol solutions of pairs of basic analytes, A1 and A2. A1 had higher solution basicity and A2 higher gas basicity. It was found that the A1 peaks are suppressed by the presence of A2. This effect increased with the concentration of A2. The dominance of gas phase energetics implies that proton transfer reactions occur in a gas-like environment.

FAB spectra were obtained for glycerol solutions of diethanolamine. The observed intensity changes of protonated molecular ions, fragment ions and cluster ions were successfully modelled on the basis of a gas phase kinetic scheme. A residence time distribution for the ions in the gas-like region was derived. Ions with longer residence times have lower internal energy.

The temperature dependence of the FAB spectra of glycerol solutions of diethanolamine was investigated in the range -30° C to +40° C. It was found that the appearance of the spectrum im-

proves noticeably as the temperature increases, i.e. more intense protonated molecular ions and clusters, and less intense fragment ions and noise ions, are observed. The same kinetic scheme based on ion-molecule reactions in a high density gas was used to reproduce the experimental results, with the assumption that the maximum reaction time t_{max} increases with the sample solution temperature.

The effect of the viscosity of the sample solution on the FAB spectra was studied. Sucrose was added to glycerol, diethanolamine and their solutions to increase the viscosity. The spectra showed strong degradation with increasing viscosity. It was concluded that the observed temperature dependence is due to viscosity changes. At high viscosities the formation of the gas-like bubble is prevented and the residence time is short, while at low viscosities the bubble expands and as it cools down there is time available for the ion-molecule reactions to take place.

The ionization cross sections for 6-7 KeV Xe atom beam and gaseous toluene, glycerol and 3-nitrobenzyl alcohol were determined. The values obtained are quite large. This indicates that ionization is produced by the atom beam and brings support to the mechanisms where ionization is assumed to occur by ion-molecule reactions.

ACKNOWLEDGEMENT

I thank Dr. P. Kebarle for his supervision and advice throughout the course of this work.

I thank Dr. J. Sunner for his valuable ideas, that made this work possible.

I thank the Venezuelan Government for the scholarship granted to me by the "Fundación Gran Mariscal de Ayacucho", to carry out my Ph. D. studies.

I thank the "Instituto Venezolano de Investigaciones Científicas" for the leave of absence granted to me to carry out my graduate studies.

I thank the Faculty of Graduate Studies and Research and the Department of Chemistry of the University of Alberta for accepting me as a graduate student and for the financial support given to me through a teaching assistantship.

My special thanks to Dr. A. Hogg and the personnel of the Mass Spectrometry Laboratory, Mr. J. Olekszyk, Mr. D. Morgan, Mr. L. Harrower and Mr. A. Jodhan, for their invaluable help, friendship and encouragement, which helped me greatly during these years.

My most sincere appreciation to Dr. M. Ralitsch for his unconditional friendship, his priceless help with the editing of this work and the moral support and encouragement given to me in good and bad times.

I wish to express my gratitude to Dr. M. Armour, who has given me not only support and friendship, but also constant encouragement to do my best as a person and as a teacher.

The completion of this work would not have been possible without the assistance of the technical staff of the Department: Machine, Electronics and Glass Shops, Library, Photocopying and Printing Services and Storerooms. I also would like to thank the General Office personnel and secretaries for their efficiency in solving any of my problems.

I also wish to thank Dr. D. Tanner, Dr. H. J. Liu and his group, Ms. D. Dowhaniuk, Dr. L. Browne, Ms. I. Takahashi, Ms. P. Campbell, Dr. T. Stelfox and other dear people, for their friendship and help in many ways.

Finally and very important, I would like to express my endless gratitude to my family, for being always on my side and for their love and respect at all times.

TABLE OF CONTENTS

INTRODUCTION 1

Chapter 1

Scope of Mass Spectrometry. 2

Conventional Techniques and its Limitations. 3

Sputtering Techniques. 15

Chapter 2

Mechanistic Studies on the Desorption and Ionization Processes in SIMS and FAB. 26

Atomic SIMS Models. 27

Molecular SIMS and FABMS. Desorption Ionization Models. 30

Early Work in Our Group. 48

EXPERIMENTAL SECTION 52

Chapter 3

General. 53

Experiments for the Study of Competition for Protons and Dominance of Gas Basicities over Solution Basicities. 61

Experiments for the Kinetic Modelling of the FAB Spectra. 63

Experiments for the Study of Temperature and Viscosity Effects. 63

Chapter 4

Experiments for the Calculation of Ionization Cross Sections in Gas Phase FAB. 65

RESULTS AND DISCUSSION 75

Chapter 5

Competition for Protons and Dominance of Gas Basicities over Solution Basicities in FABMS. 76

Chapter 6

Kinetic Modelling of the FAB Spectra. 91

Chapter 7

Effect of the Temperature and Viscosity of the Sample Solution on the FAB Spectra. 114

Chapter 8

Calculation of Ionization Cross Sections in Gas Phase FAB. 141

CONCLUSIONS 153

REFERENCES 157

LIST OF FIGURES

Figure 1.1.	Diagram of a Double Focussing Mass Spectrometer.	4
Figure 1.2.	Total Ion Current (TIC) vs. Electron Beam Energy.	5
Figure 1.3.	EI Mass Spectra of Ethyl Acetate at Different Electron Beam Energies.	7
Figure 1.4.	Diagram of a CI Reagent Gas Introduction System.	9
Figure 1.5.	EI and CI Mass Spectra of Histamine.	9
Figure 1.6.	Diagram of a EI/CI Direct Insertion Probe.	11
Figure 1.7.	Diagram of a FI/FD Ion Source.	12
Figure 1.8.	EI, FI and FD Mass Spectra of Glutamic Acid.	14
Figure 1.9.	Schematic Representation of the Sputtering Phenomenon.	17
Figure 1.10.	Diagram of a SIMS Ion Source.	18
Figure 1.11.	SI Mass Spectrum of a Silicon Surface.	20
Figure 1.12.	SI Mass Spectra of Glycine.	21
Figure 1.13.	Diagram of a FAB Ion Source.	24
Figure 1.14.	FAB Mass Spectrum of a Saccharide.	25
Figure 2.1.	Qualitative Shape of the Function E(r).	33
Figure 2.2.	Monte Carlo Simulations of the Trajectory of Recoiled Sample Atoms at Two Incidence Angles of the Primary Ion Beam.	36

Figure 2.3.	Schematic Representation of Particle Induced Desorption Techniques.	39
Figure 2.4.	Schematic Representation of Processess Involved in DI Techniques.	46
Figure 2.5.	Schematic Representation of Sputtering by Spraying.	46
Figure 2.6.	FAB Spectra of Neat Triethanolamine and 10 Molepercent Solution of Triethanolamine in 3-Nitrobenzyl Alcohol.	50
Figure 2.7.	Normalized Total Ion Current (TIC) from FAB of Glycerol Solutions of Alkali Halides.	50
Figure 3.1.	Diagram of FAB Atom Gun.	55
Figure 3.2.	Diagram of FAB Ion Source.	59
Figure 4.1.	Typical Arrangement for Determination of Ionization Cross Sections under Thin Target Conditions.	66
Figure 4.2.	Diagram of Modified FAB Ion Source for Gas Phase Sample Analysis.	68
Figure 4.3.	Diagram of the Mass Spectrometer Pumping System.	71
Figure 5.1.	Solution Basicities in Water and Glycerol vs. Gas Basicity for the Compounds Used as Analytes.	80
Figure 5.2.	FAB Spectra of the Pair Ammonia/Aniline in Glycerol Solutions. a- 1 Molepercent Ammonium Chloride, b-1 Molepercent Anilinium Chloride, c- 1 Molepercent Each, d- 10 Molepercent Ammonium Chloride, e- 10 Molepercent Anilinium Chloride, f- 10 Molepercent Each.	82

Figure 5.3. Total Intensity of Major Ammonia and Aniline Ions vs. Analyte Concentration, from FAB Spectra of Ammonia/Aniline in Glycerol Solutions. a- Ammonia Ions from Ammonium Chlloride Solutions, b- Aniline Ions from Anilinium Chloride Solutions, c- Ammonia Ions and d- Aniline Ions from Equimolar Solutions of Ammonium Chloride and Anilinium Chloride. 83

Figure 5.4. Intensity Ratios $R_{A2/A1}$ vs. ΔGB. 85

Figure 5.5. Intensity Ratios $R'_{A2'/A1'}$ vs. ΔpK_a. 87

Figure 6.1. FAB Spectra of Diethanolamine-Glycerol Solutions. a- Neat Glycerol, b- 2 Molepercent Diethanolamine, c- 10 Molepercent Diethanolamine, d- Neat Diethanolamine. 93

Figure 6.2. Intensity of Protonated Molecular Ions and Cluster Ions of Glycerol and Diethanolamine vs. Diethanolamine Concentration, from FAB Spectra of Diethanolamine-Glycerol Solutions. 94

Figure 6.3. Intensity of Protonated Molecular Ions and Some of the Main Fragment Ions of Glycerol and Diethanolamine vs. Diethanolamine Concentration, from FAB Spectra of Diethanolamine-Glycerol Solutions. 96

Figure 6.4. Fragment Ratios, Dimer Ratios and Mixed Cluster Ratio of Glycerol and Diethanolamine vs. Diethanolamine Concentration, from FAB Spectra of Diethanolamine-Glycerol Solutions. 96

Figure 6.5. Total Intensity of Glycerol-Derived Ions vs. Diethanolamine Concentration, from FAB Spectra of Diethanolamine-Glycerol Solutions. 99

Figure 6.6. Distribution Function f(t) of Ion Residence Times in FAB of Diethanolamine-Glycerol Solutions. $f(t) = 1/at+b$, $a = 1.818 \times 10^9\ s^{-1}$, $b = 0.01818$. 102

Figure 6.7. Result of Kinetic Model Calculation of Intensity of Glycerol-Derived Ions on FAB Spectra of Diethanolamine-Glycerol Solutions. Calculated Intensities Are Shown as Solid Lines and Experimental Intensities as Data Points. 104

Figure 6.8. Calculated Intensities of Diethanolamine-Derived Ions from Kinetic Model Calculation on FAB Spectra of Diethanolamine-Glycerol Solutions. 107

Figure 6.9. Predicted Time Dependence of FAB Spectrum of Neat Glycerol. 108

Figure 6.10. Intensity of Representative Noise Ions vs. Diethanolamine Concentration, from FAB Spectra of Diethanolamine-Glycerol Solutions. Dashed Lines Show the Linear Dependence of Intensities on the Concentration. 112

Figure 7.1. FAB Spectra of Neat Glycerol at Different Temperatures. 118

Figure 7.2. Intensity of Glycerol-Derived Ions vs. Temperature of the Sample Solution T_b, from FAB Spectra of Neat Glycerol. Dashed Lines Show Calculated Results. 119

Figure 7.3. Intensity of Glycerol Cluster Ions vs. Temperature of the Sample Solution T_b, from FAB Spectra of Neat Glycerol. 119

Figure 7.4. Intensity of Diethanolamine-Derived Ions vs. Temperature of the Sample Solution T_b, from FAB Spectra of Neat Diethanolamine. 120

Figure 7.5. Intensity of Major Ions vs. Temperature of the Sample Solution T_b, from FAB Spectra of 2 Molepercent Solution of Diethanolamine in Glycerol. Dashed Lines Show Calculated Results. 121

Figure 7.6. Intensity of Major Ions vs. Temperature of the Sample Solution T_b, from FAB Spectra of 10 Molepercent Solution of Diethanolamine in Glycerol. Dashed Lines Show Calculated Results. 122

Figure 7.7. Intensity of Major Ions vs. Temperature of the Sample Solution T_b, from FAB Spectra of 10 Molepercent Solution of Pyridinium Chloride in Glycerol. 123

Figure 7.8. Calculated Intensity Ratio ΣDEA-Ions/ΣGL-Ions vs. t_{max} for 2 Molepercent Solution of Diethanolamine in Glycerol. Experimental Values of T_b for each Intensity Ratio Are Shown as Data Points. 125

Figure 7.9. Dependence of t_{max} on T_b. 126

Figure 7.10. Thermodynamic PVT Surface for a Single Component System. Line D Indicates the States at Zero Pressure. 128

Figure 7.11. Viscosity of Glycerol vs. Temperature. 130

Figure 7.12. Diagram of the Gas-Like Cavity Generated at the Bombardment Point. 132

Figure 7.13. Viscosity of Aqueous Solution of Sucrose vs. Sucrose Concentration. 134

Figure 7.14. FAB Spectra of Glycerol with Increasing Concentrations of Sucrose Added to Increase the Viscosity. a- Neat Glycerol, b- 20 % Sucrose, c- 40 % Sucrose, d- 60 % Sucrose. 136

Figure 7.15. FAB Spectra of Diethanolamine with Increasing Concentrations of Sucrose Added to Increase the Viscosity. a- Neat Diethanolamine, b- 20 % Sucrose, c- 40 % Sucrose, d- 60 % Sucrose. 137

Figure 7.16. Intensity of Glycerol-Derived Ions vs. Sucrose Concentration Added to Increase the Viscosity, from FAB Spectra of Sucrose-Glycerol Solutions. 138

Figure 7.17. Intensity of Diethanolamine-Derived Ions vs. Sucrose Concentration Added to Increase the Viscosity, from FAB Spectra of Sucrose-Diethanolamine Solutions. 138

Figure 7.18. Intensity of Major Ions vs. Sucrose Concentration Added to Increase the Viscosity, from FAB Spectra of Sucrose-2 mole-percent Diethanolamine in Glycerol Solutions. 139

Figure 7.19. Intensity of Major Ions vs. Sucrose Concentration Added to Increase the Viscosity, from FAB Spectra of Sucrose-10 mole-percent Diethanolamine in Glycerol Solutions. 139

Figure 8.1. Positive Ion Current vs. Uncorrected Ion Source Pressure for Gaseous Toluene Ionized by the Xe Fast Atom Beam. 144

Figure 8.2. Positive Ion Current vs. Uncorrected Ion Source Pressure for Gaseous Glycerol Ionized by the Xe Fast Atom Beam. 146

Figure 8.3. Positive Ion Current vs. Uncorrected Ion Source Pressure for Gaseous 3-Nitrobenzyl Alcohol Ionized by the Xe Fast Atom Beam. 146

Figure 8.4. Gas-Phase FAB Spectrum (6 KeV Xe atoms) and EI Spectrum (70 eV electrons) of Toluene. 149

Figure 8.5. Gas-Phase FAB Spectrum (6 KeV Xe atoms) and EI Spectrum (70 eV electrons) of Glycerol. 150

Figure 8.6. Gas-Phase FAB Spectrum (6 KeV Xe atoms) and EI Spectrum (70 eV electrons) of 3-Nitrobenzyl Alcohol. 151

INTRODUCTION

CHAPTER 1

SCOPE OF MASS SPECTROMETRY

Mass Spectrometry (MS) is a very powerful tool in Analytical, Inorganic and Organic Chemistry, since it offers a collection of very sensitive techniques, able to provide accurate information about molecular weights, elemental composition and structures, while requiring very small amounts of sample. In its early stages, only samples with certain volatility could be analyzed, to provide molecular weight determinations and structural information by means of the fragmentation patterns. To overcome this limitation, new ionization processes have been developed to extend mass spectrometric analysis to large, non-volatile molecules, and now mass spectral data of salts and biomolecules can be obtained. In addition, further improvement of the mass analyzers have made possible high resolution techniques and with them elemental composition has become available, and the coupling of mass spectrometers to gas (GC-MS) and liquid chromatographs (LC-MS) has made possible the analysis of mixtures. Besides its versatile applications, Mass Spectrometry is also a wide area of research in Physical Chemistry and Physics, involved in the study of molecules and ions and a variety of phenomena related to them.[1-3]

CONVENTIONAL MS TECHNIQUES AND LIMITATIONS

In the first applications in Organic Analysis, Electron Impact (EI) was the fundamental ionization process on which mass spectrometric studies were based, although the ionization of atoms and molecules could be achieved in several other ways. A typical double focussing instrument is shown in Figure 1.1. Single focussing machines, with only magnetic sectors, and quadrupole analyzers are also popular and less expensive, but do not allow high resolution.

A routine EI experiment includes the introduction of the analyte into the high vacuum conditions of the ion source, where the gaseous analyte molecules are ionized by interaction with the electron beam:

$$M + \vec{e^-} \longrightarrow M^{\ddagger} + 2\vec{e^-} \qquad (1.1)$$

Molecular ions $M^{\ddagger}$ with a certain range of excitation energies are formed, and those with lower energies survive as intact species with the same mass as the original molecules, while others undergo decomposition to produce fragment ions that carry structural information. This mixture of ions is expelled from the ion source by the positive repeller electrode, accelerated and separated in the analyzer, that in Figure 1.1 includes an electric and a magnetic

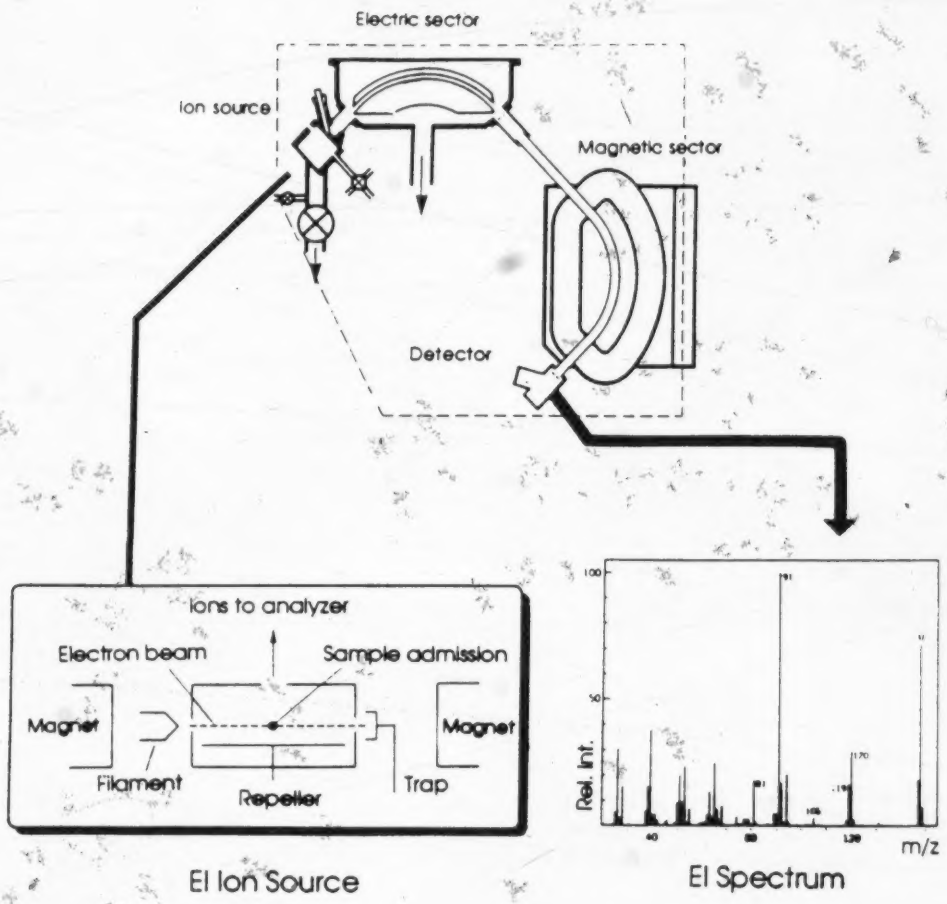

FIGURE 1.1. Diagram of a Double Focussing Mass Spectrometer

sectors. Finally the ion current is detected, amplified and recorded by a computer. The mass spectrum presents the results, usually as a bar-graph of relative ion intensity versus ion mass-to-charge ratio.

The energy of the electron beam is usually 70 eV, because the ionization efficiency is close to a maximum at that value, as shown in Figure 1.2.

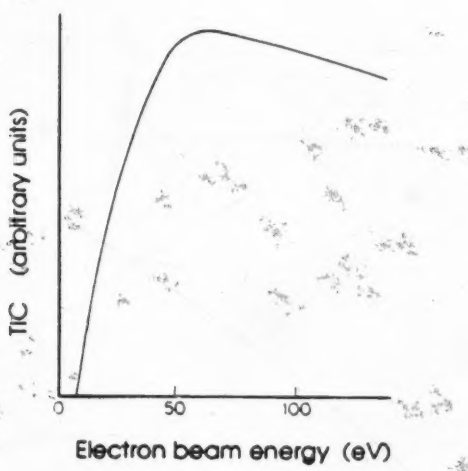

FIGURE 1.2. Total Ion Current (TIC) vs Electron Beam Energy
(Adapted from J. R. Chapman, *'Practical Organic Mass Spectrometry'*, Wiley Interscience, Great Britain, 1985).

A common problem associated with EI is that for certain compounds the molecular ions initially produced may have very short life-times, due to the high amount of excitation energy, relative to that leading to fragmentation, acquired during the ion-

ization process. When this is the case, extensive fragmentation occurs and molecular ions are not observed in the spectrum. An electron beam of lower energy can be used to help this situation. An example of the results is shown in Figure 1.3, in which the EI spectrum of ethyl acetate at three different electron beam energies is presented. However, this does not always solve the problem. Chemical Ionization (CI)[4,5] is often a better alternative. In it, a relatively high pressure (approximately 1 torr) of a reagent gas, usually ammonia, methane or isobutane, is introduced to the ion source, by means of a gas introduction system, like the one shown in Figure 1.4. The partial pressure of the sample is very much smaller and makes no significant contribution to the total pressure in the ion source. The reagent gas is ionized by the electron beam and the ions produced undergo ion-molecule reactions with other reagent gas molecules. For example, for methane at 1 torr the main reactions are:

$$CH_4 \longrightarrow CH_4^{+\cdot} \longrightarrow CH_3^+ + H^\cdot \qquad (1.2)$$

$$CH_4^{+\cdot} + CH_4 \longrightarrow CH_5^+ + CH_3^\cdot \qquad (1.3)$$

$$CH_3^+ + CH_4 \longrightarrow C_2H_5^+ + H_2 \qquad (1.4)$$

Subsequent ion-molecule reactions between the reagent gas ions and the sample molecules are responsible for the formation

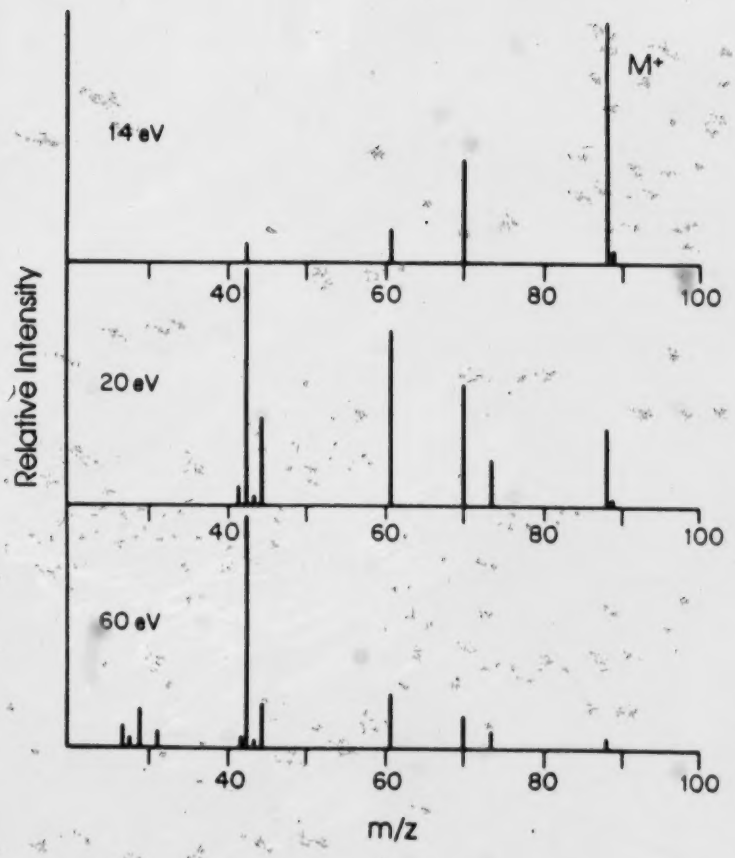

FIGURE 1.3. EI Mass Spectra of Ethyl Acetate at Different Electron Beam Energies

(Adapted from W. H. McFadden, *'Techniques of Combined GC/MS: Applications to Organic Analysis'*, Wiley-Interscience, New York, 1973.)

of the sample ions. The most important reactions that take place are:

a- proton transfer:

$$CH_5^+ + M \longrightarrow (M + H)^+ + CH_4 \qquad (1.5)$$

b- hydride abstraction:

$$C_2H_5^+ + M \longrightarrow (M-H)^+ + C_2H_6 \qquad (1.6)$$

c- electrophilic addition:

$$C_2H_5^+ + M \longrightarrow (M + C_2H_5)^+ \qquad (1.7)$$

The ions produced are closely related to the original structure of the sample molecules and are usually called "pseudomolecular ions". These reactions involve less energy transfer than direct electron impact ionization. This leads to pseudomolecular ions that have longer life-times, so that they can be detected as intact species, with very little or no fragmentation. An example is shown in Figure 1.5, where the EI spectrum of histamine is composed mainly of the fragment at m/z 82 [(M - CH_2NH)+] and other small signals, while the CI spectrum, obtained with isobutane as the reagent gas, reveals only the protonated molecular ion $(M + H)^+$ at m/z 112.

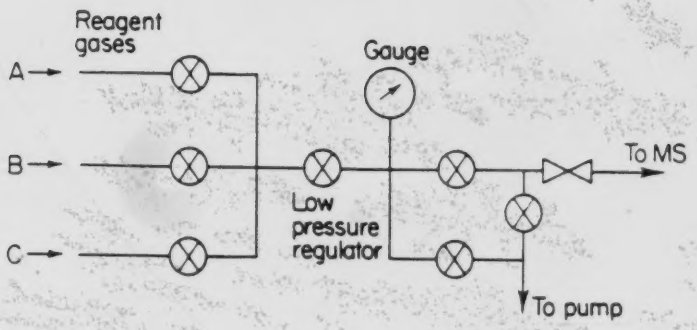

FIGURE 1.4. Diagram of a CI Reagent Gas Introduction System
(Adapted from J. R. Chapman, *'Practical Organic Mass Spectrometry'*, Wiley Interscience, Great Britain, 1985).

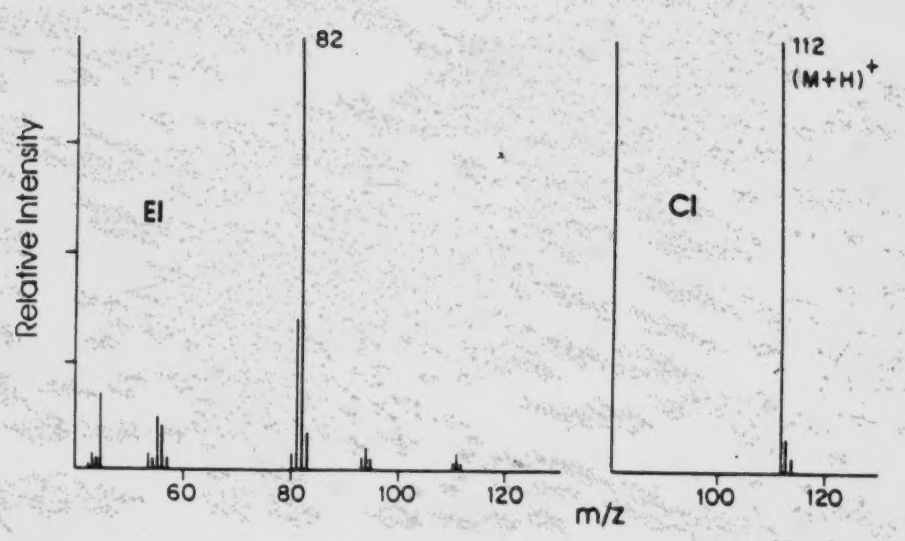

FIGURE 1.5. EI and CI Mass Spectra of Histamine
(Adapted from G. W. A. Milne, H. M. Fales and R. W. Colburn, *Anal. Chem.*, **45** (1973) 1952).

In both EI and CI, samples which have sufficient volatility are introduced into the ion source *via* a heated reservoir inlet system. However, most of the samples submitted for mass spectrometric analysis have low vapour pressure. Such compounds have to be introduced directly into the ion source. A standard direct insertion probe is shown in Figure 1.6. The sample is loaded on the tip and the probe is introduced into the ion source through a vacuum lock. An additional advantage of this arrangement is that it requires far less sample than the reservoir inlet system. If the extension of the probe is long enough, so that the sample loaded on the tip can be brought very close to the electron beam, better quality spectra are obtained for non-volatile compounds.[6] This modification is called "In-beam technique"[7] and offers, for both EI and CI,[8] improved sensitivities.[9-11]

The vaporization of the analyte is a requirement in both EI and CI. This represents a serious disadvantage and leads to limited applicability when dealing with polar, non-volatile compounds or thermally unstable molecules. This is especially true in the case of the analysis of substances of biological and medical interest.[12-14] This difficulty has encouraged the development of other techniques, able to produce diagnostically useful mass spectra from non-volatile analytes. A diagnostically useful mass spectrum should provide a relatively intense molecular or pseudomolecular ion, as well as fragment ions that would reveal structural features of the

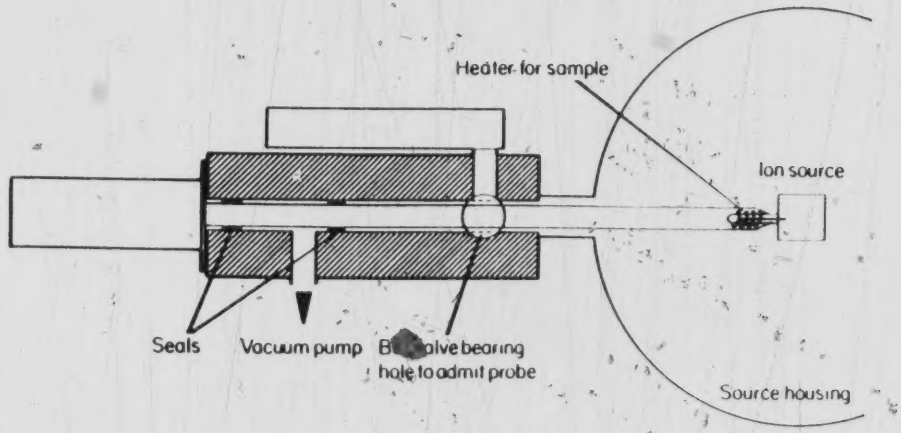

FIGURE 1.6. Diagram of a EI/CI Direct Insertion Probe
(Adapted from J. R. Chapman, "*Practical Organic Mass Spectrometry*", Wiley Interscience, Great Britain, 1985).

compound. Generally this is the case when the molecular ions are formed with low excitation energies. Techniques leading to such spectra are called 'soft' ionization methods.

Extension of Mass Spectrometry to Include Analysis of Large, Non-volatile Molecules.

FIMS, FDMS and Other Techniques.

Field Ionization (FI),[15,16] developed by Beckey in 1960, was one of the first methods used to increase the yield of molecular ions. A diagram of an FI ion source is shown in Figure 1.7.

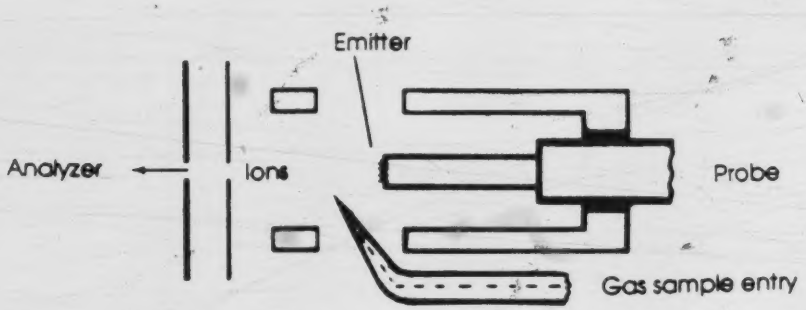

Figure 1.7. Diagram of an FI/FD Ion Source
(Adapted from J. R. Chapman, *'Practical Organic Mass Spectrometry'*, Wiley Interscience, Great Britain, 1985).

The vaporized sample is introduced from the inlet system and ionized by the action of a very intense electric field (about 10^7-

10^8 V/cm), produced by an emitter electrode, whose surface is covered by a large number of microneedles or dendrites. The very high electric fields near the tips of the microneedles pull electrons out of the analyte molecules, leading to the so-called field ionization. The energy transferred during the field ionization process is much lower than that involved in EI or CI, a fact that makes FI a very soft method. However, the vaporization of the sample is still a requirement, and the method fails for non-volatile compounds.

In 1969 Beckey modified the FI ion source to introduce Field Desorption (FD).[17-19] In this technique, the sample is coated on to the emitter prior to analysis. The source is the same as the FI source shown in Figure 1.7, but the inlet system is not required. Under the influence of the electric field, the sample is ionized and desorbed from the metallic emitter by processes not fully understood. Considerable progress was attained with FD, and an example of the improvement is shown in Figure 1.8, in which the EI, FI and FD mass spectra of glutamic acid are presented. However, this method works well only for certain compounds and the reproducibility is low. Besides, great care has to be taken to prepare the emitters, and this represents a serious problem in FD.

Soon thereafter other techniques based on very rapid heating and desorption were developed. In the middle 70's Macfarlane

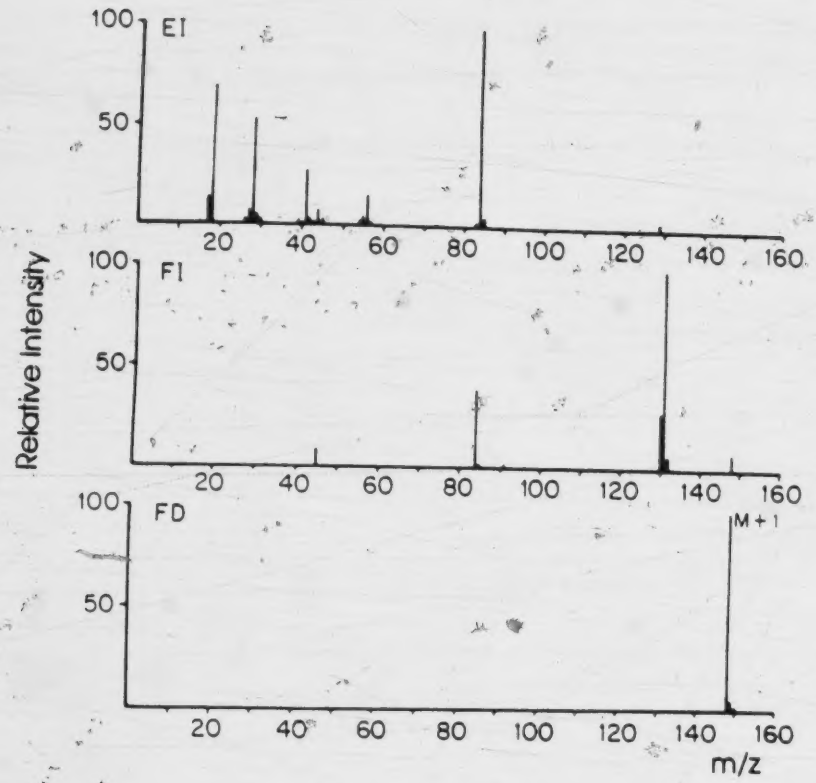

FIGURE 1.8. EI, FI and FD Mass Spectra of Glutamic Acid
(Adapted from H. D. Beckey, A. Heindrichs and H. U. Winkler, *Int. J. Mass Spectrom. Ion Phys.*, **3** (1970) App. 9).

implemented ^{252}Cf-Plasma Desorption (PD)[20-22], and later on Laser Desorption (LD),[23,24] and Thermal Desorption (TD)[25] became available. In addition, some other methods capable of sampling ions from liquid phases were developed,[26] with the aim of finding an interface for Liquid Chromatography/Mass Spectrometry (LC-MS). Included among these are Electrospray,[27] Electrohydrodynamic Ionization,[28] Liquid-ion Evaporation,[29] and Thermospray.[30] However, despite some impressive results, none of these methods proved to be convenient or versatile enough to become successful tools in routine mass spectrometric analysis of non-volatile compounds.

Sputtering Techniques

Secondary Ion Mass Spectrometry (SIMS).- A major improvement was achieved with the application of the already known technique SIMS[31-33] to the analysis of organic compounds. This method, pioneered by Bennighoven and others,[34-38] is based on the long ago discovered[39,40] and extensively studied[41-46] phenomenon of physical sputtering.

Sputtering is defined as the removal of atoms and molecules, either neutral or ionized, from solid surfaces, by bombardment with an energetic beam, usually with kinetic energies in the KeV range. A representation of the phenomenon assumed to occur is shown

in Figure 1.9. The bombarding particle transfers energy to the surface, an excited region is generated, and three different regimes can take place:[46]

a- direct knock-on: a particle is emitted because the resulting motion directs it towards the surface and the particle has enough kinetic energy to overcome the binding forces (Figure 1.9a).

b- linear cascade: recoil particles from beam-target collisions get enough energy to generate collision cascades, but the density of recoil particles is low and knock-on events dominate over collisions (Figure 1.9b).

c- thermal spike: the density and energy of recoil particles is high and multiple collisions with splitting of cascades create an excited volume in which all the particles are in random motion (Figure 1.9c).

As a result of any of the above mentioned processes, ions and neutrals are emitted from the surface. Both the bombardment conditions and the chemical nature of the sample influence the secondary particle emission. The main bombardment parameters are mass, energy and angle of incidence of the impinging particles. All these determine the size and properties of the ex-

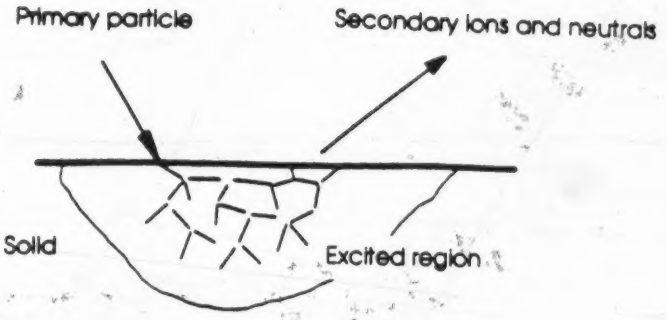

Excitation of Bombardment Site by Momentum Transfer
(Adapted from A. Benninghoven, *Int. J. Mass Spectrom. Ion Phys.*, **46** (1983) 459).

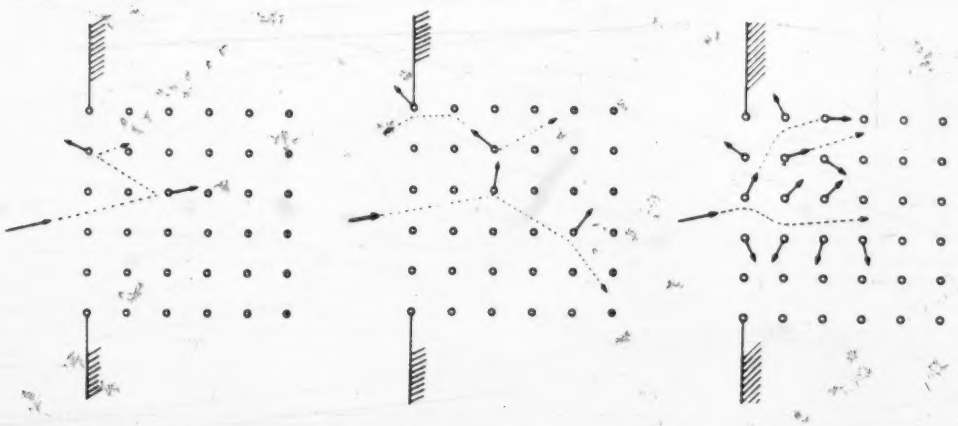

a- Direct Knock-on **b- Collision Cascade** **c- Thermal Spike**
(Adapted from P. Sigmund, in *"Sputtering by Particle Bombardment I"*, Topics in Applied Physics, Vol. 47, R. Behrisch (ed.), Springer-Verlag, Berlin, 1981).

FIGURE 1.9. Schematic Representation of the Sputtering Phenomenon

cited volume at the surface target. The chemical nature of the analyte, its concentration and the nature of its environment, influence the secondary ion yields.

A diagram of a SIMS ion source is shown in Figure 1.10. The sample is presented as a solid layer deposited on a metallic surface. Generally this is achieved by applying a solution, followed by evaporation of the solvent, on a metallic probe tip. Then, the sample is exposed to the action of the ion beam. SIMS methodology includes two distinct lines: dynamic SIMS, the first and original method, and static SIMS, a softer method introduced later.

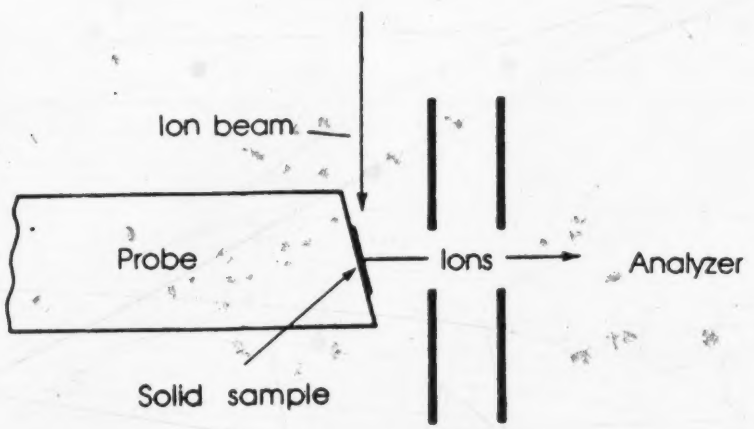

Figure 1.10. Diagram of a SIMS Ion Source

Dynamic SIMS, also called Atomic SIMS by some authors, refers to high primary ion beam flux (10^{-6} A/cm^2), and is used for depth profile and surface analysis,[47-51] involving mainly metals, semiconduc-

tors and inorganic salts. This kind of sample does not suffer extensive damage by exposure to a high ion beam flux. Figure 1.11 shows the SIMS spectrum of a silicon surface under dynamic conditions.

Static SIMS is useful for the analysis of surface monolayers and non-volatile labile compounds, like polymers and biomolecules. A low primary ion flux (10^{-9} A/cm^2) is used to avoid extensive sample damage. Under these conditions, the relative yield of diagnostically useful secondary ions is greatly increased. Static SIMS, also known as Molecular SIMS, produces similar spectra to those obtained by FD or PD for a variety of samples,[34-38,52-56] including aminoacids, drugs, vitamins, etc., with far simpler experimental conditions. Two SIMS spectra of glycine on a silver target, one from a neutral solution and the other from an acidic solution of the sample, are shown in Figure 1.12. Although aminoacids are very polar and non-volatile compounds, and thus difficult to analyze, it can be seen that very good spectra are obtained. This method, more versatile and easier to handle than FD or PD, became popular in spite of some practical drawbacks.[38,57,58] Among these, it can be mentioned: 1- low intensity of the signal, due to the low primary ion beam flux, 2- short life-time of the sample, regarding the production of diagnostically useful spectra, 3- wide kinetic energy distribution of the ions, due to the deposition of a large amount of energy, 4- surface charging of the target, due to the

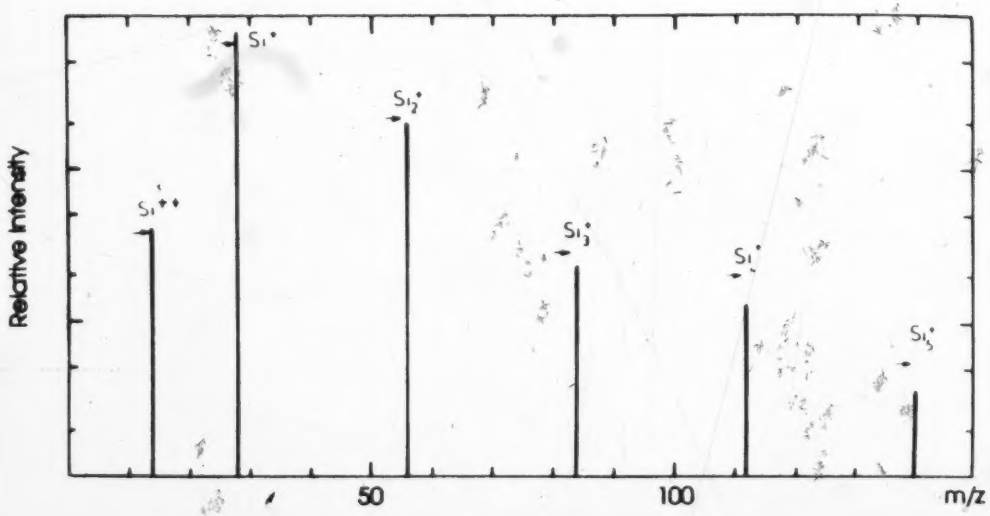

Figure 1.11. SI Mass Spectrum of a Silicon Surface
(Adapted from A. Benninghoven, *Surf. Sci.*, **53** (1975) 596).

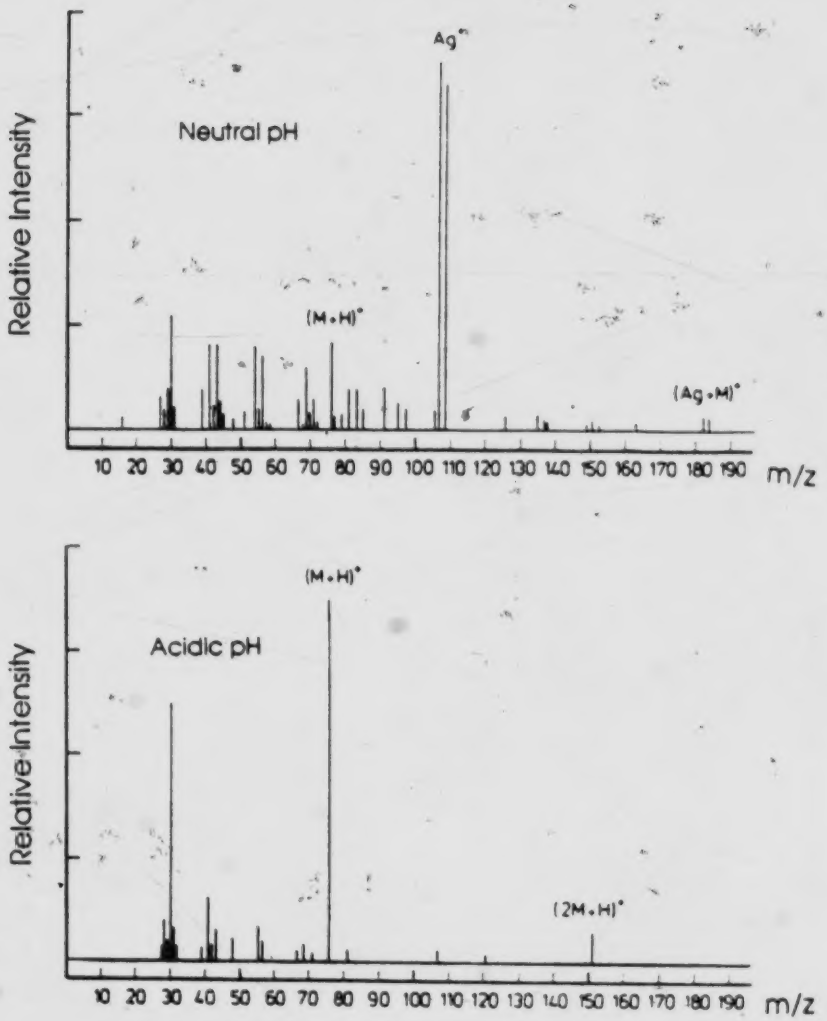

FIGURE 1.12. SI Mass Spectra of Glycine
(Adapted from A. Benninghoven and W. K. Sichtermann, *Anal. Chem.*, **50**, (1978) 1180).

ionic nature of the beam, and 5- difficulty in directing the primary ion beam towards the high voltage region of the ion source.

Fast Atom Bombardment Mass Spectrometry (FABMS).- Although the bombardment of metallic surfaces with high energy neutral beams to produce sputtering had been studied since 1929,[59] there was no knowledge about the nature of the ejected particles. In 1966 Devienne reported that ions were produced when a solid target was bombarded with a neutral molecular beam,[60] and the same group studied this effect during the following ten years, using mass spectrometric detection.[61-64] However, the major contribution that led to the most successful application to date in the analysis of non-volatile organic, organometallic and inorganic compounds, took place in 1981, when FABMS[65-68] appeared as an improved version of Static SIMS. The original idea in FAB was to use an atom beam to bombard the sample, instead of an ion beam, in order to avoid charging of the sample, and to make the technique readily adaptable to high-mass, high-resolution instruments. But the most important feature in FAB, which only became evident in a later publication by the same group,[69] was not the use of an atom beam, but rather the use of a non-volatile liquid matrix to contain the analyte when it was exposed to the action of the primary beam. This innovation allowed the use of higher flux beams, led to intense and stable secondary ion currents and produced mass spectra with relatively abundant protonated molecular ions

and structurally significant fragments, overcoming the main limitation of SIMS, which is the radiation damage associated with the bombardment of solids. A diagram of a FABMS ion source is shown in Figure 1.13. It is basically the same as a SIMS ion source, and the main difference is that the sample is exposed to the ionizing beam as a liquid solution. The fact that an atom beam is used instead of an ion beam is not relevant in terms of the sputtering, and similar spectra are obtained with FABMS or liquid SIMS.

The major contribution of the pioneers of FAB was to demonstrate that large, highly polar biomolecules can be analyzed by means of a reliable MS experiment. Soon after the appearance of FABMS many research groups began to use it. In a short time, the literature was replete with reports of a wide variety of applications[70-85] and reviews[86-95] on different aspects of this remarkable technique. Figure 1.14 shows the FAB spectra of a saccharide, a kind of compound for which mass spectrometric analysis is usually difficult because of their high polarity and thermal instability. However, the FAB spectrum shows not only the pseudomolecular ions (both protonated and sodiated) but also fragment ions which provide valuable structural information.

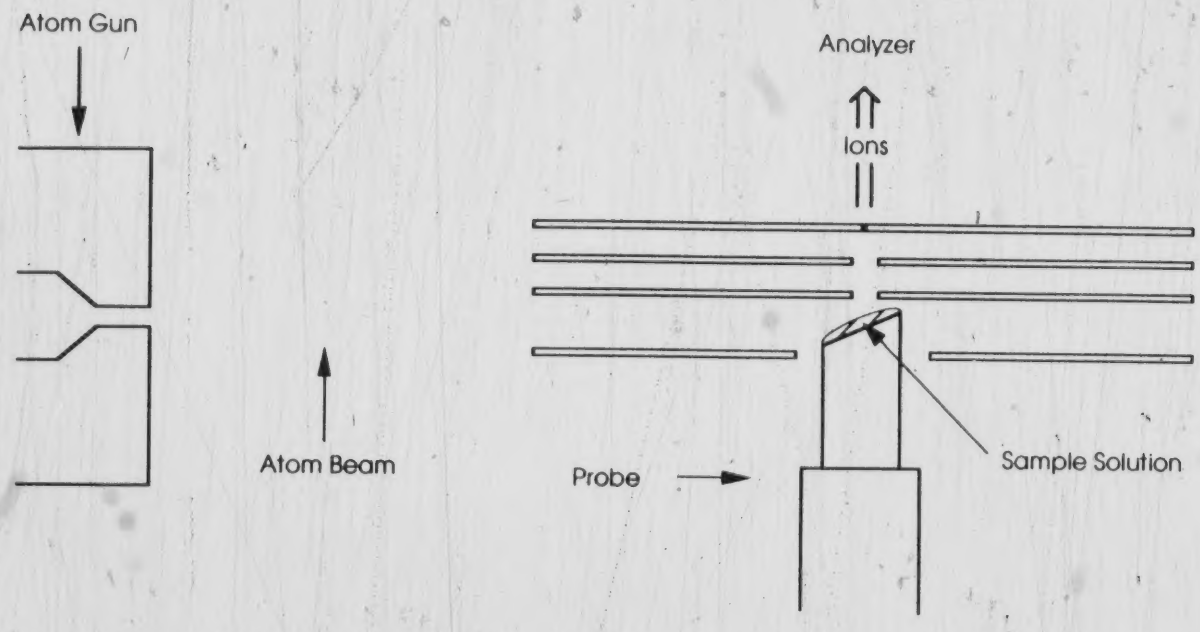

FIGURE 1.13. Diagram of a FAB Ion Source

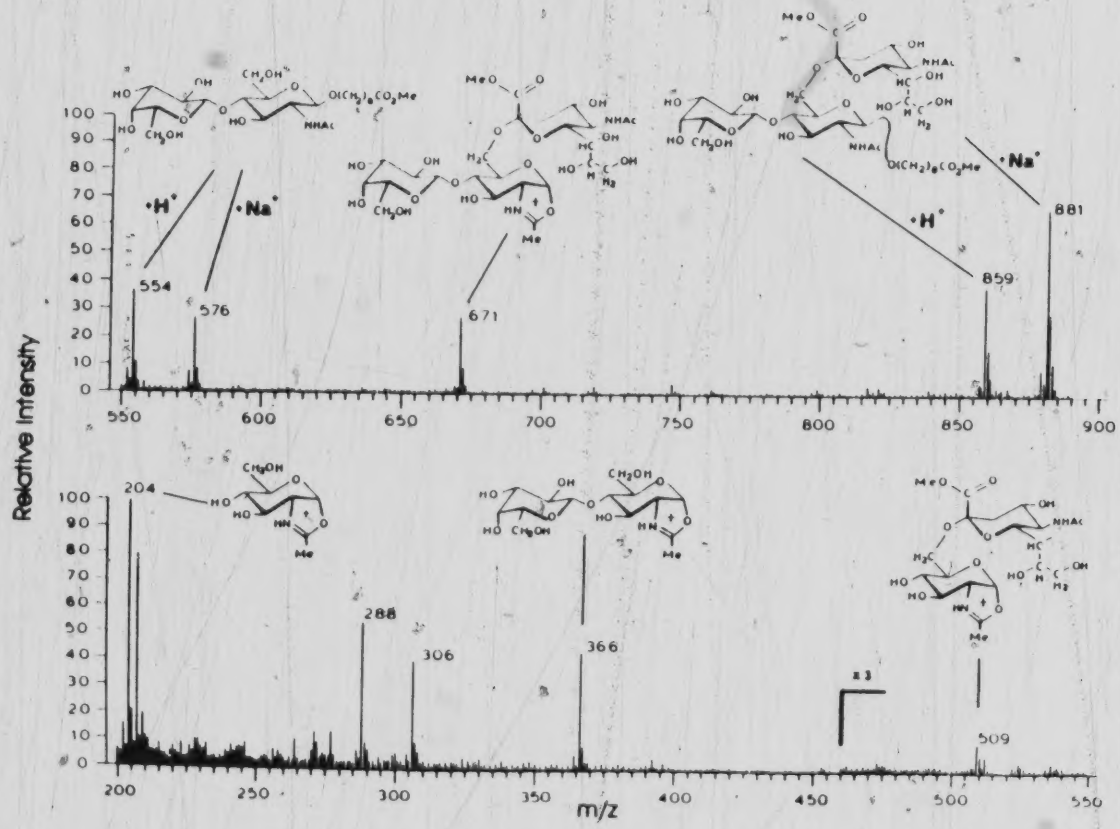

Figure 1.14. FAB Mass Spectrum of a Saccharide
(Adapted from M. M. Palic, O. P. Srivastava and O. Hindsgaul, *Carbohydr. Res.*, **159** (1987) 315).

CHAPTER 2

MECHANISTIC STUDIES ON THE DESORPTION AND IONIZATION PROCESSES IN SIMS AND FABMS.

Right after the introduction of FAB, a large volume of discussion was generated about its close similarity with SIMS, from both theoretical and experimental points of view. FAB and Liquid or Molecular SIMS became names used with practically no discrimination, despite the differences existing among the three methods. In the same explosive way, a large number of scientists, including physicists, chemists and biologists, decided to explore the intriguing phenomena underlying these techniques. This is understandable, since it is indeed surprising that the deposition of a large amount of energy in a very small volume over a short period of time could result in the desorption and ionization of intact molecules, especially when these are large, highly polar and thermally unstable biomolecules. There is no agreement in the literature regarding the mechanism by which the molecules can survive such an apparently violent process. Most of the early mechanistic research was developed in connection with Atomic SIMS, and when Molecular SIMS and FAB became widely used, the focus of attention was switched to them. As a consequence, many models have been proposed for SIMS and FAB. However, PD and LD give spectra comparable to those obtained under FAB or SIMS

conditions. This indicates that the phenomena governing the production of the detected ions in each of those cases are similar and justifies the now popular use of the collective term Desorption Ionization (DI) for such mechanisms. A very brief review will be given here, with more emphasis on Molecular SIMS and FAB.

Atomic SIMS Models

Atomic SIMS refers mainly to the analysis of inorganic materials under dynamic conditions. Mechanistic studies in this area have established the theoretical basis and terminology for Molecular SIMS and FAB as well. There is extensive information in the literature about models that apply satisfactorily to Atomic SIMS. A large number of references are included in several reviews and monographs on this topic.[96-102] The different models can be divided in two main groups: Sputtering and Ionization Models.

Sputtering Models.- These models are concerned with the energy transfer process between the primary ion beam and the target, and with the removal of the particles from the bombarded surface.

Among the Sputtering Models, the Thermal Spike Models[103-107] have been proposed to explain the existence of sputtered atoms with energies in the thermal range (less than 1 eV). According to

these models, élastic collisions between the atoms of the solid occur when the surface is bombarded, and the excited region or spike acts like a high density gas that is being heated. As a result, atoms are emitted by evaporation from the surface of the spike. In addition, atoms with higher energies, in the order of hundreds of eV, are also emitted by a knock-on process, due to direct momentum transfer from the bombarding particles, followed by ejection after undergoing a small number of collisions with other atoms, or by recoiling along the linear trajectory of the primary particle and reaching the surface with enough energy to overcome the binding forces. However, the presence of the majority of the atoms, with intermediate energies between 1 and 20 eV, is not explained by these models.

The Collision Cascade Models[108-110] offer an explanation for the emission of particles with translational energies. In these models, the impinging particle penetrates into the surface, altering its originally linear trajectory, and transfers its excess of kinetic energy to the target atoms. The energized atoms hit other atoms and a collision cascade is generated. The process continues until the impact energy is dissipated, and those atoms that have enough energy and are directed towards the surface are ejected. The sputtering time-scale is considered to be very short, less than 10^{-12} s after the impact.

Ionization Models.- A large proportion of neutrals to ions are produced by sputtering. Ions, although in smaller percentage, have the advantage that they can be easily detected. These models are concerned with the processes governing the production of ions. Among them, the models based on the band structure concept are quite popular.

The Bond Breaking Model[111-113] is used to explain the ion emission from simple ionic compounds that contain in the lattice a valence band of anionic states and a conduction band of cationic states, with a gap between the two bands. According to this model half of the lattice energy is consumed when a cation is removed, but in order to remove a neutral an electron has to cross the band gap and the atom must go to the gas phase, which is energetically less favorable. Then, for ionic compounds the emission of ions is preferred, when the lattice energy is much less than the band gap. This model is useful only for polar materials.

A more general model is the Band Structure Model,[114-116] that assumes that the band structure of the solid controls the electron transfer between excited species and the surface. In the case of a metal, the sputtered ions can undergo neutralization by means of electron transfer to or from the conduction band. The amount of ions is reduced as more neutrals are produced. For a covalent surface, like an oxide, neutralization is less probable because

there are no electrons available in the conduction band, and the electrons in the valence band have not enough energy to be exchanged between the excited species and the solid. Therefore, higher positive ion ejection is expected, and an increase in negative ion production is explained by electron attachment to departing neutrals.

These models based on the concept of band structures are not completely acceptable, because the bombarded area is highly disturbed and this picture of organized bands seems unrelated to the real situation. A variety of other models, like the Local Thermal Equilibrium Model,[117] the Surface Polarization Model,[118] the Electron Tunneling Model[119,120] and others, have proliferated, each one trying to explain different aspects of Atomic SIMS. Some models are qualitative and applied to very specific cases, and others are quantitative. However, none of them is able to account for all the experimental facts.

Molecular SIMS and FABMS. Desorption Ionization Models

The development of Static SIMS led the way to Molecular SIMS and FAB, and soon models for the mechanism of ejection of organic molecules began to populate the literature. This subject became a greater challenge compared to Atomic SIMS, because the sputtering and ionization of intact molecules was even

more difficult to explain. When trying to do so, the first obvious tendency is to adapt some of the many approaches available from Atomic SIMS models. However, although atomic and molecular emission are similar, a more sophisticated set of events must be present in the case of molecules. In such a state of continuous controversy, there was a time when it seemed to be as many models as authors, as it is reflected in several reviews of the topic.[58,89,94,102,121-126]

Despite the diversity of opinions, there are some basic points on which most models seem to agree. A logical assumption, present in practically all models, is that the sputtering phenomenon is an important part of the whole process. The obvious starting point is that, similar to the situation in Atomic SIMS, the impact generates an excited region by energy transfer from the bombarding particle to the target. As the energy is dissipated through the liquid or solid surface, the molecules begin to move and eventually they are ionized and/or ejected. However, how the dissipation of the energy occurs and how, when and where the molecules undergo ionization and fragmentation to produce the detected species, are controversial issues. From this point of view, the models for organic emission can be split in two categories: translational models and thermal/vibrational models.[102] A further classification, that applies to both these groups, distinguishes between empirical or intuitive models and those based on calculations.[125] In addition, from a

more theoretical standpoint, the models can be divided according to two aspects, the first related to the principle governing the energizing mechanism, and the second regarding the expansion process.[123] This classification includes five groups of models: RRKM,[127,128] Coulomb Explosion,[129,130] Thermal,[131,132] Expansion[133,134] and Excitation models.[135,136] However, in the context of the present work, the first classification mentioned (translational and thermal/vibrational models) is the most important, and only that one will be briefly covered.

Translational Models.- These models are based on collision cascade regimes. Among them, the Precursor Model proposed by Benninghoven[122,137] is one of the most widely accepted. According to this model, before any bombardment event, preformed ions exist in the sample. An excited region is formed around the path of the bombarding particle, due to the dissipation of energy in a volume of 10-100 Å in diameter. Very rapid energy transfer causes emission of these precursor ions from the surface, with high probability of keeping the same charge during the process. Rapid transfer of small amounts of energy leads to emission of non-fragmented parent-like secondary ions, while transfer of large amounts of energy results in the emission of fragment ions, formed by decomposition of the precursor ions, although fragmentation might also occur by decomposition of excited molecular ions. This model rationalizes the dissipation of energy along the

track of the collision cascade by means of an energy distribution E, that describes the average energy transferred to the particles as a function of the distance r from the impact point. The qualitative shape of E is shown in Figure 2.1.

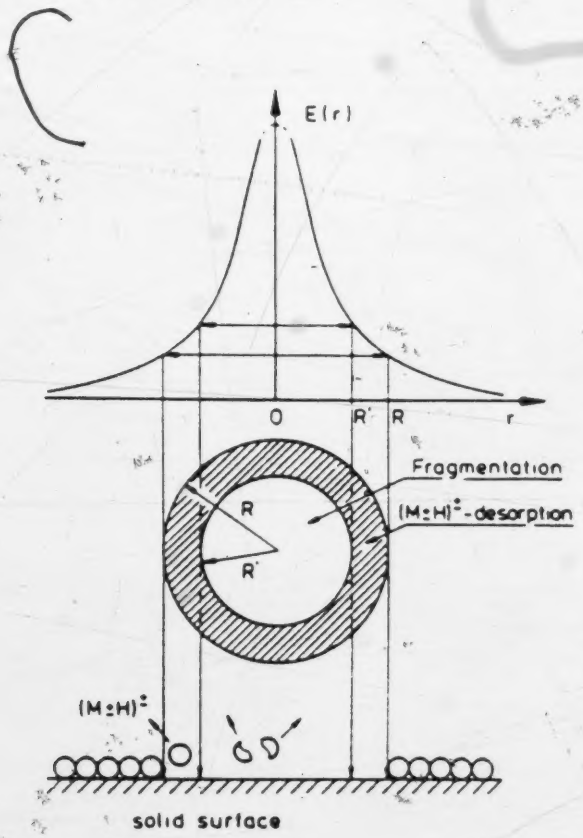

Figure 2.1. Qualitative Shape of the Function E(r).
(Adapted from A. Benninghoven, *Int. J. Mass Spectrom. Ion Phys.*, **53** (1983) 85).

Close to the bombardment site, ($r < R'$), a large amount of energy is transferred and the probability of emission of fragments is very high. At intermediate distances, ($R < r < R'$), the amount of energy

transferred is small and results in the ejection of parent-like ions, *via* a very fast evaporation. At long distances, ($r > R$), the amount of transferred energy is very small and no ejection takes place. As a consequence, relatively high kinetic energies are expected for the fragment ions, whereas parent-like ions are expected to be emitted with low kinetic energies.

Other translational models are based on computer simulations and offer a more quantitative treatment of the ejection of the particles.[105,138-147] A good picture of the particle motion generated at the surface target by bombardment with energetic atoms or ions has been obtained by means of three-dimensional Monte Carlo calculations to metal surfaces.[105,138,139] The method uses interatomic potential equations and requires initial information such as energy, position and direction of the observed particle, which is assumed to change direction when participating in binary nuclear collisions and to follow straight free paths between those events. Its energy is reduced due to nuclear and electronic losses and the calculation finishes when the energy drops below a certain value, or when the particle is out of the target. These calculations allow determination of energy and angular distributions. Based on these simulations, Magee[105] concludes that in the case of organic solids the ejected fragments come from direct impact in the vicinity of the bombardment site (direct-knock-on), while the molecular species come from further away, where the energy has dissipated

enough to produce no fragmentation but only ejection (linear collision cascade). The dependence of the molecular ion yield on the incidence angle of the primary beam, and on the nature (liquid or solid) of the surface, are also discussed on the basis of Monte Carlo simulations. Figure 2.2 shows the trajectory of recoiled sample atoms produced by a 10 KeV Ar^+ beam on a Cu surface, at two incidence angles.[138] It can be seen that many more of the low energy collision cascades intersect the surface when the angle of incidence is 70°. This results in a higher yield of the sputtering of non-fragmented particles. The importance of liquid matrices is explained as the result of rapid renewal of the surface exposed to the radiation.

The Classical Dynamics Model,[110,125,140-142] based on earlier computer simulations[143,144] and developed by Garrison and coworkers, also proposes a collision cascade to deal with the energy transfer and dissipation, but differs from Monte Carlo calculations in some aspects. The model shows that the intact molecules can be ejected from regions either close to or far away from the initial impact area, and gives three possible explanations for such an intact ejection. First, the energy of the impinging particle can be rapidly dissipated by the target, and by the time it reaches the organic molecule, the kinetic energies involved are only in the order of tens of eV. Second, the molecules contain many vibrational

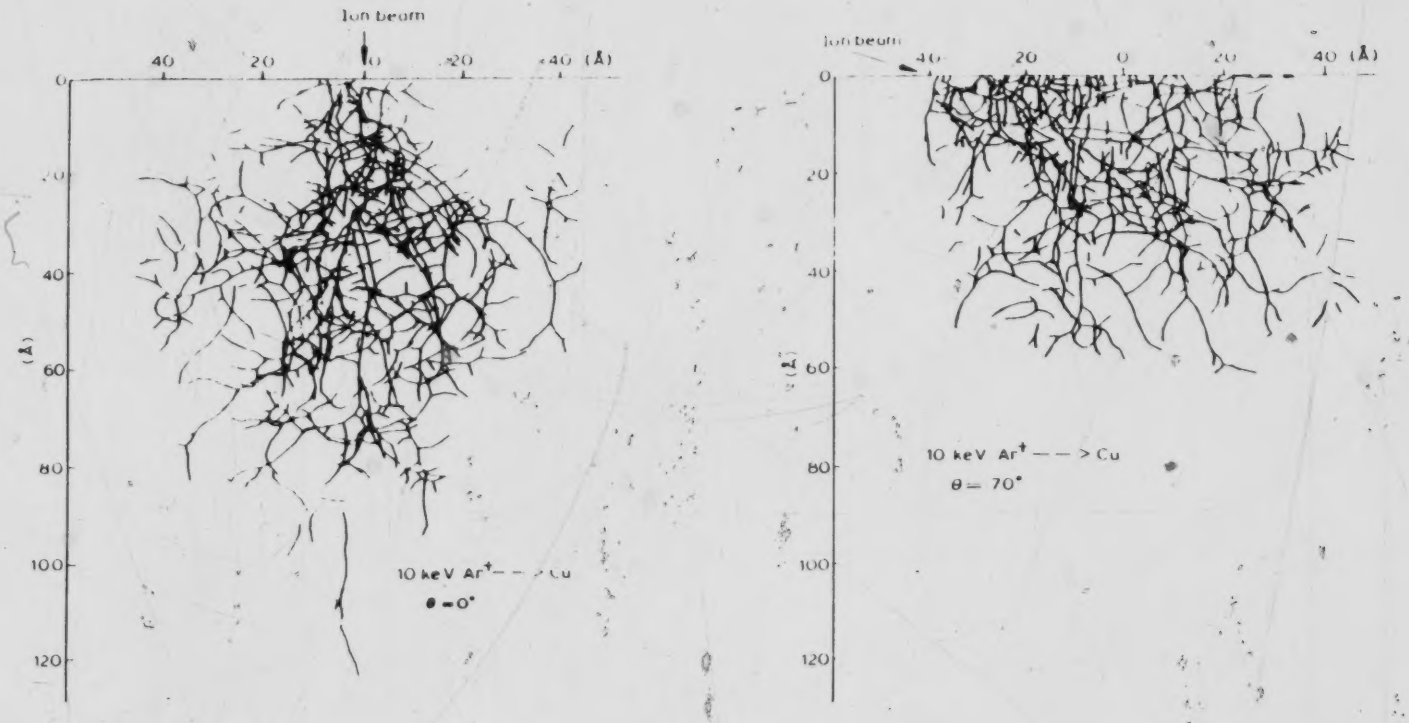

Figure 2.2. Monte Carlo Simulations of the Trajectory of Recoiled Sample Atoms at Two Incidence Angles of the Primary Ion Beam.

(Adapted from C. W. Magee, *Int. J. Mass Spectrom. Ion Phys.*, **49** (1983) 211).

modes that can efficiently absorb energy from the collision without dissociating. Third, in the case of large organic molecules, individual atoms or groups are small compared to the metal atoms that support the sample, and it is possible to hit the molecule at several points in a concerted fashion, causing the entire entity to move in one direction. These calculations also anticipate that the fragments can be formed not only in the region directly bombarded, but also in areas far away from it. In order to predict sputtering effects, cluster formation and emission and fragmentation of adsorbed molecules, the model applies classical motion equations to predefined parameters such as mass and energy of the primary particle, size and structure of the surface target, incidence angle of the beam, etc. This information is used to predict the experimental results, such as total yield of ejected particles, energy distributions, cluster formation, etc. Additionally, computer simulations also show that the ejected species can undergo transformations in the near-surface region, and therefore their charge and composition as they reach the detector may not be the same as when they left the surface. Possible reactions are proton transfer, cationization, anionization, etc. Furthermore, it is predicted that when the species leave this near-surface region with enough internal energies, there is the possibility of unimolecular reactions and formation of new fragments on the way to the detector.

Thermal/Vibrational Models.- The thermal/vibrational models do not completely contradict the translational models, but consider them incomplete and try to further explain the ejection and ionization processes as a consequence of thermal disturbance after the initial collision cascade. Some of the models are general for DI techniques, and some others are more specific for a particular method.

Macfarlane,[124,148,149] although working mainly on PD of a wide variety of samples, from ice to insulin, supports the idea that even if the mechanism of deposition of energy varies when the projectile is a collection of coherent infrared photons (LD), or a MeV heavy ion (PD), or a KeV ion (SIMS) or atom (FAB), the spectra produced by different particle-induced desorption methods are essentially the same. Based on this, he suggests that the sequence of events that directly influence the production of the spectrum is common to all of them. A representation of the four main variations of particle induced desorption techniques is shown in Figure 2.3. In all the methods, the deposition of energy is highly concentrated and the excitation lasts for only a very short period of time. Under those conditions the sample molecules, even large, thermally labile molecules, survive the desorption process. Macfarlane divides the events into three categories: chemical transformations, desorption and surface ionization. The molecules to be desorbed are bound through polar interactions. These forces are strong enough to form aggregates that, in the presence of an additional

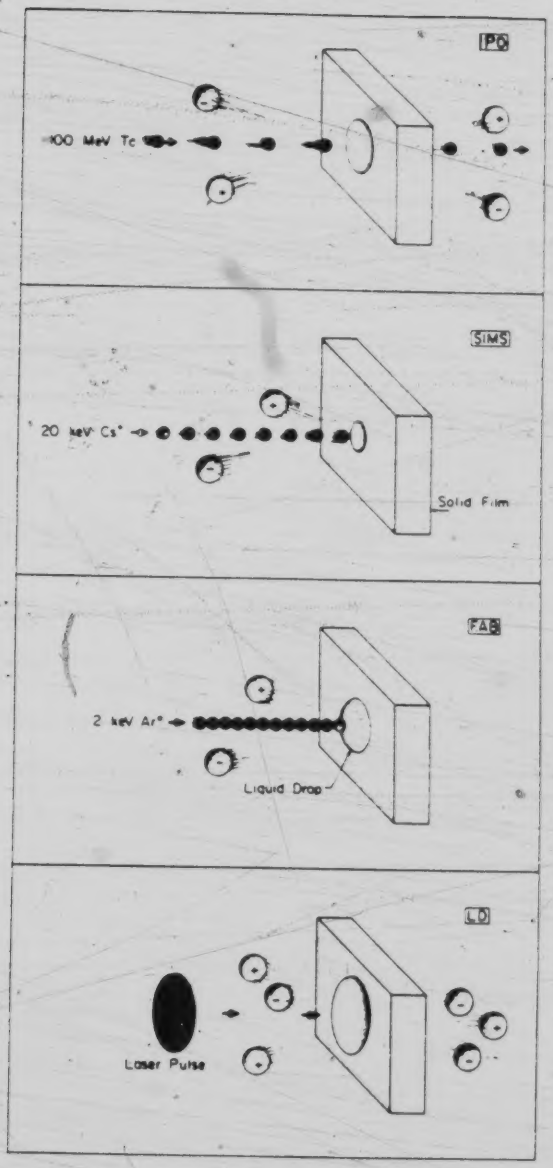

Figure 2.3. Schematic Representation of Particle Induced Desorption Techniques.
(Adapted from R. D. Macfarlane, *Acc. Chem. Res.*, **15** (1982) 268).

energy source, can react. There are two possible places where chemical reactions can take place: on the surface or in the gas phase. For non-volatile biomolecules, the main transformations to yield ionization are assumed to occur on the surface, and the final charge states of the desorbed species are determined by the substrate-absorbate interactions during the desorption process. For the ejection mechanism, two approaches are proposed: evaporation or kinetics transformation. In the thermal spike approach the desorption is considered to occur by thermal evaporation. If the process is treated as a chemical kinetics problem, it is described by the Arrhenius' equation, with the pre-exponential factor related to the surface-adsorbate vibrational mode, and the activation energy as the heat of sublimation necessary to break the bond between the molecule and the surface.

Rabalais' model,[116,150,151] based on SIMS experiments of solid samples, such as alkali halides, ice, frozen benzene and nickel tetracarbonyl, is among the early and most important contributions to this topic. The spectra show sequences of cluster ions, with exponential decrease of the intensities as the size of the cluster increases. Rabalais proposes that the observed spectra originate from processes involving molecules on the surface of the probe, rather than from gas phase species, since the sample pressures are very low, in the order of 10^{-9} torr. This model divides the particle emission into two steps: ejection dynamics and electronic pro-

cesses. The initial impact and transfer of energy from the primary particle to the surface involves the generation of a non-equilibrium situation, caused by the almost instantaneous deposition of a high amount of energy into a small region. This results in the localized heating of the bombarded area up to very high temperatures, and the situation is relieved by irreversible expansion into the vacuum. Some species are ejected without recombination with other particles, if they have enough energy to overcome the binding forces and if the velocity vectors are oriented in the appropriate direction towards the surface. This process is called non-reactive ejection. Some other particles are induced to move through the surface with a broad velocity distribution, determined by the momentum transfer, forming a high density, thermally activated region near the impact site, where reactions can take place. This transient, high density plasma is the so-called selvedge, situated at the interface between the condensed and gaseous phases and populated with neutrals and ions formed by single collisions. As these species propagate, large clusters are formed in the selvedge if the time and velocity of the species are synchronized in such a way that the attractive potential between them is large enough to bind them together as a single entity. These clusters are ejected to the vacuum, and some of them undergo unimolecular dissociations during their flight to the detector. The particles are emitted predominantly with the same charge they had in the original material. However, the final charge of the ejected

particles may be altered by electron-exchange processes between the particles and the surface, explained in terms of the band structure of the solid.

Extensive work developed by Michl and coworkers[152-163] with frozen gases such as nitrogen, noble gases, carbon monoxide, etc., at cryogenic temperatures, lead to the conclusion that momentum transfer, direct charge transfer, association reactions and ion-molecule reactions are all important process in the formation of the secondary ions. Regular progressions of cluster ions, with a nearly exponential decrease of the intensities as the size of the cluster increases, are observed for all the samples. Based on these results the Gas-flow Model is assembled. In it, Michl assumes that the impinging particle penetrates into the surface, transferring its energy to the sample molecules. Fragmentation and ionization generate a damage track, and the immediate result is the ejection of secondary particles from the layers near the surface. These high energy species are called the "first batch of ejected particles" and have a broad energy distribution. They have no opportunity to react with other constituents of the solid, even if they are highly reactive. They correspond mainly to the fragment ions observed in the spectrum, and to some fraction of the molecular ions. The atomic motion is quenched by energy transfer to the cold areas nearby, and the collision cascade regime is converted to a thermal regime. The impact region can be viewed now as the re-

sult of the thermal spike, a high pressure, high density, high temperature gas, in which the identity of the individual layers of the solid has been lost by random mixing. As the collision cascade develops into the thermal spike, time becomes available for the hot species to react among themselves and also with their cold neighbors. To relieve the non-equilibrium situation, an explosive expansion of the high pressure gas into the vacuum takes place, accompanied by evaporation from the surface surrounding the thermal spike region. This causes cooling and promotes large cluster formation. The species ejected at this point are the "second batch of secondary particles" and their energy distribution is narrower and at lower energy values that those of the first batch particles. They correspond mainly to molecular ions and clusters observed in the spectrum. The gas flow from the hot spike into the vacuum is an essential idea in this model. The final step of the proposed mechanism is the metastable decay of the clusters. Electron exchange is not considered significant, due to the lack of identity of the solid bands in the sputtered region and the solvated nature of the emitted ions.

In broad agreement with some of the ideas of Rabalais and Michl, Cooks and coworkers[58,88,164-171] have reviewed some aspects of the Molecular SIMS/FAB mechanism, especially those related to chemical effects. Their experimental work covers a variety of organic salts and polar compounds in ammonium chloride

and other solid and liquid matrices. According to Cooks, irrespective of the initial method of energy deposition, there is a point in all DI methods at which the energy is in a common form, and this accounts for the resemblance observed in the spectra obtained with all DI techniques. This transformation to a common form of energy is called "energy isomerization" by Cooks, and it is the result of energy transfer to low-energy vibrational and translational modes of the sample molecules. This causes heating and emission of electrons, photons, neutral molecules and ions. The thermal spike leads to the formation of the selvedge or high density gas region, and the reactions occurring there are considered very important. Cooks explains that molecular ions arise from three different processes: ion-molecule reactions, direct desorption and some minor electron ionization by electrons present in the selvedge as the result of secondary electron emission. Ions formed in the selvedge can react with other ions or with neutrals to form clusters and other secondary particles. The observed fragmentation is considered mainly as a result of unimolecular decay of metastable ions in the vacuum. Figure 2.4 summarizes Cooks' view of the processes occurring in the DI mechanism.

A traditional idea introduced during the early FAB experiments[69] is that the liquid surface continuously renews itself by diffusion and that this fact explains the long life-time of the signal during the sputtering. However, more recent experiments by Ligon[172-173] with deuterated

glycerols, and by Wong and coworkers[174-175] with glycerol solutions of carbohydrates and peptides, indicate that this assumption is probably incorrect, since diffusion is a very slow process in the time-scale of the sputtering. These authors consider that the layers of the sample solution are removed by evaporation. Wong[175] proposes a mechanism of sputtering by spraying, involving the formation of a high pressure gas by evaporation of the sample solution from the dense cascade region, as shown in Figure 2.5. Large clusters are ejected, and they decompose to produce molecular ions. Sputtering of radiation damage products also takes place. As for the ionization process, it is assumed that the clusters initially formed are randomly charged, and their rapid decomposition leads to the most stable ions. Therefore, the ion intensity distribution reflects the ion chemistry in solution. Ligon,[173] based on his measurements of the ratio MD^+/MH^+ from the spectra of solutions of deuterated glycerols in glycerol, proposes an ionization mechanism *via* radical cation intermediates, in contrast with the widely accepted explanations regarding the existence of preformed ions in solution, or the ionization in the selvedge. This mechanism involves the formation of radicals by primary radiation damage, which are able to abstract protons from nearby molecules and ionize other species in solution by proton exchange.

Additional information about radical formation during particle bombardment is found in the literature.[176-178] For instance, Field[176-177]

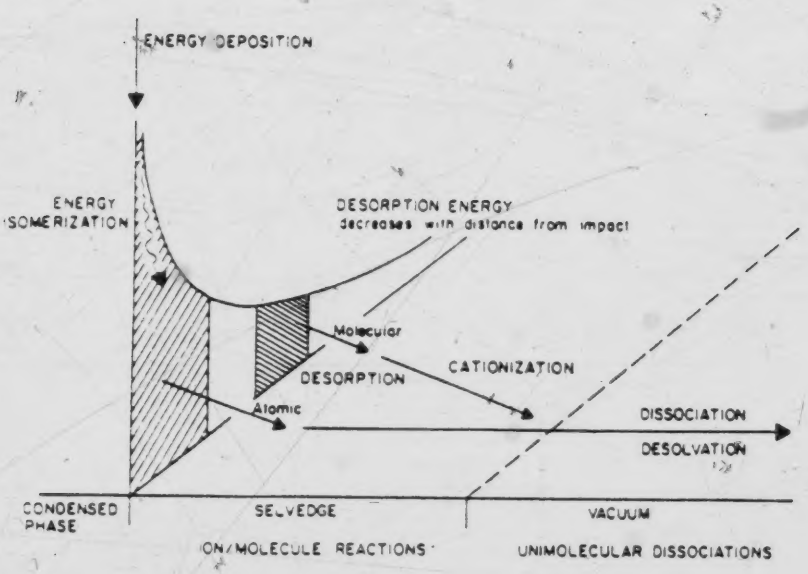

Figure 2.4. Schematic Representation of Processes Involved in DI Techniques.
(Adapted from R. G. Cooks and K. L Busch, *Int. J. Mass Spectrom. Ion Phys.*, **53** (1983) 111).

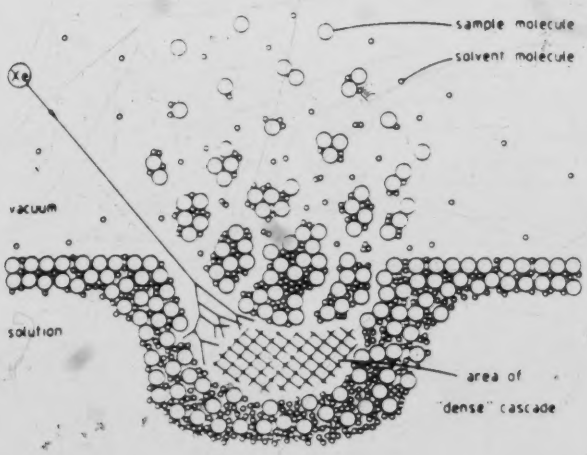

Figure 2.5. Schematic Representation of Sputtering by Spraying.
(Adapted from S. S. Wong and F. W. Röigen, *Nucl. Instrum. Methods Phys. Res. B*, **14** (1986) 436).

reports marked changes in the glycerol FAB spectrum as the bombardment proceeds. Protonated molecular ion and cluster peaks decrease almost completely as new peaks appear, indicating that the bombardment causes glycerol reactions to produce new compounds. Field suggests that a special case of hot atom chemistry, with no incorporation of the bombarding entity into the molecule being transtormed, is responsible for the radiation damage and formation of the radicals. This assumption is based on the premise that a fast atom beam carrying an energy of several KeV cannot be considered ionizing radiation, according to adiabatic principle calculations.[179,180] Even if interesting and important in some cases,[181,182] the mechanism of radical formation is probably not directly responsible for most of the significant ions observed in FAB spectra. FAB analysis usually involves the very first scans, with a minimum of exposure to the bombardment, which leads to the observation of clean and meaningful spectra.

Budzikiewicz and coworkers[183,184] have performed FAB experiments with non-ionic compounds in order to demonstrate that ion formation is due essentially to chemical ionization in the gas phase by a matrix plasma. The vapor pressure of the matrix during the FAB experiments is in the CI range[185] and their results with glycerol, thioglycerol and other compounds commonly used as FAB matrices,[183] show that the FAB matrix spectra are similar to those obtained by evaporation of the matrix directly into the ion source

and followed by ionization by EI or collision with the fast atom beam. The ionization of non-ionic FAB samples is assumed to occur in three steps: first, the sample molecules are transported to the surface of the solution by convection or diffusion during the bombardment; second, neutrals from both matrix and analyte are sputtered from the surface and/or from lower layers of the solution into the gas phase, and third, ionization of the matrix molecules occurs by collision with the atom beam. Chemical ionization of analyte molecules takes place in the matrix plasma. Experiments using divided targets,[184] with two different compounds in each side of the target, show the production of mixed ions, giving support to the idea of ionization in the gas phase. Therefore, properties of molecules in the gas phase, like gas basicities (GB), proton affinities (PA), electron affinities (EA), etc., have influence in the results of FAB experiments. There are a few reports in the literature[76,78,186,187] where the low PA of the analyte compared to that of the matrix is considered the main reason for the low intensity observed for the analyte signals in the FAB spectrum. However, in many other cases different properties are assumed to be responsible for the success or failure of FAB experiments.

Early Work in Our Group

In view of all this abundant and sometimes contradictory information, our research group decided that it would be interesting to develop a more systematic series of experiments to further clarify

the role of GB values in the production of FAB spectra. This could lead to some conclusions about the dominance of gas phase chemistry or solution chemistry in the ionization mechanism involved.[188-190] The FAB spectra of a series of liquid compounds with different GB were recorded.[189] The compounds studied are commonly used as FAB matrices and the spectra were recorded for the neat liquids and for 10 molepercent solutions. The observed result in most of the cases is that the spectrum of the compound with lower gas basicity is strongly suppressed. Figure 2.6 shows the spectrum of neat triethanolamine (GB = 225 Kcal mol^{-1}) and 10 molepercent solution of triethanolamine in 3-nitrobenzyl alcohol (GB = 186 Kcal mol^{-1}). It can be seen that the presence of 3-nitrobenzyl alcohol is not detected and both spectra are practically the same. In a separate set of experiments, the total ion current (TIC) of the FAB spectra of salts in glycerol was measured as the concentration of the salt was increased.[190] It was observed that there is no increase of TIC with the concentration of the salt. As shown in Figure 2.7, a slight decrease is observed. This disagrees with the widely accepted idea that ions already existing in solution are responsible for the production of the spectrum, as proposed in the Precursor Model.[137] These results led to the proposed Gas Phase Collision Model, which states that analyte ions and matrix ions produced by the atom impact, suffer extensive recombination as a high density, high temperature gas-like region is formed,

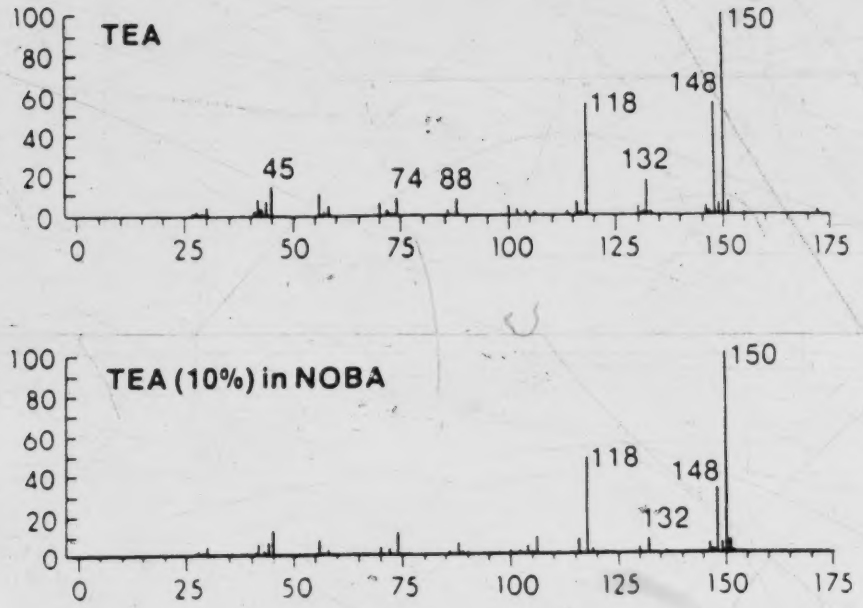

Figure 2.6. FAB Spectra of Neat Triethanolamine and 10 Molepercent Solution of Triethanolamine in 3-Nitrobenzyl Alcohol.

(Adapted fom J. A. Sunner, R. Kulatunga and P. Kebarle *Anal. Chem.*, **58** (1986) 1312).

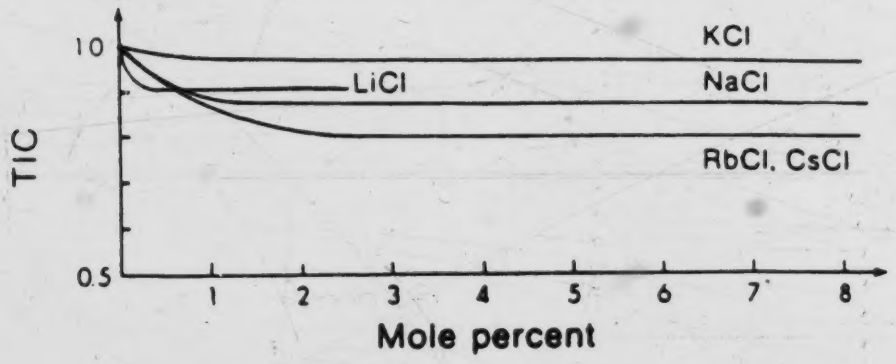

Figure 2.7. Normalized Total Ion Current (TIC) from FAB of Glycerol Solutions of Alkali Halides.

(Adapted from J. A. Sunner, R. Kulatunga and P. Kebarle *Anal. Chem.*, **58** (1986) 2009).

and when this hot gas is being expelled into the vacuum, ion-molecule reactions take place to produce the detected ions. However, it has been argued[102] that it is inappropriate to conclude that ejection of preformed ions is not significant in the formation of the FAB spectrum, since the compounds chosen for the mentioned experiments[189] do not propitiate the formation of ions in solution. The objective of the present work is to go further in this line of research, in order to clarify whether gas phase chemistry or solution chemistry is dominant in FAB experiments, and to propose a more detailed mechanism for the ionization process involved.

EXPERIMENTAL SECTION

CHAPTER 3

GENERAL

The experiments carried out in this study were performed on a modified AEI/Kratos MS9 double focussing mass spectrometer. This instrument has features which make it suitable to be converted to a FAB mass spectrometer,[191] among those:

a- adequate mass range (0 to 1500 daltons).

b- direct insertion lock, mounted on the ion source flange, useful to admit the sample probe.

c- spare source port in direct line with the ionization region, on which the atom gun can be mounted.

d- good source-region pumping capacity, to handle both the flow of gas from the gun and the vapor pressure from the sample matrix.

e- double focussing geometry, which handles ions with a wide range of energies.

f- sector geometry, which prevents neutrals from reaching the detector.

The instrument is equipped with a saddle field atom gun, a sample introduction probe, and a FAB ion source.

Atom Gun.- A diagram of the atom gun installed in the MS9 is shown in Figure 3.1. Its major components are:

a- two identically shaped aluminum cathodes. The one at the front has one central exit channel for the beam, and the one at the back has one channel to accommodate the ceramic sleeve insulated spring connector for the high voltage supplied to the anode, and five other channels to admit the operating gas.

b- the anode, a circular stainless-steel plate with a central hole where the saddle point of the electric field is located. The plasma of ionizing electrons oscillate through this point. The plate has six symmetrical notches on its periphery, to provide the proper location for six 5 mm diameter ruby ball insulators.

c- a thin-walled stainless-steel tube, where the three electrodes are stacked. The alignment and insulation are provided by the ruby balls. The whole arrangement is kept inside the tube by a retaining ring.

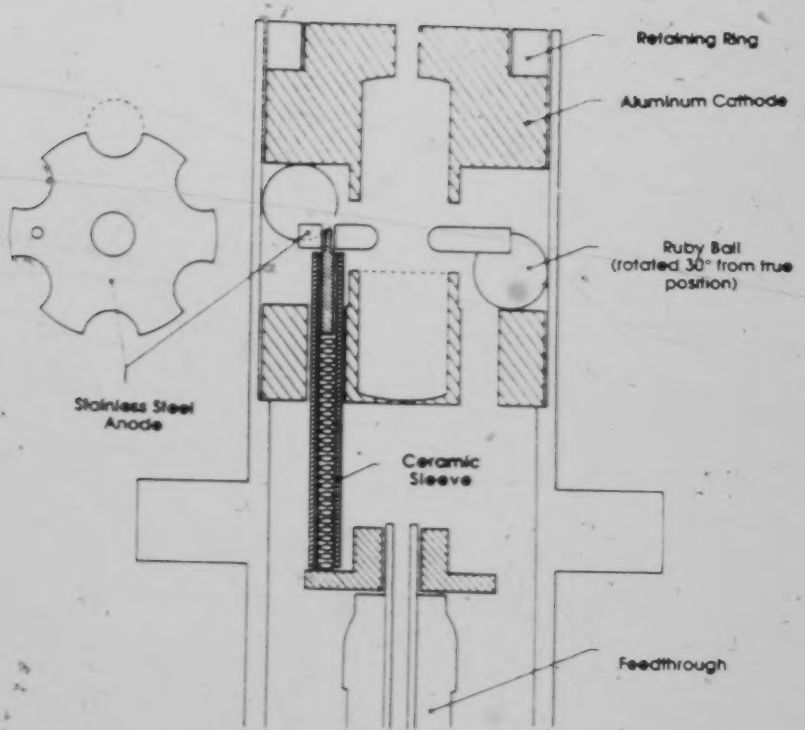

FIGURE 3.1. Diagram of FAB Atom Gun

d- a 10 KV-rated feed through, which carries the anode voltage *via* a disk slipped over the end and connected to the anode by the insulated spring that goes through the rear cathode.

e- a capillary stainless-steel tube, through which the operating gas, usually Xe, is admitted.

f- a 0-10 KV, 0-10 mA Spellman RHR-10P60/CR power supply, to provide the anode potential. The gun is usually operated at a voltage of 6-8 KV and the discharge current flowing between anode and cathode is controlled by varying the voltage and/or the gas flow. The pressure of the gas is set at about 1 psi at the pressure regulator on the cylinder of Xe, and the actual pressure inside the gun is controlled by a Negretti and Zambra needle valve.

The beam of fast atoms (actually a mixture of neutrals and ions) is easily generated by first producing a beam of fast ions, and allowing them to be neutralized with little or no loss of kinetic energy. In order to produce the initial ions, the charged particle oscillator principle is used.[192-194] Electrons present in the space between the two cathodes oscillate around the saddle point of the electrostatic field applied between the positive anode and the grounded cathodes. Initially the electrons are accelerated from the cathode region toward the anode and pass through the cen-

tral hole, where the saddle point is located. Once past the anode, they are decelerated as they approach the other cathode and eventually return toward the anode again, following the reverse path. When electrons hit atoms of the gas, the required ionization occurs. The electrons knocked out in this process are a constant source for renewal of the ionizing plasma. The ions produced are accelerated towards both cathodes. Those which strike the cathodes, produce more secondary electrons which contribute to the plasma, and those ions going through the front cathode exit channel are neutralized on their way out by means of two major processes:

1- resonant charge transfer:[195-198]

$$\vec{A}^{+} + A \xrightarrow{\text{no energy transfer}} \vec{A} + A^{+} \qquad (3.1)$$

2- electron capture:[199]

$$\vec{A}^{+} + e^{-} \longrightarrow \vec{A} \qquad (3.2)$$

As a result, a beam of fast atoms, together with some surviving ions,[200] is generated.

Sample Probe.- The sample is introduced into the ion source by means of a direct insertion probe, equipped with a cylindrical

gold tip. The flat surface of the tip is about 2 mm^2 with a slant of 20°, as shown in Figure 3.2. Solid analytes are usually presented as solutions in a non-volatile matrix, whereas liquids are handled in neat form. The ideal volume to use is 1-2 µL, in order to cover the surface of the probe tip with a uniform thin film of sample. The probe is inserted through a vacuum lock in a coaxial direction to the secondary ion beam. The atom beam has an incidence angle of 70°, relative to the normal to the tip surface. The tip is brought to the same voltage as the ion source by means of a spring contact, which is attached to the extraction plate support and touches the probe tip when fully inserted. The tip is mounted on a nylon probe extension, in order to provide insulation from the grounded steel probe shaft.

Ion Source.- The ion source used to run FABMS in the MS9 instrument is shown in Figure 3.2. Together with the probe, it includes the extraction plates, held at the full acceleration voltage, either 6 KV or 8 KV, and two beam-centering plates, kept at a voltage about 500 V lower than that of the extraction plates and the probe tip. The extraction slit is wider than the one used in EIMS, and its dimensions are not critical.

The mass spectrometer is coupled to a Data General Nova 4/X minicomputer, through a Kratos preprocessor interface. The Kratos DS-55 data acquisition system and processing software were used for all the experiments.

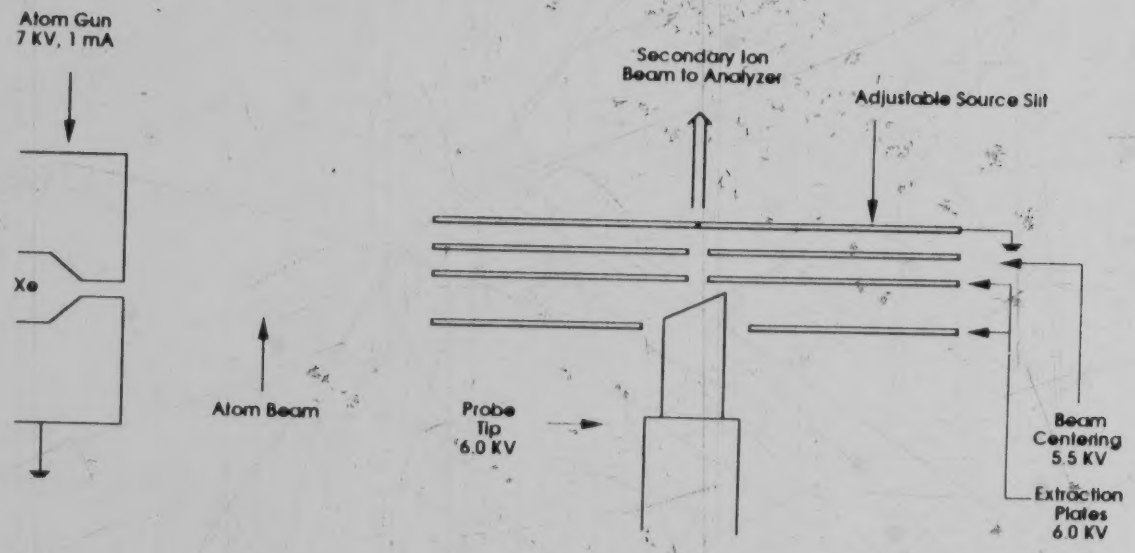

FIGURE 3.2. Diagram of FAB Ion Source

The chemicals used are commercially available, mainly from Aldrich Chemical Co., and were used without further purification, except for the following:

1- diethanolamine was purified by fractional distillation, followed by melting and fractional crystallization.[201]

2- sulfolane was distilled under reduced pressure.

3- 4-cyanopyridine and 4-N,N-dimethylaminopyridine hydrochloride salts were prepared by bubbling hydrogen chloride through an ether solution of the respective free base and collecting the precipitated salt by vacuum filtration.

For all the experiments, 2 μL of sample solution or neat liquid were applied to the gold tip with a 1-5 μL adjustable Scorex micropipette, and then the probe was introduced just in time to take the first scan, with the atom gun already set and working at the desired conditions, usually 7 KV, with a discharge current of 1 mA. The time for rough pumping and exposure to the high vacuum were kept to a minimum. Only the first two or three scans were used.

Experiments for the Study of Competition for Protons and Dominance of Gas Basicities over Solution Basicities

The gas basicity (GB),[202,203] and pK_a[204,205] values were taken from the literature. The absolute pK_a values of the analytes in glycerol were not available in the literature. Accurate measurements of pK_a may be difficult when non-aqueous solvents are involved.[208,209] The pK_a values in glycerol are expected to be lower than those in water,[208] and to follow roughly the same trend. Approximate relative pK_a values in glycerol were obtained by titration of 100 mL of 0.01 M solutions of the compounds of interest in glycerol, with both 0.1 M solutions of hydrochloric acid and perchloric acid in glycerol. The pH measurements were taken with a Fisher 520 pH/ion meter, equipped with a conventional glass/Calomel pair of electrodes. Aqueous buffer solutions of pH 10 (borax), pH 7 (phosphate) and pH 4 (hydrogen phthalate) were used to calibrate the pH meter in the usual manner. The titrating solution was added at a constant rate of 0.19 mL/min into the magnetically stirred solution to be titrated, by means of a Sage Instruments 341A syringe pump. These precautions were necessary due to the high viscosity of the solvent. The titration curves were registered on a Hewlett-Packard 17503A strip chart recorder. The pK_a values were obtained from the pH values at half neutralization volume, according to:

$$pK_a = pH - \log \frac{[A]}{[AH]} \qquad (3.3)$$

The errors related to this approximation should not be neglected.[206-210] Activity considerations and corrections for interactions with the solvent (ion association and homoconjugation become important for low dielectric constant solvents) are not included.[208, 209] Furthermore, for non-aqueous solvents this approximation may not longer work, especially because of the fact that the electrodes used may not function reversibly, and the measured potentials may not follow the Nernst equation.[207,210] The use of indicators is adviced. Fortunately, glass electrodes have wide applicability in solvents other that water, and the values obtained do have some meaning as an empirical measure of basicity-solvation effects.[206]

Sixteen pairs of analytes were chosen according to their relative values of GB[202,203] and pK_a[204,205] in order to carry out the title study. These pairs were: 1) ammonia/4-dimethylaminopyridine, 2) ammonia/diethanolamine, 3) ammonia/pyridine, 4) ammonia/4-hydroxypyridine, 5) aniline/diethanolamine, 6) 3-hydroxyaniline/diethanolamine, 7) aniline/4-hydroxypyridine, 8) ammonia/3-hydroxyaniline, 9) aniline/pyridine, 10) ammonia/aniline, 11) 3-hydroxyaniline/4-hydroxypyridine, 12) 4-hydroxypyridine/diethanolamine, 13) pyridine/diethanolamine, 14) hydrazine/aniline, 15) diethanolamine/triethanolamine, 16) ammonia/hydrazine. For each pair, 1 and 10 molepercent solutions in glycerol were prepared. For the pair ammonia-aniline, five additional solutions in the

concentration range from 1 to 10 molepercent (2, 3, 4, 6 and 8 molepercent) were also used. The FAB spectra were obtained following the general procedure outlined above.

Experiments for the Kinetic Modelling of the FAB Spectra

Thirteen solutions of diethanolamine in glycerol, covering the whole range of concentration from 0 to 100 molepercent, were used for this study (0, 0.5, 1, 2, 4, 6, 8, 10, 20, 40, 60, 80, 100 molepercent). The FAB spectra were recorded according to the general procedure. The kinetic calculations were performed on an IBM PC-XT and a Zenith-200 PC equipped with a numeric coprocessor, using the MathCad software package (version 1.01) by numerical integration of the rate equations.

Experiments for the Study of Temperature and Viscosity Effects

The standard FAB probe used in these experiments does not have a temperature control. Since temperature changes were required in the study of temperature effects, the probe tip was cooled by immersing it in dry-ice or liquid nitrogen, or heated with a heat gun, before applying the sample on it. The temperature was measured by using a Type-J thermocouple attached to an Omega HH-70KC digital thermometer. In all the experiments, the temperature measurements were done just before inserting the

sample probe to run the spectrum, and right after removing the probe from the ion source. The change was found to be no more than 2° C during that elapsed time. The samples used were glycerol, diethanolamine and 2 and 10 molepercent solutions of diethanolamine in glycerol, and the bulk sample temperature was varied from -30° C to +40° C.

It was necessary to make a correction by subtracting 1 molepercent from the nominal concentration of the diethanolamine solutions, since when these experiments were carried out, consistent lower ion intensities were obtained with respect to the signals observed before in the experiments for the kinetic modelling. This kind of variation is not unusual in FAB spectra, although a clear explanation for it cannot be presently provided.

In the case of the study of viscosity effects, sucrose was used to increase the viscosity of the samples. Those were: glycerol, diethanolamine and 2 and 10 molepercent solutions of diethanolamine in glycerol. Sucrose was added to the samples in a range from 5 to 80 weightpercent. The solutions were prepared by gently heating the mixtures, and leaving them standing overnight before running the FAB spectra.

CHAPTER 4

EXPERIMENTS FOR THE CALCULATION OF IONIZATION CROSS-SECTIONS IN GAS PHASE FAB

The ionization cross section σ can be measured on the basis of equation 4.1, and the schematic of the experimental arrangement is shown in Figure 4.1.

$$i_+ = \sigma_M \rho_M d q_e f_A \qquad (4.1)$$

A beam of atoms with a flux f_A fast atoms per second, enters the ionization box B, which contains a number density of ρ_M molecules per unit volume of the compound M, whose ionization cross section σ_M is to be determined. The length of the box is d, and the positive current to the negative (bottom) plate of the box, measured with a current meter, is equal to i_+. The elementary charge q_e is 1.6×10^{-19} C. Equation 4.1 holds under thin target conditions, i.e. when the average number of collisions per fast atom are much less that one.

For an accurate determination of σ, the box B would be placed inside a vacuum chamber, which contains a known pressure of the gas M, such that ρ_M could be evaluated from the ideal gas law as shown in equation 4.2.

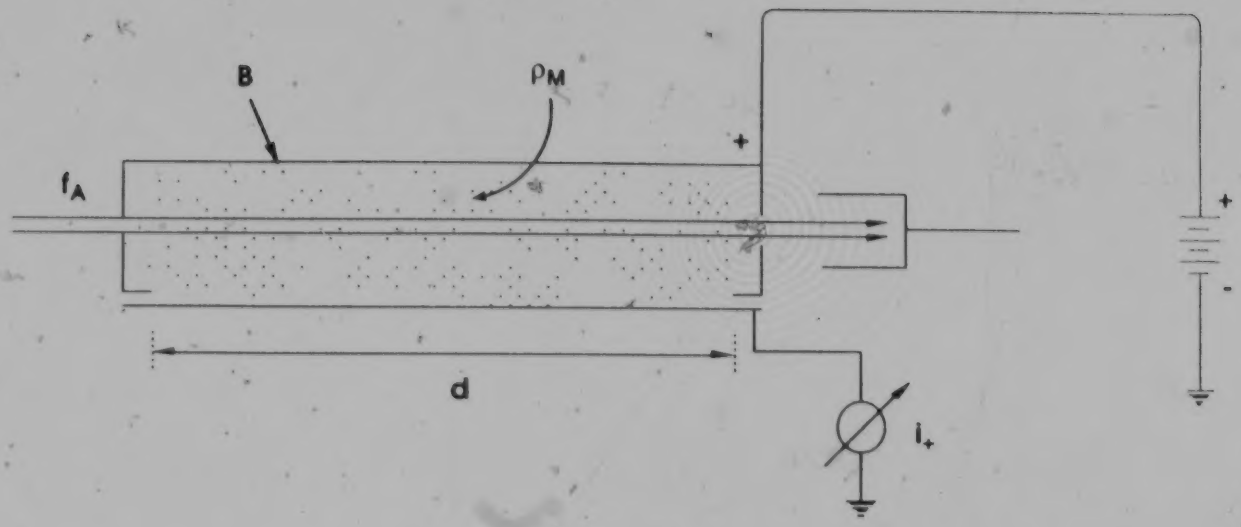

Figure 4.1. Typical Arrangement for Determination of Ionization Cross Sections under Thin Target Conditions

$$p_M = \frac{nN_A}{V} = \frac{PN_A}{RT} \qquad (4.2)$$

Furthermore, the neutral fast atom flux f_A entering the box must also be accurately known.

While an arrangement equivalent to the schematic shown in Figure 4.1 is not difficult to construct, the task is time consuming, and since cross sections of an accuracy within a factor of 2 or even only a factor of 4 would be sufficient for the present purposes, the measurements were executed directly on the ion source of the mass spectrometer used in the present work.

Fast atoms striking the metal surfaces produce secondary electrons which, if accelerated into the ion source, can cause electron impact ionization on collision with neutral molecules. Such ionization, if it occurs in the region between the beam centering plates, can lead to grossly erroneous measurements of the fast atom ionization. To avoid such an artefact, several precautions were taken. The arrangement is illustrated in Figure 4.2. The FAB gun provides the Xe atoms beam, which enters the space between the equipotential extraction plates, generally kept at +6 KV. The Xe beam is collimated by means of an aluminum nozzle, 1.8 cm long and 1.5 mm I.D., so that its width is smaller than the width of the space between the extraction plates. Any secondary electrons created in the channel of the collimator are prevented from being

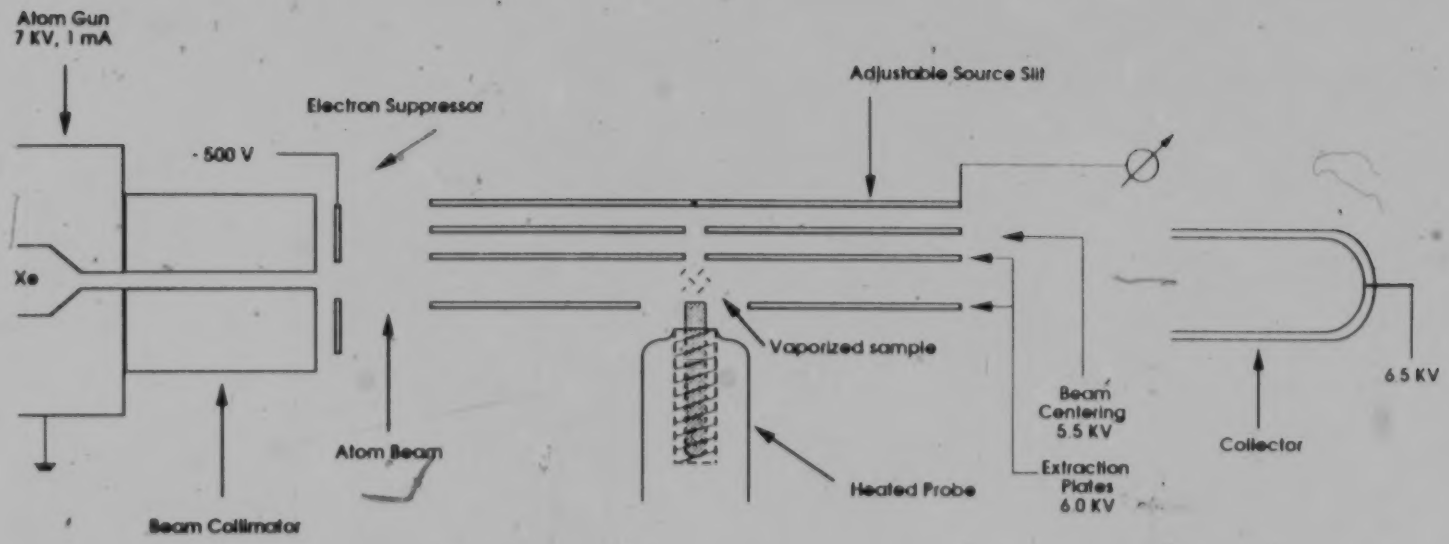

Figure 4.2. Diagram of Modified FAB Ion Source for Gas Phase Sample Analysis

accelerated to the ion source by an electron suppressor, consisting of a 1.6 cm diameter copper plate, with a 3 mm diameter hole at its center, attached to the exit of the nozzle by means of a teflon screw and a quartz insulator. The plate is held at -500 V. The beam exits the ion source and enters a beam collector, which consists of a pyrex tube 6 cm long and 1 cm I.D., sealed at one end, aluminized in the inside and kept at +6.5 KV. The fast atom beam collector is operated at +6.5 KV, a voltage more positive than that of the ion source (+6 KV). The negative potential of the ion source relative to the beam collector should prevent electrons escaping the beam collector from entering the ion source. Positive ions created in the ion source, due to collisions of the beam with neutral molecules M, are extracted by the penetration of the potential of the beam centering plates, +5.5 KV, which is negative relative to the ion source (+6 KV). The positive ions arriving at the closed off and grounded adjustable source slit produce the positive ion current i_+ which is measured with a Keithley 610B current meter.

Two parameters required for the determination of σ by using equation 4.1, had to be estimated. These are the effective length d of the path of the beam for which the ionization is measured with the current meter, and the pressure of the gas M in the ion source.

The width of the gap between the two beam centering plates of the ion source, through which the ions are extracted and acceler-

ated towards the ion collector (adjustable source slit), is 2 mm. Thus, the minimum effective length is d_{min} = 2 mm. However, the field penetration from the 5.5 KV beam centering plates into the ion source is probably appreciable and since only a few volts are sufficient to extract the ions from the ion source, the effective length d should be perceptibly larger. A value d = 10 mm was arbitrarily chosen. These value may be somewhat too large but, for the present purposes, errors on the conservative side, i.e. predictions of σ that are smaller than the true value, are to be preferred.

The pressure of the gas M in the ion source was estimated on the basis of pressure reading with an ionization gauge. As indicated in Figure 4.3, which gives a schematic of the vacuum system, the ion gauge is located downstream from the ion source. To correct for the pressure difference between the pressure in the ion source P_{is} and the pressure at the gauge P_{ig} the conductances F_1 and F_2 of the pumping elements between the ion source and the ion gauge are evaluated using standard vacuum technique equations.[211] The equivalent conductance of these two elements is (all values for air):

$$F_{eq} = 500 \text{ L/s} \qquad (4.3)$$

The conductance of the lead connecting the ion gauge volume to the diffusion pump and cooling baffle is:

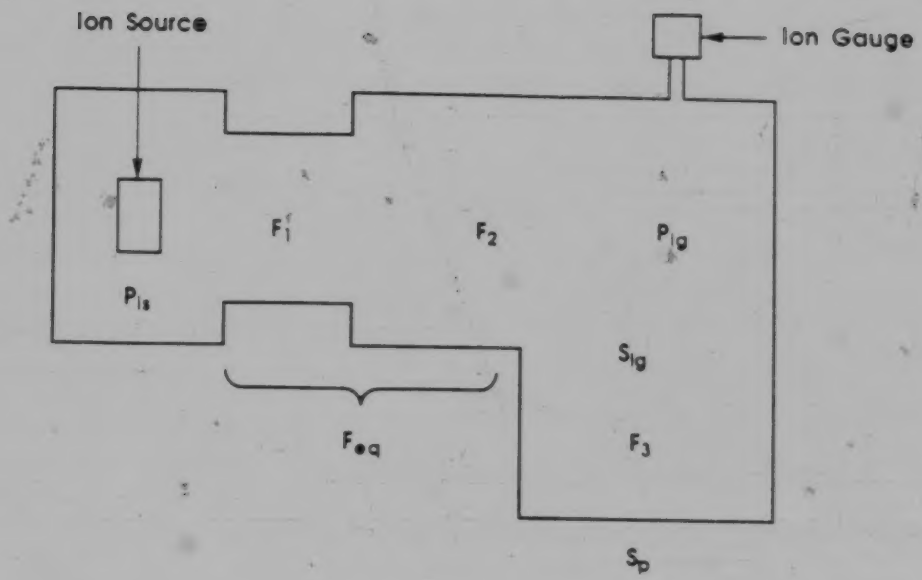

Figure 4.3. Diagram of the Mass Spectrometer Pumping System

$$F_3 = 700 \text{ L/s} \tag{4.4}$$

The combined pumping speed of the pump with baffle is:

$$S_p = 150 \text{ L/s} \tag{4.5}$$

The equivalent pumping speed at the ion gauge is thus:

$$S_g = \frac{F_3 S_p}{F_3 + S_p} = 123 \text{ L/s} \tag{4.6}$$

At the ion source:

$$S_{is} = \frac{F_{eq}\, S_{ig}}{F_{eq} + S_{ig}} = \frac{500 \times 123}{500 + 123} = 99 \text{ L/s} \qquad (4.7)$$

The pressure ratio P_{is} to P_{ig} can thus be evaluated from:

$$P_{is}\, S_{is} = P_{ig}\, S_{ig} \quad \text{or}$$

$$P_{is} = P_{ig} \frac{S_{ig}}{S_{is}} = P_{ig} \frac{123}{99} = 1.24\, P_{ig} \qquad (4.8)$$

The above correction was applied to the ion gauge readings.

The analytes used were glycerol, 3-nitrobenzyl alcohol and toluene. In addition to the ion gauge pressures and total ion current measurements, their gas phase FAB spectra were also recorded.

Since the ion gauge is calibrated to read for air, a correction based on the electron impact ionization cross sections for air and for the gas M was applied. The ionization cross sections were estimated with the procedure described by Stevenson,[212] based on the atomic ionization cross sections. For toluene this correction amounted to dividing the ion gauge pressure reading by a factor of 6, while for glycerol and 3-nitrobenzyl alcohol the factors were equal to 4 and 7 respectively.

Toluene was admitted into the ion source region *via* a probe equipped with a reservoir, suitable for volatile compounds. The tip of the probe terminated close to, but still outside, the ion source. For this type of gas introduction, the pressure inside the ionization region and in the neighboring volume around the ion source are expected to be equal and therefore the ion source pressure, evaluated with equation 4.8, should be accurate.

Glycerol and 3-nitrobenzyl alcohol have relatively low vapor pressures and were introduced into the ion source with the arrangement shown in Figure 4.2. A narrow glass tube sealed at one end contained the liquid. It was placed in a heated solid-liquid insertion probe and held in a position such that the opening of the glass tube was partly inside the ion source. Sufficient pressures to observe measurable total ion currents are obtained on heating the glass tube. With this method of gas supply, the effective pressure in the ionization region is somewhat higher than the pressure immediately outside the ion source. The conductance of the ion source was estimated from its dimensions:

$$F_{is} = 19 \text{ L/s} \qquad (4.9)$$

This value, combined with the pumping speed at the ion source (S_{is} = 99 L/s) leads to a pressure inside the ion source approximately five times higher than that immediately outside. However, this pressure correction is not very reliable and therefore actual

cross section values for glycerol and 3-nitrobenzyl alcohol vapors cannot be quoted.

The Xe atom flux produced by the gun had been measured previously[200] and corresponds to 4 x 10^{13} atoms/s. The output of the FAB gun[200] produces a beam that contains Xe atoms and Xe^+ ions, roughly in a 1:1 ratio. It is assumed that the large majority of the Xe^+ ions do not enter the ion source, since the it is at +5.5 KV potential relative to the gun cathode. The kinetic energy of the Xe^+ ions produced by the beam source is close to 7 KeV, i.e. corresponds almost to the full potential applied to the FAB gun.[200] Therefore, the Xe^+ beam ions have enough energy to enter the ion source. However, as it could be visually observed, the ion beam is deflected by the positive potential of the ion source plates and does not enter the ionization region.[213]

RESULTS AND DISCUSSION

CHAPTER 5

COMPETITION FOR PROTONS AND DOMINANCE OF GAS BASICITIES OVER SOLUTION BASICITIES IN FABMS

As already mentioned in the Introduction, the mechanism of ion formation in FAB and other related DI techniques has received considerable attention in the last few years and it is still a subject of controversy.

There is experimental evidence in support of the Precursor Model,[122,137] in which it is assumed that the observed spectrum is due to desorption of ionic species already existing in solution. It has been elsewhere proposed that reactions occurring at the region near the surface or selvedge might be responsible for the final spectrum produced,[150,151] and also that unimolecular reactions taking place in the vacuum play an important role in this matter.[65,214] In addition, there are results that indicate that gas phase ion-molecule reactions are important.[158,171,184,188] Among those, experiments carried out in our group show that the gas phase basicity (GB) of both analyte and matrix are crucial for the successful production of the FAB spectrum,[189] and that the increase of ion concentration in solution does not result in an increase of the total ion current (TIC) in the spectrum.[190] Rather, there is indication that the cationization of molecules may occur *via* ion-molecule reac-

tions. These results are interpreted in terms of a Gas Collision Model. This model assumes that the fast atom beam causes some ion formation as the collision cascade develops, and a cavity filled with hot gas-like molecules and ions is formed, as a result of the energy released from the bombarding particles to the target. More collisions occur prior to the entrance of the ions into the vacuum and some of these collisions result in proton transfer. In order to explain the preference of higher GB compounds, at least an average of 10-20 ion-molecule collisions are required. This fact is in accordance with the idea of a high temperature, high density gas formed at the impact site.[67,158] During this process, extensive ion-recombination occurs to form ion pairs, fragment ions and neutrals. In addition, proton transfer and cationization reactions also take place. The reactions that lead to the formation of protonated molecular ions MH^+ are:

1- bombarding atoms cause fragmentation of matrix molecules M to produce positive Pi^+ and negative Ni^+ ions:

$$\overrightarrow{Xe} + M \rightarrow \overrightarrow{Xe} + Pi^+ + Ni^- \qquad (5.1)$$

2- positive ions react with matrix molecules to produce matrix protonated molecular ions MH^+:

$$M + Pi^+ \rightleftharpoons MH^+ + (Pi^+ - H) \qquad (5.2)$$

3- analyte molecules A receive a proton from protonated matrix molecules or from positive ions to form analyte protonated molecular ions AH^+:

$$A + MH^+ \text{ (or } Pi^+) \rightleftharpoons AH^+ + M \text{ (or } (Pi^+ - H)) \qquad (5.3)$$

The observation that the GB of the analyte should be higher than that of the matrix, in order to produce significant intensity of analyte protonated molecular ions, is explained by the occurrence of the reaction 5.3, that is favoured by such a condition. Otherwise it would be an endothermic process and its rate constant would be low.

Since a compound with high GB generally has high solution basicity as well, it could be argued that the competition for protons expressed in the reaction 5.3 occurs in the liquid. In order to clarify the situation, the study of the competition for protons between pairs of analytes was carried out. In the chosen pairs, the crucial condition is that one of the compounds must be more basic in the gas phase, and the other one more basic in solution. Despite the correlation between GB and pK_a values, it is possible to find such pairs.

The use of a non-aqueous solvent, glycerol in this case, has the disadvantage that basicities in solution are not available in the lit-

erature, although they are expected to follow the same trend as that in water, with probably lower individual values.[206-208] To ensure that the relative pK_a values are close to those in water, pK_a determinations in glycerol were carried out, as described in the Experimental Section, for the compounds used as analytes. The values obtained are summarized in Figure 5.1, together with the values of GB[202,203] and pK_a in water.[204,205] The observed basicity order is the same in both liquids, except for two of the compounds, diethanolamine and 4-dimethylaminopyridine, which exchange positions. Diethanolamine is the strongest base in glycerol, while 4-dimethylaminopyridine is the strongest base in water. From the plot of the solution basicities in both water and glycerol vs. GB it is easily seen that for most of the chosen pairs, one compound is more basic in solution and the other more basic in the gas phase.

Another problem related to this study is that the GB values are generally known only for small, relatively volatile molecules. Evaporation from the FAB probe under the vacuum conditions inside the ion source occurs for most of such compounds. In order to avoid this inconvenience, the compounds were used as the respective hydrochloride salts in most cases. Both free bases and salts produce practically the same FAB spectra, therefore no significant differences are introduced.

In this study, the FAB spectra of 1 molepercent and 10 molepercent solutions of each analyte (A1 and A2) in the matrix (M) glycerol

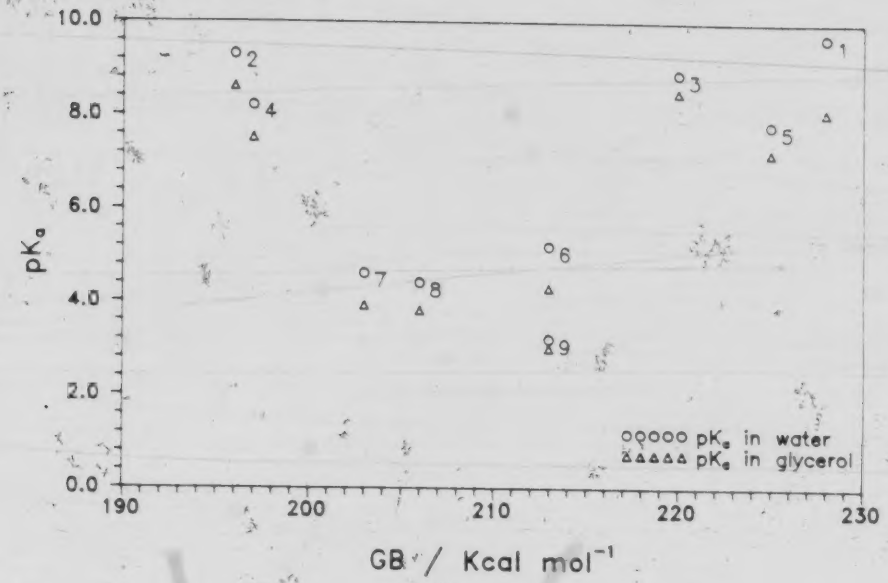

	Analyte	GB (Kcal mol^{-1})	pK_a (Aq. soln.)	pK_a (Gly. soln.)
1	4-dimethylaminopyridine	228	9.7	8.1
2	ammonia	196	9.3	8.6
3	diethanolamine	220	8.9	8.5
4	hydrazine	197	8.2	7.5
5	triethanolamine	225	7.8	7.2
6	pyridine	213	5.2	4.3
7	aniline	203	4.6	3.9
8	3-hydroxyaniline	206	4.4	3.8
9	4-hydroxypyridine	213	3.2	3.0

Figure 5.1. Solution Basicities in Water and Glycerol vs. Gas Basicity for the Compounds Used as Analytes

were taken, as well as the spectra of glycerol solutions of both analytes together at a concentration of 1 and 10 molepercent each. In each pair, A2 is the analyte with higher GB in all cases, and A1 the one with higher pK_a in ten of the sixteen pairs. Figure 5.2 shows an example of the kind of result observed, in this case for pair 10 (A1= ammonia, A2= aniline). It can be seen that when both analytes are present together at a concentration of 1 molepercent (Figure 5.2c), their respective peaks have intensities which are very close to those observed in the spectra of the individual compounds at the same concentration (Figure 5.2a,b). Therefore, the presence of one of them does not significantly influence the spectrum of the other. It can be said that their contributions to the FAB spectrum are additive. In contrast to this situation, when 10 molepercent solutions are used, the presence of A2 in the solution results in a suppression of the peaks of A1 in the FAB spectrum (Figure 5.2f), when compared to the intensities observed for the 10 molepercent solution of A1 by itself (Figure 5.2d).

The total intensities of the ammonia and aniline major peaks, with and without the presence of the other analyte, are shown in Figure 5.3 for the concentration range from 1 to 10 molepercent. The ammonia peaks (5.3a) are always less intense than the aniline peaks (5.3b) at the same concentration, and when those curves (5.3a,b) are compared with the ones that represent the intensities of the ammonia and aniline peaks in the presence of each other

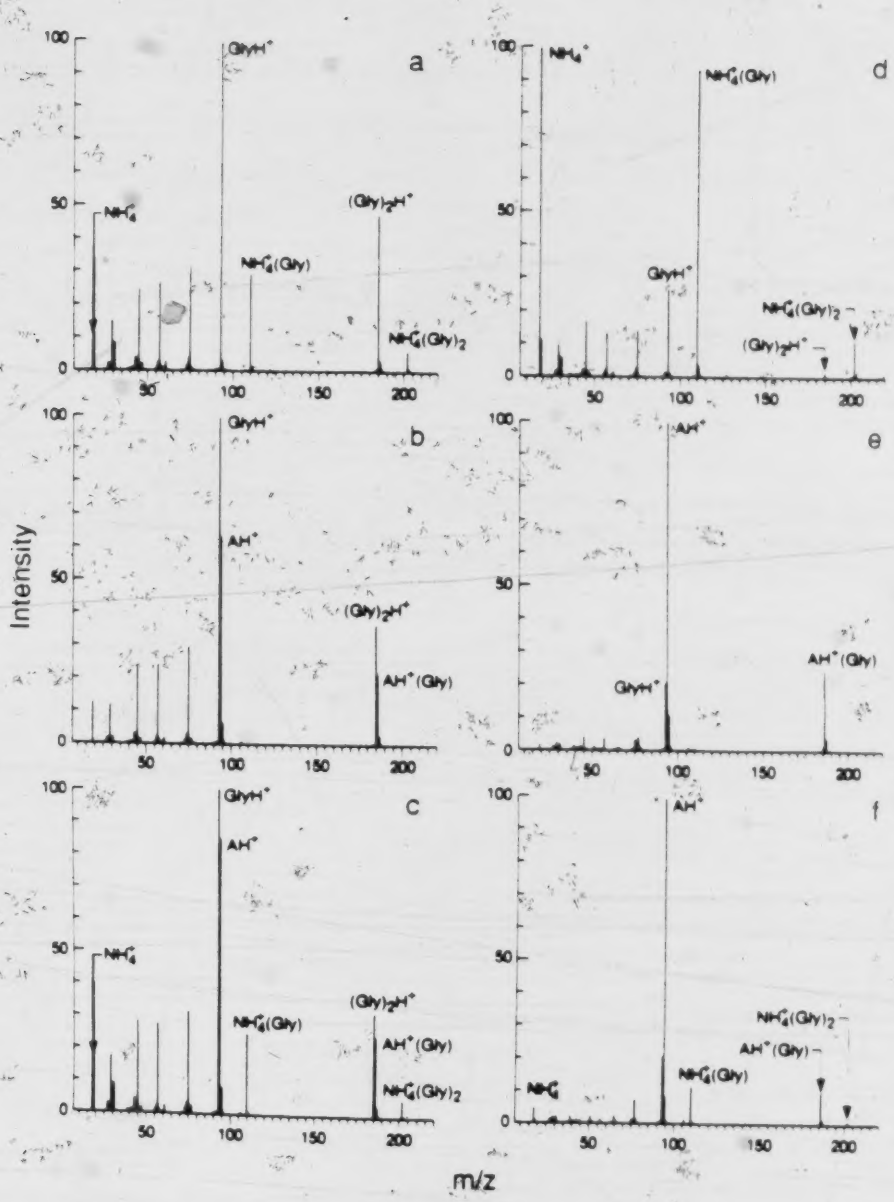

Figure 5.2. FAB Spectra of the Pair Ammonia/Aniline in Glycerol Solutions. a- 1 Molepercent Ammonium Chloride, b-1 Molepercent Anilinium Chloride, c- 1 Molepercent Each, d- 10 Molepercent Ammonium Chloride, e- 10 Molepercent Anilinium Chloride, f- 10 Molepercent Each

(5.3c,d), the increasing suppression of ammonia by aniline is clearly observed.

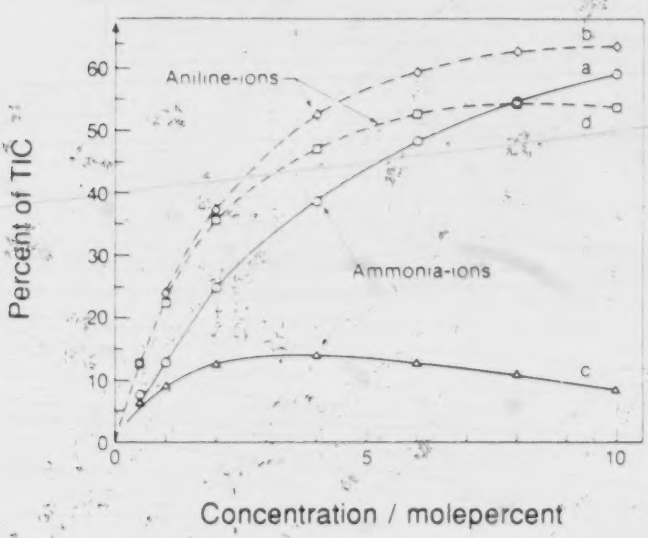

Figure 5.3. Total Intensity of Major Ammonia and Aniline Ions vs. Analyte Concentration, from FAB Spectra of Ammonia/Aniline in Glycerol Solutions. a- Ammonia Ions from Ammonium Chloride Solutions, b- Aniline Ions from Anilinium Chloride Solutions, c- Ammonia Ions and d- Aniline Ions from Equimolar Solutions of Ammonium Chloride and Anilinium Chloride

In order to quantify this effect, Suppression Factors SF_{A1} and SF_{A2} are defined for the 10 molepercent concentration , as a measure of the suppression of the peaks of one analyte by the presence of the other, according to the expressions:

$$SF_{A1} = \frac{I_{A1,A2}}{I_{A1}} \qquad (5.4)$$

$$SF_{A2} = \frac{I_{A2,A1}}{I_{A2}} \qquad (5.5)$$

where I_{A1} and I_{A2} are the intensities in percent TIC for the analyte peaks from FAB spectra of 10 molepercent glycerol solutions of A1 or A2 separately, and $I_{A1,A2}$ and $I_{A2,A1}$ are the intensities of the same peaks from the FAB spectrum of glycerol solution of both analytes, together, at 10 molepercent each.

The Intensity Ratio $R_{A2/A1}$ is defined as:

$$R_{A2/A1} = \frac{SF_{A2}}{SF_{A1}} = \frac{I_{A2,A1}}{I_{A1,A2}} \frac{I_{A1}}{I_{A2}} \qquad (5.6)$$

From this definition, the value of $R_{A2/A1}$ would be equal to 1 if the analytes do not compete, since the peak intensities for each of them would be the same regardless the presence of the other compound in the solution. If there is competition, R must be greater than 1 if A1 is suppressed by A2, or less than 1 if A2 is suppressed by A1. Figure 5.4 summarizes the results for the sixteen pairs used in these experiments. It can be seen that, with only one exception for the pair aniline/pyridine (probably due to higher surface concentration of aniline), all the values of $R_{A2/A1}$ are greater than 1, which clearly indicates that A2, the analyte with higher GB,

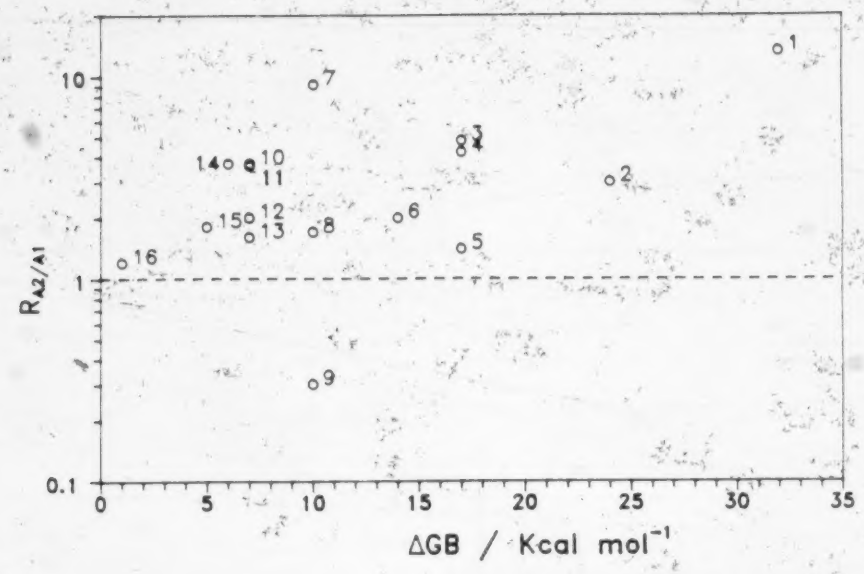

Pair	A1	A2	ΔGB (Kcal mol^{-1})	ΔpK_a (Aq. soln.)	ΔpK_a (Gly soln.)	$R_{A2/A1}$
1	ammonia	4-dimethylaminopyridine	32	+0.4	-0.5	13.3
2	ammonia	diethanolamine	24	-0.4	-0.1	3.0
3	ammonia	pyridine	17	-4.1	-4.3	4.8
4	ammonia	4-hydroxypyridine	17	-6.1	-5.1	4.2
5	aniline	diethanolamine	17	+4.3	+4.6	1.4
6	3-hydroxyaniline	diethanolamine	14	+4.5	+4.7	2.0
7	aniline	4-hydroxypyridine	10	-1.4	-0.4	9.1
8	ammonia	3-hydroxyaniline	10	-4.9	-4.8	1.7
9	aniline	pyridine	10	+0.6	+0.4	0.3
10	ammonia	aniline	7	-4.7	-4.6	3.7
11	3-hydroxyaniline	4-hydroxypyridine	7	-1.2	-0.3	3.6
12	4-hydroxypyridine	diethanolamine	7	+5.7	+5.5	2.0
13	pyridine	diethanolamine	7	+3.7	+4.2	1.6
14	hydrazine	aniline	6	-3.6	-3.6	3.7
15	diethanolamine	triethanolamine	5	-1.1	-0.7	1.8
16	ammonia	hydrazine	1	-1.1	-1.1	1.2

Figure 5.4. Intensity Ratios $R_{A2/A1}$ vs. ΔGB

dominates over A1, the analyte with higher pK_a, in the competition for protons. It is observed in the plot of $R_{A2/A1}$ vs. ΔGB that $R_{A2/A1}$ tends to increase when increasing ΔGB, although the data are very scattered.

For the sake of comparison, the Intensity Ratio $R'_{A2'/A1'}$ is defined in a similar way for the same set of data, but in this case, A2' is the analyte with higher pK_a for all the pairs used.

$$R'_{A2'/A1'} = \frac{SF_{A2'}}{SF_{A1'}} = \frac{I_{A2'A1'} \; I_{A1'}}{I_{A1'A2'} \; I_{A2'}} \qquad (5.7)$$

Figure 5.5 summarizes the values obtained. It is seen in the plot of $R'_{A2'/A1'}$ vs. ΔpK_a, that for most of the pairs $R'_{A2'/A1'}$ is less than 1 and no clear correlation is observed between the competition for protons and the solution basicities.

The following set of reactions describes the suggested process leading to the formation of protonated analyte ions, cluster ions and fragment ions, according to the Gas Collision Model:[190]

$$MH^+ + A1 \rightleftharpoons M + A1H^+ \qquad (5.8)$$

$$A1H^+ \rightarrow \text{cluster ions, fragment ions} \qquad (5.9)$$

$$MH^+ + A2 \rightleftharpoons M + A2H^+ \qquad (5.10)$$

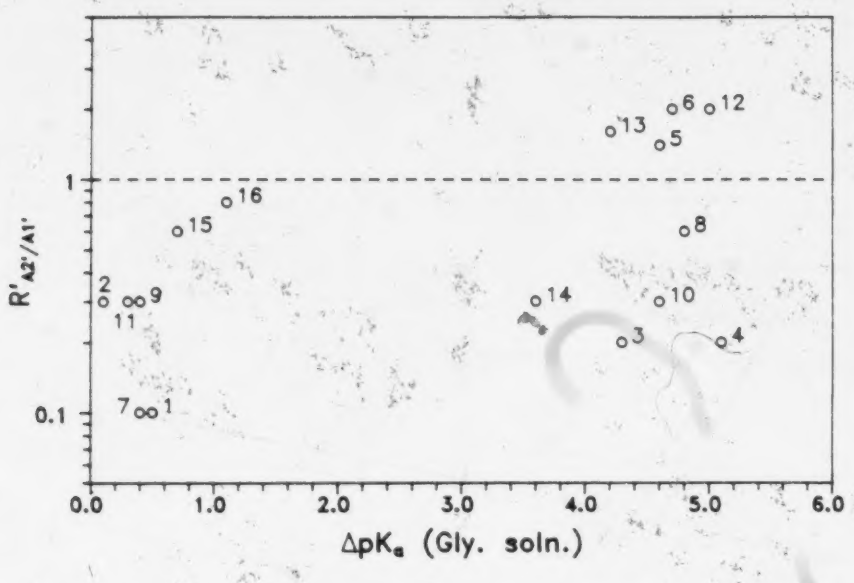

Pair	A1'	A2'	ΔpK_a (Aq. soln.)	ΔpK_a (Gly. soln.)	$R'_{A2'/A1'}$
1	4-dimethylaminopyridine	ammonia	-0.4	+0.5	0.1
2	diethanolamine	ammonia	+0.4	+0.1	0.3
3	pyridine	ammonia	+4.1	+4.3	0.2
4	4-hydroxypyridine	ammonia	+6.1	+5.1	0.2
5	aniline	diethanolamine	+4.3	+4.6	1.4
6	3-hydroxyaniline	diethanolamine	+4.5	+4.7	2.0
7	4-hydroxypyridine	aniline	+1.4	+0.4	0.1
8	3-hydroxyaniline	ammonia	+4.9	+4.8	0.6
9	aniline	pyridine	+0.6	+0.4	0.3
10	aniline	ammonia	+4.7	+4.6	0.3
11	4-hydroxypyridine	3-hydroxyaniline	+1.2	+0.3	0.3
12	4-hydroxypyridine	diethanolamine	+5.7	+5.0	2.0
13	pyridine	diethanolamine	+3.7	+4.2	1.6
14	aniline	hydrazine	+3.6	+3.6	0.3
15	triethanolamine	diethanolamine	+1.1	+0.7	0.6
16	hydrazine	ammonia	+1.1	+1.1	0.8

Figure 5.5. Intensity Ratios $R'_{A2'/A1'}$ vs. ΔpK_a

$$A2H^+ \rightarrow \text{cluster ions, fragment ions} \qquad (5.11)$$

$$A1H^+ + A2 \rightleftharpoons A2H^+ + A1 \qquad (5.12)$$

Equation 5.12 represents the competition for protons between the two analytes, that efficiently takes place, as indicated by the results observed. For this reaction to occur, A2 should be present as a neutral in the gas phase. Prior to bombardment, the analytes may be protonated in the glycerol solution, but they must be effectively deprotonated *via* recombination reactions occurring in the hot cavity generated at the bombardment site:

$$AH^+_{soln} + Ni^-_{soln} \rightleftharpoons (AH^+Ni^-) \rightarrow A_{gas} + NiH_{gas} \qquad (5.13)$$

Because of the ion-pair formation and subsequent dissociation, it should not make any difference whether the free bases or the salts are used to make the solutions to run the FAB spectra. In effect, as it has been mentioned before, no significant difference is observed in the FAB spectra of the free bases or the respective hydrochlorides. However, even taking that precaution, attention has to be paid to both volatility and solution basicity. For example, when ammonium chloride and diethanolamine were present together as analytes, no ammonia peaks were observed. This could be happening due to the close values of solution basicities of the two compounds, which allows proton transfer reactions to

take place in solution, followed by loss of ammonia by evaporation.

The most likely explanation for the scatter observed in Figure 5.4, is that the concentration of some analytes at the surface may not be the same as that at the bulk of the solution. It is known that surface activity influences the appearance of FAB spectra, and surfactants have been used to enhance the sensitivity of this technique.[215] The compounds used here are small molecules with far less surface activity than actual surfactants, and it does not seem to be information about surface enrichment for any of them. But even so, it may be still meaningful to speculate that FAB spectra are determined by gas phase reactions, especially by proton transfer, which is governed by GB values, and that there is no better correlation in these results because the concentration of the analytes at the bombardment site may not be the same as that at the bulk of the solution, due to surface enrichment in some cases. Obviously, it would be very valuable to be able to determine surface concentrations by an independent method.

The solution basicities used for this discussion are room temperature values. It could be argued that higher temperature values should be more appropriate, since the temperatures of the sample solutions must be higher under bombardment conditions, and the relative basicities in water, and probably also in glycerol, are

temperature dependent. However, the important point in this study is that, even if the competition for protons takes place in what could be called a metastable liquid, the energetics of the proton transfer reactions is more characteristic of the gas phase. The basicity reversals from gas to solution are due to solvation effects. It has been shown that solvent effects are present even with the attachment of a relatively small number of solvent molecules to the solute.[216,217] Therefore, since GB dominance is observed in the FAB spectra, the degree of solvation of the molecules in the hot cavity has to be very low.

The present experimental findings, together with previous results in our group,[188-190] show that the presence of preformed ions in the matrix solution is not a direct cause for the signals observed in the spectrum.[137] These results also appear incompatible with the idea that FAB mass spectral data reflect acidic or basic properties in solution and that pK_a's can be estimated from this kind of experimental information.[74] On the contrary, gas phase properties seem to be more important in the context of the present discussion, and some aspects of the Gas Collision Model are similar to Rabalais' Selvedge Theory[150,151] and to Michl's Gas Flow Model.[158,161]

CHAPTER 6

KINETIC MODELLING OF THE FAB SPECTRA

Many spectral features of FAB can be explained on the basis of gas phase ionic processes and their energetics. The idea that the intermediate state, in which the observed spectrum originates, may be best described as a gas goes back to the late 70's, when the ionization mechanism of SIMS was a topic of wide discussion.[150,153] More recently, Cooks[58] also describes the selvedge as a gas and considers the reactions occurring in that region as an important source of the detected ions, in addition to the direct desorption of ions already existing in solution.

The importance of proton transfer reactions and relative GB values for the formation of the protonated molecular ions was demonstrated by showing that it is the GB rather than the pK_a that determines the direction of the proton transfer. This fact, together with the previous results obtained in our group, which showed that the TIC of the spectrum does not increase with the electrolyte concentration in the sample solution[188,190], led to the Gas Collision Model. In this model the central idea is that extensive ion-molecule chemistry occurs during the FAB desorption process in a region that is best described as a high density gas. This gas is generated by a rapid irreversible expansion of the liquid sample solution near the track of

the impinging atom. The exploding gas contains ions formed out of neutral molecules during the collision cascade, in addition to ions already existing in solution prior to bombardment. Fast and extensive positive-negative ion recombination reactions result in neutral molecules, ion pairs and fragment ions. As the gas escapes into the vacuum, the ions undergo collisions with neutral molecules and ion-molecule reactions take place. Very significant are the proton transfer reactions that lead to the formation of the protonated molecular ions.

In order to establish a kinetic scheme for the reaction mechanism in FAB on the basis of the Gas Collision Model, a study of the FAB spectra of diethanolamine (DEA) in glycerol (GL) was carried out. Diethanolamine was chosen as the analyte (A), due to its high GB relative to that of the matrix glycerol (M) and because both compounds are completely miscible. In this set of experiments, the concentrations of the solutions were varied from the neat matrix to the neat analyte. Examples of the spectra obtained are shown in Figure 6.1 for neat glycerol, 2 and 10 molepercent solutions of diethanolamine in glycerol and neat diethanolamine.

Figure 6.2 shows the intensities of the protonated molecular ions and cluster ions in the FAB spectra of diethanolamine-glycerol solutions as a function of the diethanolamine concentration. In the concentration range below 10 molepercent, the effect of dietha-

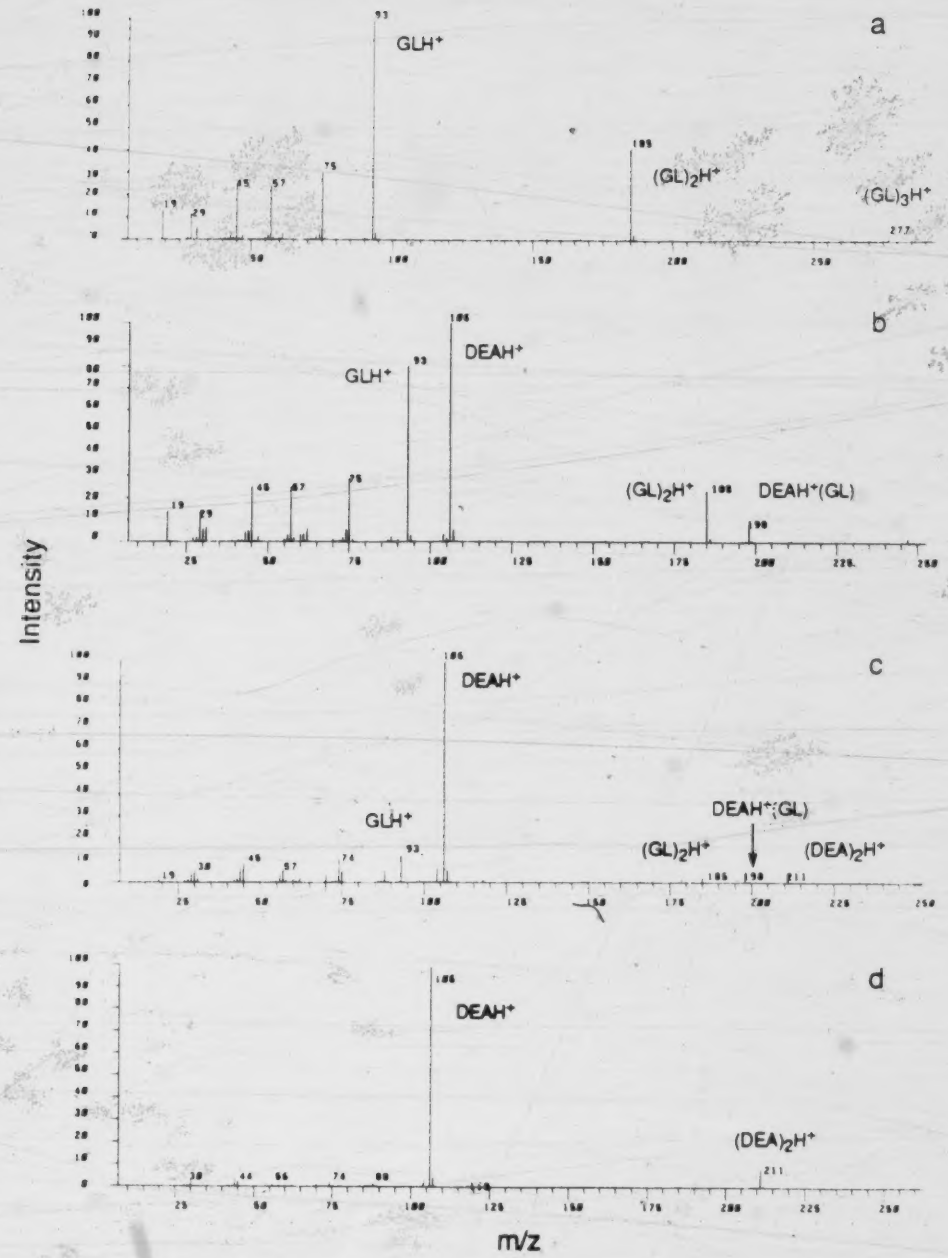

Figure 6.1. FAB Spectra of Diethanolamine-Glycerol Solutions. a- Neat Glycerol, b- 2 Molepercent Diethanolamine, c- 10 Molepercent Diethanolamine, d- Neat Diethanolamine

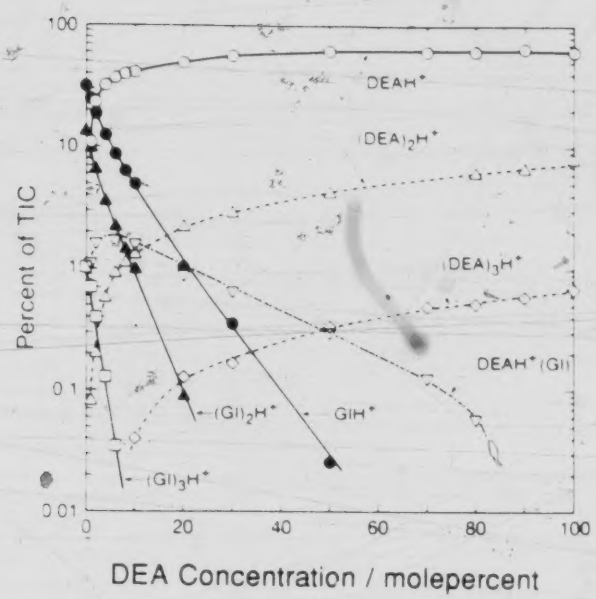

Figure 6.2. Intensity of Protonated Molecular Ions and Cluster Ions of Glycerol and Diethanolamine vs Diethanolamine Concentration, from FAB Spectra of Diethanolamine-Glycerol Solutions

nolamine over glycerol is typical of a high GB compound. The diethanolamine peaks $DEAH^+$ and $(DEA)_nH^+$ increase rapidly as the diethanolamine concentration increases, while the glycerol peaks markedly decrease. It can be seen that the concentration dependence is quite regular. Above 10 molepercent the diethanolamine ion intensities become less dependent on the concentration, as the intensities of the glycerol peaks continue to decrease exponentially at approximately the same rate. It is also observed that the intensity of the glycerol dimer $(GL)_2H^+$ decreases more rapidly than that of the protonated molecular ion

GLH^+. The decrease is even faster for the trimer $(GL)_3H^+$. In addition, the FAB spectra also show fragment ions for both analyte and matrix. Figure 6.3 shows the intensity changes of the protonated molecular ions and of some of the main fragments from diethanolamine and glycerol, as the analyte concentration is increased. The diethanolamine fragment intensities initially increase and for high concentrations, above 20 molepercent, a slight decrease is observed. The glycerol fragment ion intensities decrease nearly exponentially, but less rapidly than the GLH^+ intensity. Thus, as the analyte concentration is increased, the glycerol fragment intensities increase with respect to GLH^+, while the analyte fragment ion intensities decrease relative to $DEAH^+$. This is summarized in Figure 6.4, where the Fragment Ratios, Dimer Ratios and Mixed Cluster Ratio defined below, are plotted vs. DEA concentration.

$$\text{Fragment Ratio} = \frac{\sum \text{major fragment ion intensities}}{\text{protonated molecular ion intensity}} \qquad (6.1)$$

$$\text{Dimer Ratio} = \frac{\text{dimer ion intensity}}{\text{protonated molecular ion intensity}} \qquad (6.2)$$

$$\text{Mixed Cluster Ratio} = \frac{\text{mixed cluster ion intensity}}{\text{protonated molecular ion intensity}} \qquad (6.3)$$

The regularities observed in the experimental data provide clues to the possible reaction sequence and mechanism. Most of these

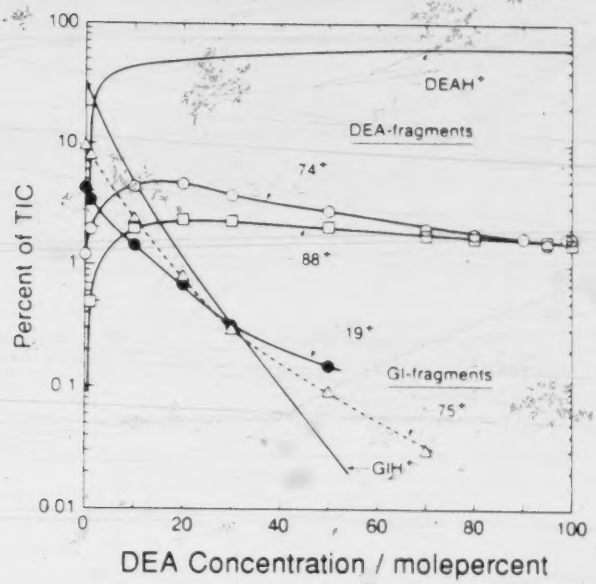

Figure 6.3. **Intensity of Protonated Molecular Ions and Some of the Main Fragment Ions of Glycerol and Diethanolamine vs. Diethanolamine Concentration, from FAB Spectra of Diethanolamine-Glycerol Solutions**

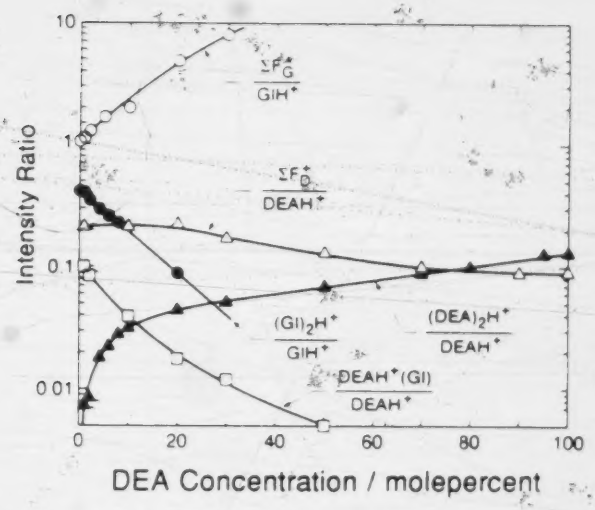

Figure 6.4. **Fragment Ratios, Dimer Ratios and Mixed Cluster Ratio of Glycerol and Diethanolamine vs. Diethanolamine Concentration, from FAB Spectra of Diethanolamine-Glycerol Solutions**

observations can be reproduced using a kinetic scheme based in the Gas Collision Model. When modelling the ion-molecule reactions occurring during the desorption process in FAB, the initial situation at the bombardment site can be visualized as a hot track generated by the collision cascade. As a consequence, a hot gaseous core develops very rapidly as neutral molecules undergo a transition from the liquid to a metastable gas.[218,219] The existence of metastable phases is due to the difficulty to attain the initial stage of the transition. If initiating influences (heterogeneous nucleation) are not present in the system, the nuclei of the new phase arise spontaneously (homogeneous nucleation) due to thermal fluctuations and intermolecular interactions.[219] The temperature increases rapidly and the nuclei are formed at a high rate, in a process that is termed explosive boiling[219] or phase explosion. A microscopic cavity or bubble containing the excited gas is formed. A number of ions M^+ is present there, either because they were already in the liquid solution or else because they were formed during the collision cascade. At a time equal to zero these ions react with neutral molecules A with a rate constant k:

$$M^+ + A \xrightarrow{k} A^+ + M \qquad (6.4)$$

The rate equation is:

$$\frac{-[d\,M^+]}{d\,t} = k\,[M^+]\,[A] \qquad (6.5)$$

Since $[A]_0 >> [M^+]_0$, the reaction is considered to be pseudo-first order and the integration at constant [A] gives $[M^+]$ as a function of time:

$$[M^+] = [M^+]_0 \, e^{-k\,t\,[A]} \qquad (6.6)$$

Assuming that all the ions in the bubble have a single residence time t, and that the observed ion intensities I_{M^+} are proportional to the ion concentrations $[M^+]$, the following expression is obtained:

$$I_{M^+} = I_{M^+_0} \, e^{-k\,t\,[A]} \qquad (6.7)$$

As mentioned before, in the present experiments M^+ is identified with the matrix M (glycerol, GL) ions and A with the analyte A (diethanolamine, DEA) molecules. The decay of the glycerol-derived ions is due to the general reaction:

$$GLH^+ + DEA \xrightarrow{k} DEAH^+ + GL \qquad (6.8)$$

The experimental decay of the total glycerol ion intensity with increasing diethanolamine concentration is shown in the semilogarithmic plot in Figure 6.5. It clearly deviates from a straight line, which indicates that the assumption of a single residence time for all the ions is not justified. Therefore, a residence time distribution has to be considered:

$$\int_0^\infty f(t)\ dt = 1 \qquad (6.9)$$

The new expression for the ion current I_{M^+} is:

$$I_{M^+} = \int_0^\infty \left\{ f(t)\, I_{M^0}\, e^{k^+[A]} \right\} dt \qquad (6.10)$$

Since the physical nature of the sample at the bombardment site is described as a high density gas inside the bubble, with molecu-

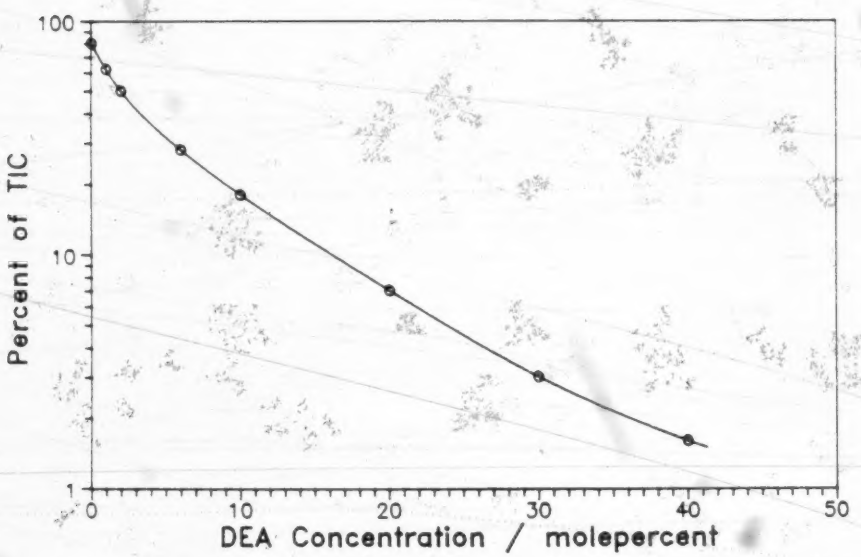

Figure 6.5. Total Intensity of Glycerol-Derived Ions vs. Diethanolamine Concentration, from FAB Spectra of Diethanolamine-Glycerol Solutions

lar densities close to that of a liquid, the total rate constant k for the reaction between glycerol ions and diethanolamine molecules was set to a typical diffusion-limited rate constant, with an approximate magnitude of 10^{10} M^{-1} s^{-1}. This rate constant is expected to be dependent on both density and temperature, but this had to be ignored in the present calculations and the value was used in expression 6.10 as a constant. Actually, the gas expands and both [A] and t depend on that process. This can be illustrated with an exponential gas expansion, described by:

$$\frac{-d[A]}{dt} = a\,[A] \qquad (6.11)$$

Integration of the expression gives:

$$[A] = [A]_0\, e^{-at} \qquad (6.12)$$

where $[A]_0$ refers to the concentration of A in the liquid. Substituting this expression into equation 6.6 and solving:

$$[M^+] = [M^+]_0\, e^{-\frac{k[A]_0}{a}(e^{-at}+1)} \qquad (6.13)$$

In the limit of large t the expression simplifies to:

$$[M^+] = [M^+]_0\, e^{-\frac{k[A]_0}{a}} \qquad (6.14)$$

Comparison of 6.14 with 6.6 gives t= 1/a.

In the present calculations, it is assumed that the effective residence time is mainly the time that the ions spend in the high density gas bubble. If this is correct, most of the ion-molecule reactions that produce the observed spectrum, take place during that time, when the density of such a gas is still close to that of the liquid.

In order to calculate I_{M^+} from expression 6.10, the I_{M^0} value was taken as the observed intensity of the total glycerol ions for neat glycerol, and [A] as the diethanolamine concentration, based on an assumed gas density equal to 0.1-0.3 of the density of the liquid at room temperature. Different functional forms of f(t) and values for the integration limits were introduced in expression 6.10, in order to examine which functional form best reproduced the experimental intensities I_{M^+} of the total glycerol ion intensity in Figure 6.5. By a computer aided trial and error procedure, the following inverse function of t was found to give the best fit:

$$f(t) = \frac{1}{a\,t + b} \qquad (6.15)$$

where $a = 1.818 \times 10^9\ s^{-1}$ and $b = 0.01818$.

The time scale results from the magnitude of the initially chosen rate constant k. This function is shown in Figure 6.6. The cut-off times, t_{min} =

0.035 ns and t_{max} = 0.70 ns, come from the integration limits that led to the best fit of the data.

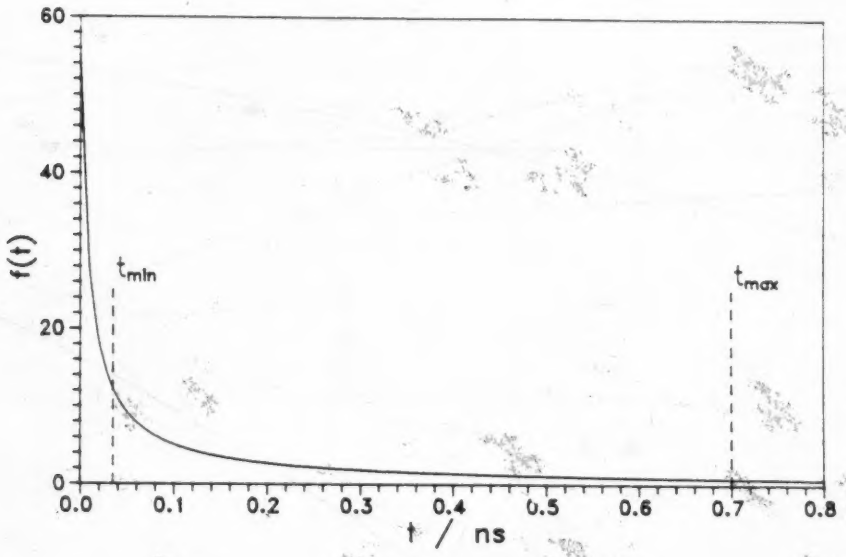

Figure 6.6. Distribution Function f(t) of Ion Residence Times in FAB of Diethanolamine-Glycerol Solutions. $f(t) = 1/at+b$, $a = 1.818 \times 10^9\ s^{-1}$, $b = 0.01818$

The distribution function f(t), as defined in expression 6.15, was used for the kinetic model calculation of the glycerol peaks in the diethanolamine-glycerol solutions, according to the following set of reactions, which are assumed to take place after the initial formation of the glycerol fragment ions F^+_{GL} during the collision cascade:

$$F^+_{GL} + GL \xrightarrow{k_1 = 0.42 \times 10^9\ M^{-1}\ s^{-1}} GLH^+ + \text{neutrals} \qquad (6.16)$$

$$GLH^+ + GL \xrightarrow{k_2 = 0.175\times10^9\ M^{-1}s^{-1}} (GL)_2H^+ \qquad (6.17)$$

$$(GL)_2H^+ + GL \xrightarrow{k_3 = 0.035\times10^9\ M^{-1}s^{-1}} (GL)_3H^+ \qquad (6.18)$$

The values of the rate constants were fitted with the condition that they should lead to the product distribution observed in the FAB spectrum of neat glycerol, shown in Figures 6.2 and 6.3, and their order of magnitude came from the diffusion-limited total rate constant k chosen initially. The experimental decays were well reproduced by using these rate constants and the function f(t). The results are shown in Figure 6.7. It can be seen that there is good agreement between the experimental points and the calculated curves.

The exact functional form of f(t), as defined in expression 6.15 and shown in Figure 6.6, cannot be deduced from an simple fitting procedure like this, but still the fit to the experimental points is very good and the shape of the distribution function f(t) does not depend on any fitted parameters.

The expression for f(t) has the same form as the integrated rate law of a second order reaction. This is very suggestive, since f(t) could be determined by ion-ion recombinations, which are second order reactions that rapidly reduce the initial ion concentration,[190] rather than by the time dependence of the desorption process. If

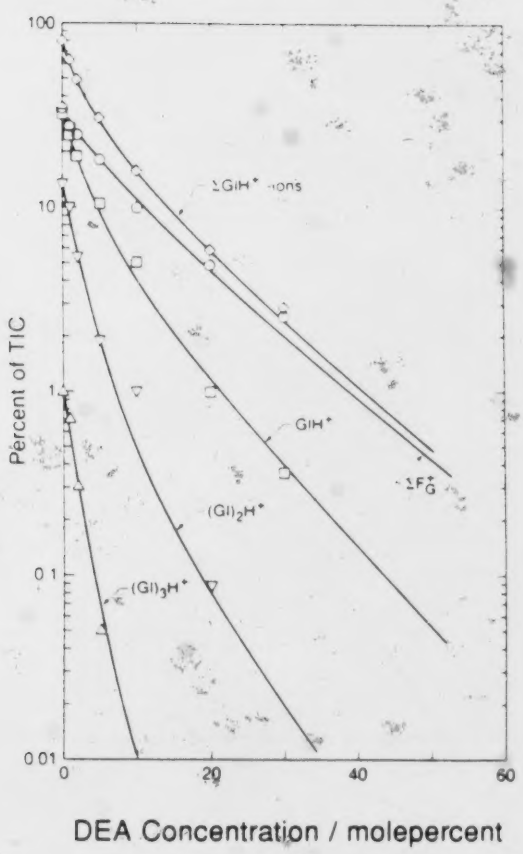

Figure 6.7. **Result of Kinetic Model Calculation of Intensity of Glycerol-Derived Ions on FAB Spectra of Diethanolamine-Glycerol Solutions. Calculated Intensities Are Shown as Solid Lines and Experimental Intensities as Data Points**

this were correct, it would mean that the residence time distribution for the neutrals decreases more slowly with time than that for the ions and this assumption would justify the use of a constant [A] in the integration of equation 6.5.

The cut-off time t_{min} may be interpreted as the time required for the expansion process to occur and for the ion molecule reactions to begin. During that time, recombination reactions reduce the initial concentration of the ions, whether formed already in the liquid or during the collision cascade. As for t_{max}, it is interpreted as the time after which the ion emission stops completely.

In the presence of diethanolamine, all the glycerol ions protonate diethanolamine molecules:

$$\{F^+_{GL}, GLH^+, (GL)_nH^+\} + DEA \xrightarrow{k_4 = 8.7\times10^9\ M^{-1}s^{-1}} DEAH^+ + \text{neutrals} \quad (6.19)$$

Glycerol ions are also expected to produce diethanolamine fragment ions F^+_{DEA}:

$$\{F^+_{GL}, GLH^+, (GL)_nH^+\} + DEA \xrightarrow{k_5 = 1.3\times10^9\ M^{-1}s^{-1}} F^+_{DEA} + \text{neutrals} \quad (6.20)$$

Diethanolamine fragment ions, produced by the collision cascade as well, protonate diethanolamine molecules:

$$F^{+}_{DEA} + DEA \xrightarrow{k_6 = 1.95\times10^{9}\ M^{-1}s^{-1}} DEAH^{+} + \text{neutrals} \qquad (6.21)$$

Once formed, diethanolamine protonated molecular ions undergo clustering, to form dimer ions $(DEA)_2H^+$, trimer ions $(DEA)_3H^+$ and mixed clusters:

$$DEAH^{+} + DEA \xrightarrow{k_7 = 0.054\times10^{9}\ M^{-1}s^{-1}} (DEA)_2H^{+} \qquad (6.22)$$

$$(DEA)_2H^{+} + DEA \xrightarrow{k_8 = 0.039\times10^{9}\ M^{-1}s^{-1}} (DEA)_3H^{+} \qquad (6.23)$$

$$DEAH^{+} + GL \xrightarrow{k_9 = 0.025\times10^{9}\ M^{-1}s^{-1}} DEAH^{+}.GL \qquad (6.24)$$

$$DEAH^{+}.GL + GL \xrightarrow{k_{10} = 0.020\times10^{9}\ M^{-1}s^{-1}} DEAH^{+}.(GL)_2 \qquad (6.25)$$

Ligand exchange reactions also take place:

$$DEAH^{+}(GL)_n + DEA \xrightarrow{k_{11} = 3.0\times10^{9}\ M^{-1}s^{-1}} (DEA)_2H^{+}(GL)_{n-1} + GL \qquad (6.26)$$

The rate constants given above were chosen to reproduce the experimental product distribution observed in the FAB spectrum of neat diethanolamine, shown in Figures 6.2 and 6.3, and used with f(t) for the kinetic model calculation of the diethanolamine peaks in the FAB spectra of diethanolamine-glycerol solutions. The mixed cluster formation was also modelled, with rate constants adjusted to reproduce the observed decays of the intensities with increas-

ing diethanolamine concentration. Figure 6.8 shows the calculated curves, which are in good agreement with the experimental data.

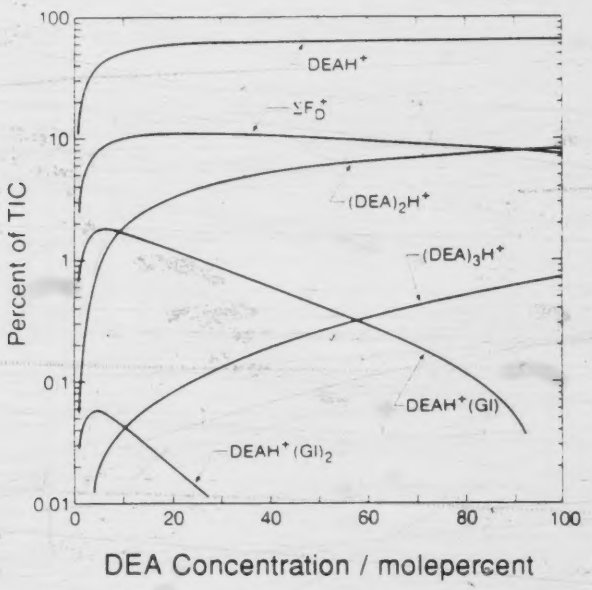

Figure 6.8. Calculated Intensities of Diethanolamine-Derived Ions from Kinetic Model Calculation on FAB Spectra of Diethanolamine-Glycerol Solutions

The proposed kinetic scheme predicts a time dependent glycerol ion distribution for the FAB spectrum of neat glycerol, as shown in Figure 6.9 Short residence times correspond to low mass ions (fragments), due to few reactive ion-molecule interactions, and long residence times correspond to high mass ions (protonated

molecular ions and clusters) that result from extensive ion-molecule chemistry.

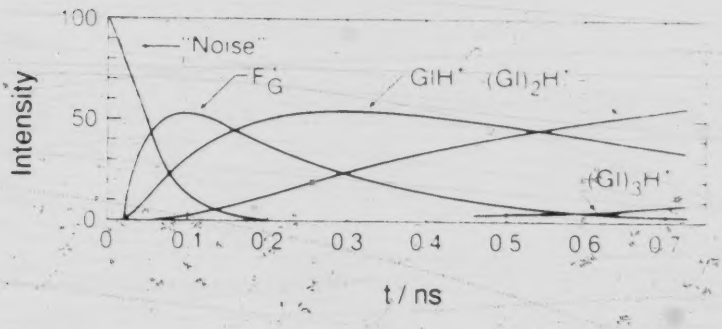

Figure 6.9. Predicted Time Dependence of FAB Spectrum of Neat Glycerol

The model considered so far could be called "clustering model", since in it the sequence of reactions goes from fragments, to protonated molecular ions, to dimers, to trimers and so on, for both matrix and analyte. This sequence is based on ion clustering events, actually observed in true gas phase ion-molecule reactions.[220] This progression from fragments to high clusters explains the main features of the FAB spectra of diethanolamine-glycerol solutions.

However, the same experimental features could be explained by a very different picture, that could be called "declustering model".

In it, instead of assuming a gas phase like clustering sequence, it is considered that cluster ions $(GL)_nH^+$ (n>>1), with a range of excitation energies, are initially produced, in the very first stages of the rapid liquid to gas phase transition. The cluster ions with higher internal energies, $(GL)_nH^{+\cdots}$, quickly decompose to fragments, while those with lower energies, $(GL)_nH^{+\cdot\cdot}$ and $(GL)_nH^{+\cdot}$, only decluster. The extent of declustering is assumed to be proportional to the internal energy:

$$(GL)_nH^{+\cdots} \longrightarrow F_{GL}^+ + (n-1)\,GL + \text{neutrals} \qquad (6.27)$$

$$(GL)_nH^{+\cdot\cdot} \longrightarrow GLH^+ + (n-1)\,GL \qquad (6.28)$$

$$(GL)_nH^{+\cdot} \longrightarrow (GL)_mH^+ + (n-m)\,GL \qquad (6.29)$$

In addition, glycerol clusters protonate diethanolamine molecules and form mixed clusters:

$$(GL)_nH^+ + DEA \longrightarrow DEAH^+(GL)_m + (n-m)\,GL \qquad (6.30)$$

The mixed clusters, depending on their excitation energies, dissociate to produce fragments, protonated molecular ions and lower clusters:

$$DEAH^+(GL)_m^{\cdots} \longrightarrow F_{DEA}^+ + m\,GL \qquad (6.31)$$

$$DEAH^+(GL)_m^{**} \longrightarrow DEAH^+ + m\,GL \qquad (6.32)$$

$$DEAH^+(GL)_m^{*} \longrightarrow DEAH^+(GL)_p + (m-p)\,GL \qquad (6.33)$$

Additional ligand exchange reactions, followed by declustering, result in the formation of diethanolamine cluster ions:

$$DEAH^+(GL)_m + DEA \longrightarrow (DEA)_2H^+(GL)_{m-1} + GL \qquad (6.34)$$

$$(DEA)_2H^+(GL)_{m-1} \longrightarrow (DEA)_2H^+ + (m-1)\,GL \qquad (6.35)$$

The observed fragment ions come from unimolecular dissociation of excited protonated molecular ions and clusters. As the gas bubble gradually cools down during the expansion, an apparent progression from fragments to clusters is observed.

The clustering and declustering models have in common that short residence times correspond to low mass ions, due to few reactive ion-molecule interactions, and that long residence times correspond to high mass ions, due to extensive ion-molecule chemistry.

The experimental results summarized in Figure 6.3 show that the fragmentation of diethanolamine decreases with increasing diethanolamine concentration. This is reproduced in the clustering model, as shown in Figure 6.8. This is explained as a consequence

of the assumed lack of reactivity of the fragments of diethanolamine towards glycerol. Therefore, at low diethanolamine concentration, the diethanolamine fragments have more chance of entering the vacuum, while at higher concentrations most of them react with diethanolamine molecules.

The declustering model does not seem to provide an obvious explanation for the experimental observations in Figure 6.3. However, a reasonable interpretation can be found if the origin and relative stability of the protonated molecular ions is considered. Assuming that the bond $DEAH^+$-DEA is stronger than the bond $DEAH^+$-GL,[221,222] diethanolamine protonated molecular ions formed by unimolecular declustering of diethanolamine cluster ions, should have lower energy (and thus show lower fragmentation) than diethanolamine molecular ions formed by declustering of mixed cluster ions, since the dissociation energy is taken from the internal energy of the clusters. This would lead to less fragmentation as the mixed cluster population decreases with increasing diethanolamine concentration.

A significant amount of low intensity ions or "chemical noise" is typically observed in FAB spectra. As mentioned in the Introduction, several explanations have been suggested for the origin of such ions.[70,137,176] In the present work, the observed dependence of some noise ions parallels that of the major fragments as the com-

position of the sample solution is changed. For example, Figure 6.10 shows the intensity changes of several noise ions as a function of the diethanolamine concentration. It is seen that the ion at m/z 39 behaves like a glycerol fragment, while the intensity of the ion at m/z 86 varies as that of the diethanolamine ions. Fragments at m/z 162 and m/z 85 behave like the mixed cluster ions and the intensity

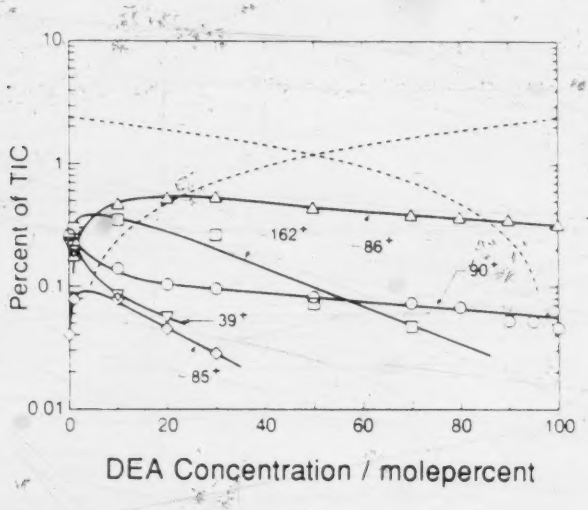

Figure 6.10. Intensity of Representative Noise Ions vs. Diethanolamine Concentration, from FAB Spectra of Diethanolamine-Glycerol Solutions. Dashed Lines Show the Linear Dependence of Intensities on the Concentration

of the ion at m/z 90 changes as that of a glycerol ion at low concentration, but more like that of a diethanolamine ion at high concentration. This kind of result indicates that background ions probably have a "kinetic history" similar to that of the major ions in the

spectrum, rather than being formed at hot spots or at the surface, by direct impact in the collision cascade and subsequent ejection to the vacuum[137], without further interaction. If this were the case, the intensity of the noise ions would be proportional to the composition of the sample solution, but that is not observed. The dashed curves in Figure 6.10 show the kind of intensity changes that would be expected if the composition of the liquid sample solution were followed in a direct desorption mechanism. Comparison with the experimental data in solid curves clearly shows that the observed changes of the noise ion intensities are quite different.

It was shown above that FAB spectra can be consistently modelled on the basis of gas phase reaction mechanisms, and that the intensity of the observed ions does not directly correlate with the concentration of the liquid sample solution.

CHAPTER 7

EFFECT OF THE TEMPERATURE AND VISCOSITY OF THE SAMPLE SOLUTION ON THE FAB SPECTRA

The work presented so far about the study of the ionization mechanism in FAB is based on systematic changes in the sample composition. By using glycerol as the matrix and analytes with different basicities, it was shown that it is the GB values rather than the pK_a values that determine the direction of the proton transfer reactions responsible for the formation of the protonated molecular ions during the FAB desorption process. In addition, a kinetic model based on high pressure ion-molecule reactions reproduced successfully the intensity changes observed in the FAB spectra of solutions of diethanolamine in glycerol, over the whole concentration range. The intensities of the major peaks for both matrix and analyte were calculated as a function of the analyte concentration. This analysis also yielded a tentative residence or reaction time distribution for the ions in the high pressure gas cavity generated by the atom impact. The functional form of f(t) that produced the best fit for the experimental data, showed an inversely proportional dependence on time. This was interpreted to be due to attenuation of the initial ion concentration by positive-negative ion recombination. The proposed kinetic scheme resulted in the prediction of a time dependent spectrum, with fragment ions domi-

nating at short times, right after the atom impact, and pseudo-molecular ions and clusters dominating at long times.

In the study of the DI mechanism, in addition to the sample solution composition, other properties must be important and could be experimentally varied to get more insights into the actual phenomena governing the production of the FAB spectrum. For example, Field[223,224] has reported strong temperature dependence of the FAB/SIMS spectra of neat methanol,[223] ethylene glycol and glycerol.[224] In all the cases, a deterioration of the spectrum is observed, from a series of cluster ions to a series of low intensity peaks or chemical noise, as the temperature is decreased.

In the continuation of the present work, variation of the temperature of the sample solution is a clear next choice, not only because it is relatively easy to work with it, but also and most important, because the temperature is a logical parameter that may be expected to influence the formation of the bubble containing the high density gas.

When the temperature of a liquid is increased up to its boiling point, gas nuclei are generally formed at active solid sites acting as heterogeneous nucleation centers. In the absence of such active solid sites, heterogeneous nucleation is eliminated and the formation of the gas is delayed. Rapid heating of the liquid brings the

temperature beyond the boiling point and violent vaporization occurs as a result of homogeneous nucleation at sufficiently high temperatures.[218,219] The temperature of maximum superheat, at which very rapid homogeneous nucleation takes place, appears to be well defined and it is found to be 0.9 times the critical temperature of the liquid.[219,225] Such values have been tabulated for a number of organic liquids at low pressure.[225]

As mentioned before, it is proposed in this work that a liquid to gas transition occurs in FAB, and that a high density gas is the reaction medium for the reactions that play an important part in the generation of the FAB spectrum. The formation of the bubble of excited gas may be viewed as the result of a very rapid homogeneous evaporation of the metastable liquid in the impact region.[218-219] The number of glycerol molecules that are desorbed from the liquid per incident Xe atom is estimated at about one thousand.[174] The kinetic energy of the Xe atom is enough to theoretically desorbe about ten thousand glycerol molecules, so that the volume that is excited by the collision cascade is relatively large and contains much more than one thousand molecules. Extensive collisions occur and the internal energies of ions and molecules have an effect on the extent of the reactions that produce the final species. Ions that spend short times in the gas cavity are highly excited and fragment extensively before they are detected. On the other hand, ions that spend long times in the bub-

ble are vibrationally cool and are detected mainly as protonated molecular ions and clusters. Therefore, the term temperature may be used as a convenient way to refer to the average excitation energy of the ions and molecules.

In the present set of experiments, the samples used were neat glycerol, neat diethanolamine, 2 and 10 molepercent solutions of diethanolamine in glycerol and 10 molepercent solution of pyridinium chloride in glycerol. The bulk sample temperatures T_b were varied from −30° C to +40° C.

Figure 7.1 shows an example of the kind of variation observed, in this case for neat glycerol at −30° C, 0° C and +30° C. The deterioration of the spectra with decreasing temperature is clearly observed. The ion intensities from the spectra of neat glycerol are shown in Figure 7.2 as a function of the sample temperature. There is a significant increase of the protonated molecular ion GLH^+ and dimer ion $(GL)_2H^+$ intensities with increasing T_b, while the sum of the major glycerol fragment ion intensities F^+_{GL} stays approximately constant and the total intensity of the noise ions strongly decreases. Figure 7.3 shows the temperature dependence of the glycerol cluster ions $(GL)_nH^+$. The intensities of these clusters increase with increasing T_b.

In the case of neat diethanolamine, the same kind of changes are observed, as shown in Figure 7.4, for the protonated molecular

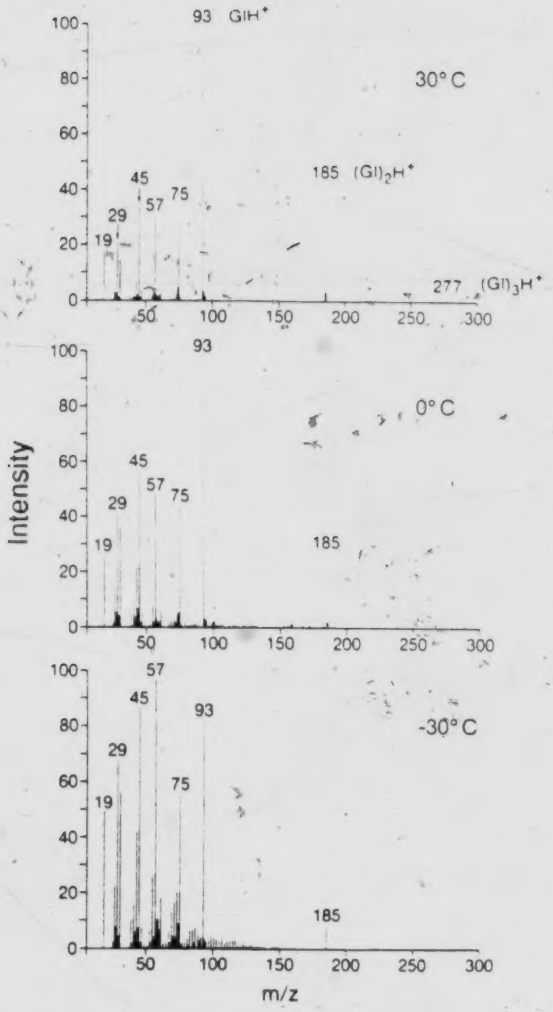

Figure 7.1. FAB Spectra of Neat Glycerol at Different Temperatures

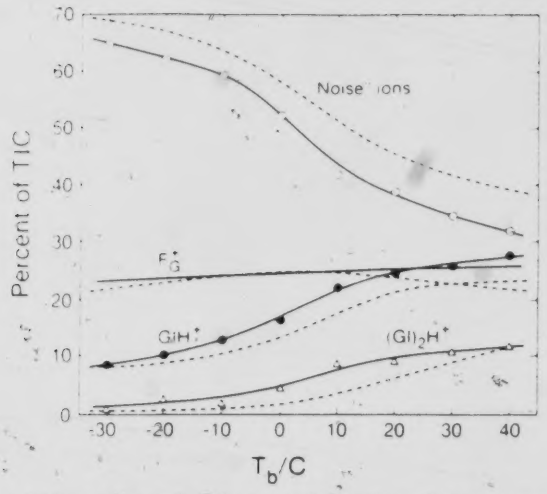

Figure 7.2. **Intensity of Glycerol-Derived Ions vs. Temperature of the Sample Solution T_b, from FAB Spectra of Neat Glycerol. Dashed Lines Show Calculated Results**

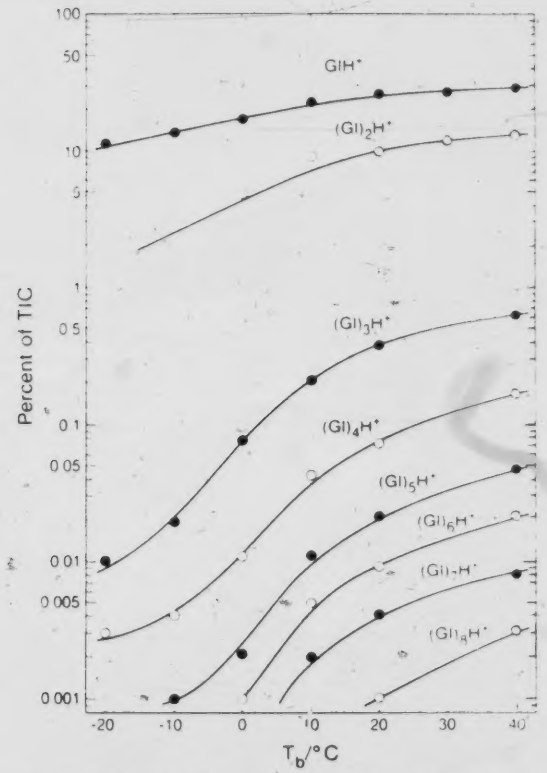

Figure 7.3. **Intensity of Glycerol Cluster Ions vs. Temperature of the Sample Solution T_b, from FAB Spectra of Neat Glycerol**

ion $DEAH^+$, the dimer ion $(DEA)_2H^+$, the major fragments F^+_{DEA} and the noise ions.

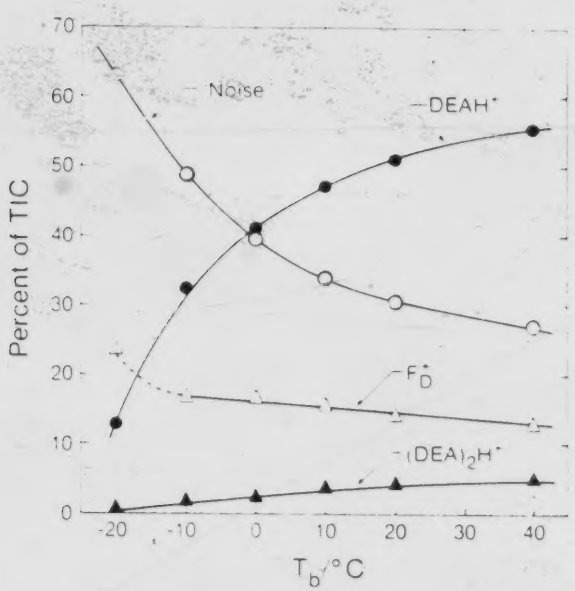

Figure 7.4. Intensity of Diethanolamine-Derived Ions vs. Temperature of the Sample Solution T_b, from FAB Spectra of Neat Diethanolamine

Figures 7.5 and 7.6 show the temperature dependence of the major ions detected in the FAB spectra of 2 and 10 molepercent solutions of diethanolamine in glycerol. Again, the same general behavior as in the neat liquids is observed for each kind of ion. In both cases, the intensities of the diethanolamine-derived ions are larger than expected in term of the concentrations involved. This is due to the higher GB value of diethanolamine relative to that of

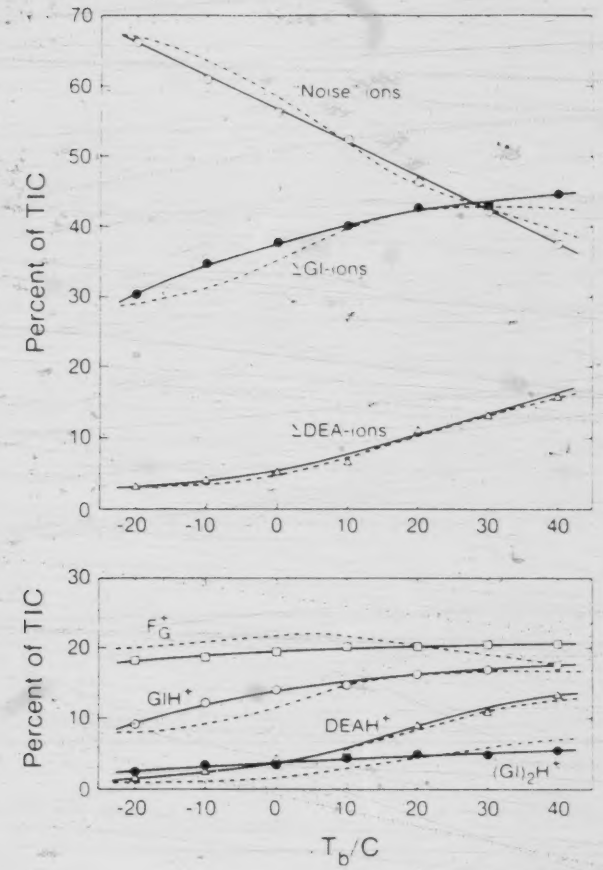

Figure 7.5. Intensity of Major Ions vs. Temperature of the Sample Solution T_b, from FAB Spectra of 2 Mole-percent Solution of Diethanolamine in Glycerol. Dashed Lines Show Calculated Results

glycerol. The dominance of high GB compounds was discussed previously in this work. In the present set of spectra, it is additionally observed that the diethanolamine ion intensities increase faster than the glycerol ion intensities with increasing temperature. The intensity changes of the major peaks in the FAB spectra of 10

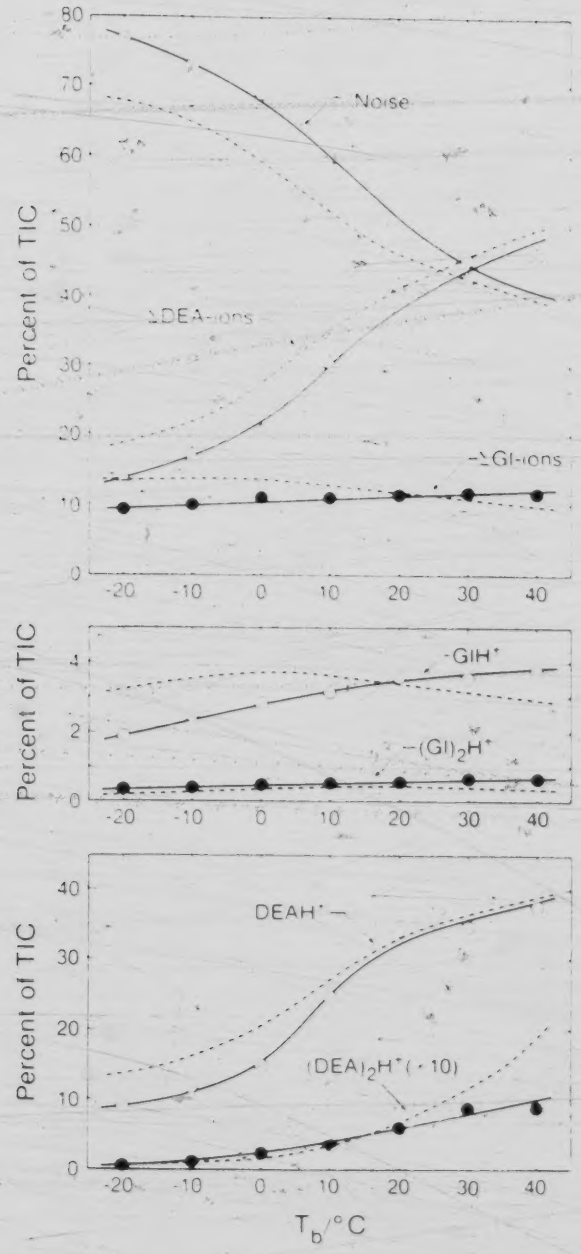

Figure 7.6. **Intensity of Major Ions vs. Temperature of the Sample Solution T_b, from FAB Spectra of 10 Mole-percent Solution of Diethanolamine in Glycerol. Dashed Lines Show Calculated Results**

molepercent solution of pyridinium chloride, shown in Figure 7.7, follow the same trend, i.e. the intensity of pyridine protonated molecular ions increases faster with the temperature than the intensities of the glycerol-derived ions.

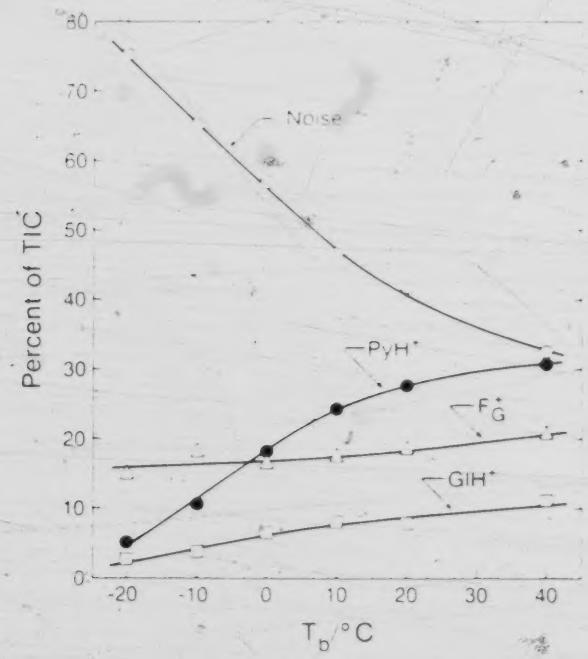

Figure 7.7. Intensity of Major Ions vs. Temperature of the Sample Solution T_b, from FAB Spectra of 10 Molepercent Solution of Pyridinium Chloride in Glycerol

These results lead to the conclusion that the dominance of the higher GB compound is favoured at higher temperatures. The preference for the high GB analyte were explained earlier as the result of proton transfer reactions taking place in the high density

gas. The increase of the analyte peak intensities with increasing T_b indicates an increase in the extent of such reactions. In addition, the decrease of both fragment and noise ion intensities, together with the increase of cluster ion intensities, suggest that the average excitation energy of the desorbed species decreases with increasing T_b.

In general, the observed order in which the intensities change with increasing temperature is: noise ions > fragment ions > molecular ions > clusters, with the noise ions having the strongest decrease and the cluster ions the strongest increase with increasing T_b. The same order was previously observed for the glycerol ions with increasing diethanolamine concentration. Since the kinetic model was successful in that case, it could be expected that the similar changes now obtained could also be explained as the result of a kinetic scheme.

The same kinetic scheme used earlier to model the FAB spectra of diethanolamine-glycerol solutions, was applied to the present set of experimental results. As mentioned before, the ion intensities change with T_b at a constant concentration, indicating a decreasing extent of the reactions in the gas-like medium as the temperature decreases. Therefore, the additional assumption was made that the maximum cut-off time t_{max} is a function of T_b.

There is not *a priori* way to calculate the changes in t_{max} as a function of T_b. However, a connection can be established by comparing the experimental ratios of diethanolamine-derived ions to glycerol-derived ions ΣDEA ions/ ΣGL ions, for the 2 molepercent solution (in which there is no strong dominance of the analyte) at different T_b, with the same ratios calculated from the kinetic model for different t_{max}. Figure 7.8 shows the connection between both sets of data and from there the dependence of t_{max} on T_b shown in Figure 7.9 is determined. From there, t_{max} is observed to decrease with decreasing T_b, as expected from inspection of the experimental data in Figures 7.2 to 7.7.

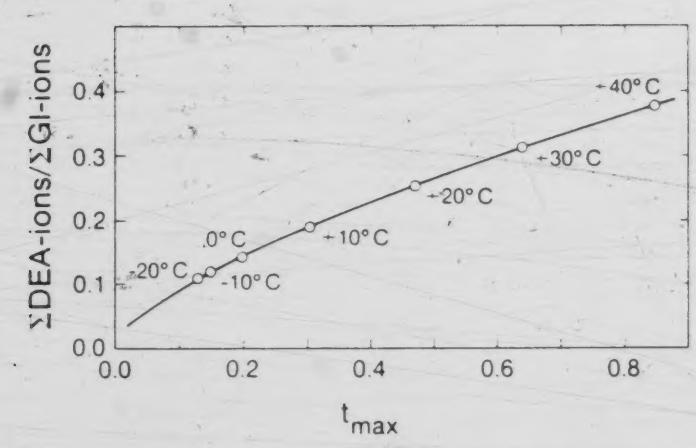

Figure 7.8. Calculated Intensity Ratio ΣDEA-Ions/ΣGL-Ions vs. t_{max} for 2 Molepercent Solution of Diethanolamine in Glycerol. Experimental Values of T_b for each Intensity Ratio Are Shown as Data Points

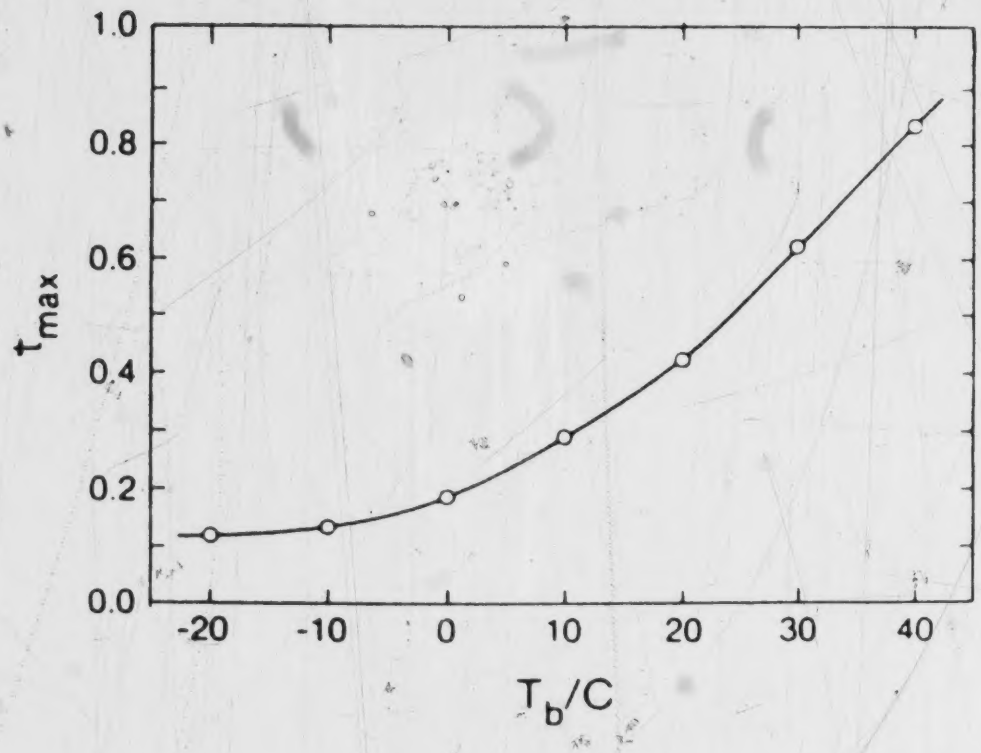

Figure 7.9. Dependence of t_{max} on T_b

Once the dependence of t_{max} on T_b was obtained, the kinetic calculations were carried out as before for neat glycerol and for both 2 and 10 molepercent diethanolamine solutions in glycerol. The same rate constants and distribution function f(t) as in Chapter 6 were used. The results are shown as dashed lines in Figures 7.2, 7.5 and 7.6 respectively. The agreement between calculated and experimental values is fairly good.

The results discussed above show that the bulk solution temperature has a strong effect on the nature of the FAB spectrum. This change cannot be interpreted as the result of changes in the average internal energy of the reacting species in the excited volume. A temperature change between -30° C and +40° C represents only a change of approximately 0.002 eV $Å^{-3}$. This magnitude is not significant compared to the estimated values of the energy density, in the range 0.01 to 0.16 eV $Å^{-3}$, deposited by the collision cascade at the bombardment site.[147] A more likely explanation could be that, rather than the energy deposition *per se*, the distribution of such energy and the response of the system to it are influenced by the solution temperature.

It was proposed before that homogeneous gas nucleation and a very rapid expansion take place as a consequence of the sudden energy deposition in the collision cascade. The process can be more easily visualized by means of a liquid-gas phase dia-

gram for a single component system. The thermodynamic PVT surface derived from the van der Waals equation of state is shown in Figure 7.10. In it, the critical point CP, at which the phase equilibrium is interrupted and the liquid and gas become identical, is a common vertex to two lines: binodal and spinodal.[218,219] The binodal is the boundary of absolute stability of the system.[218] It is defined by the equality of the chemical potential in the two phases, and joins the two experimentally possible volumes on each isotherm at a given pressure. The spinodal is the phase significant instability boundary[218] and connects the minimum (metastable liquid) and maximum (metastable gas) extrapolated pressures on each isotherm.

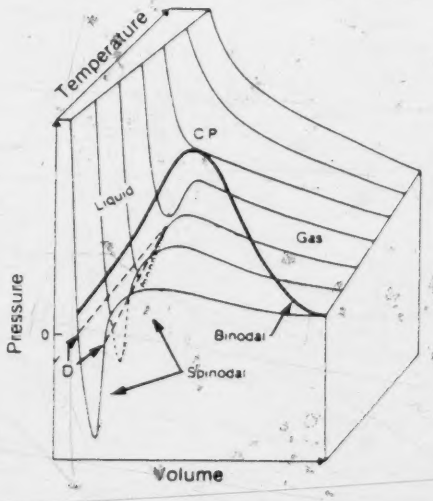

Figure 7.10. Thermodynamic PVT Surface for a Single Component System. Line D Indicates the States at Zero Pressure

In addition to the regions where the homogeneous system is stable, either as a liquid or as a gas, the binodal and spinodal lines define two zones. The metastable region, where still $(\partial p/\partial v)_T < 0$, is enclosed between the binodal and spinodal. In it, each phase is metastable with respect to the other phase. A forbidden region in which $(\partial p/\partial v)_T > 0$, is enveloped by the spinodal. In that zone the homogeneous system is absolutely unstable. A set of values of the volume for each isotherm at a given pressure, predicted by the equation of state and not experimentally possible, is included in this region, at positive pressures. Line D in Figure 7.10 indicates the states at zero pressure.

At the very low pressure inside the ion source, the sample solution is suddenly heated by the atom bombardment, and the system goes into the metastable region. If no heterogeneous nucleation is present, the formation of the gas phase is prevented and the increasing temperature brings the system into the region of absolute instability. When the limit of superheat is reached, rapid homogeneous nucleation occurs,[225] causing an irreversible expansion into an excited gas.[226] The rate of homogeneous nucleation increases very rapidly with the temperature.[219,227-230] The heat transfer between the separating phases greatly influences the process,[230] and as the gas cools down due to the expansion, the system goes back into the stable region and the gas bubble collapses into the liquid phase. This offers a possible explanation for the cut-

off time t_{max}, at which the ion emission stops. However, the limit of superheat is reached due to the energy obtained from the atom impact, and the small changes in the initial temperature of the sample do not seem to be important in this matter. Therefore, the presented arguments cannot account for the strong temperature dependence observed in the FAB experiments.

It is proposed in the present work that the dependence of the FAB spectrum with the sample temperature is related to the solution viscosity, which greatly influences the interaction between the excited gas bubble and the surrounding liquid. The viscosity of glycerol decreases greatly with the temperature,[205] as shown in Figure 7.11.

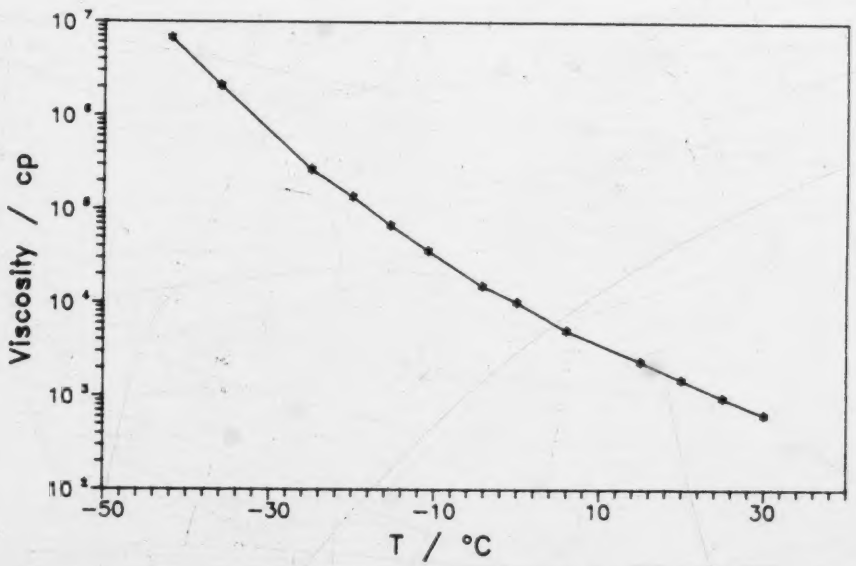

Figure 7.11. Viscosity of Glycerol vs. Temperature

In the temperature range used in these experiments, the viscosity of glycerol changes by three orders of magnitude.[205] This strong variation is the basis of the present proposal, since it may be assumed that the initial expansion of the channel depends on how the liquid responds to the high pressure initially exerted by the hot gas. The higher the viscosity of the liquid, the lower the ability to form the gas cavity.

This situation can be visualized by means of Figure 7.12, that shows a diagram of the gas-like cavity formed at the impact point. When the collision cascade takes place, a very high temperature gas is initially formed. The temperature of the hot track is high enough to rapidly increase the pressure. If the solution has high viscosity (low temperature), the bottom of the channel is not free to expand and a rapid expulsion of the gas at the top occurs. The residence time is short and the temperature of the ejected gas is high, producing a noisy spectrum. On the other hand, if an initial expansion is possible because the solution has low viscosity (high temperature), the whole channel expands and cools down as the pressure decreases. More time is available for heat transfer, and the expansion can reach the bottom of the bubble. The conditions for irreversible expansion are approached more slowly and the residence time is longer. Both hot ions from the top and cold ions from the bottom of the bubble are ejected and a clean spectrum is produced. In summary, at low viscosities the expan-

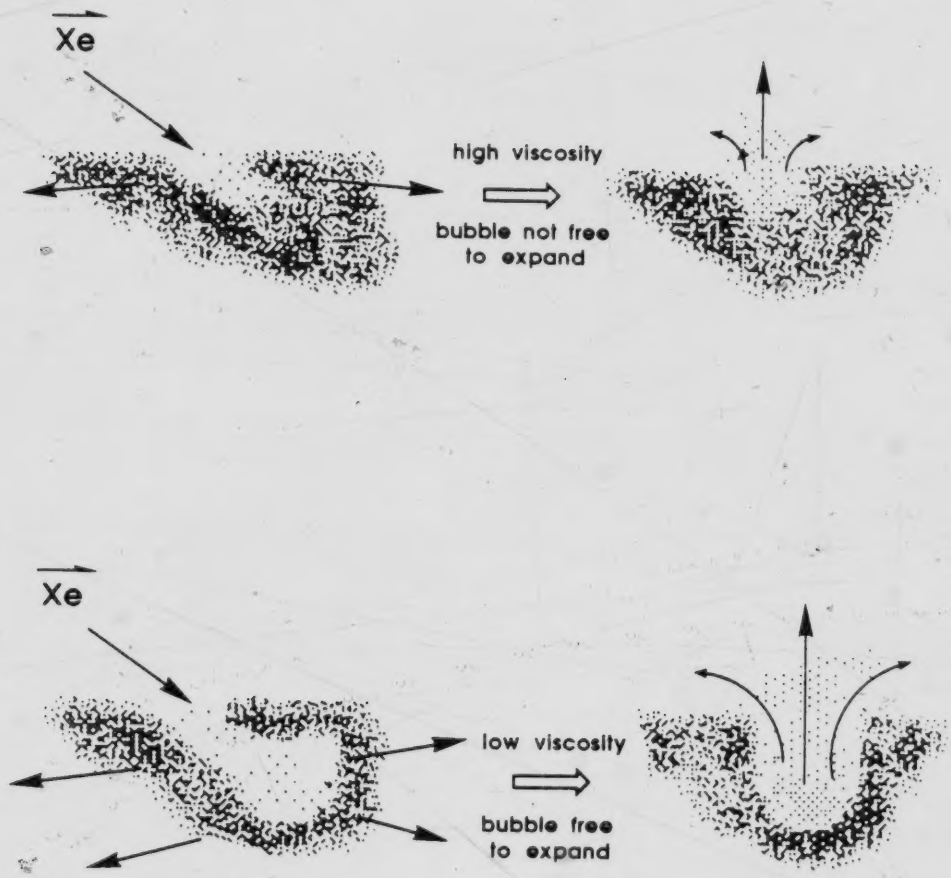

Figure 7.12. Diagram of the Gas-Like Cavity Generated at the Bombardment Point

sion of the excited gas slows down the ejection process, while at high viscosities the expansion of the cavity is prevented and the ejection dominates.

In order to check the validity of this proposal, the viscosity should be varied independently from the temperature. A series of experiments were carried out at constant temperature, and the viscosity of the sample solutions were varied by increasing addition of sucrose. The samples used were neat glycerol, 2 and 10 molepercent solutions of diethanolamine in glycerol, and neat diethanolamine.

It is well known that the viscosity of aqueous solutions of sugars, such as glucose, fructose or sucrose, strongly increases with increasing sugar concentration. Figure 7.13 shows the viscosity of sucrose aqueous solutions as a function of sucrose concentration.[205] The viscosity changes over three orders of magnitude from neat water to 75 weightpercent sucrose solution. In addition, sucrose, as well as the other sugars, can be considered inert in the context of the FAB experiments, since they are compounds with lower basicities than glycerol and produce low intensity peaks in the positive mode. Furthermore, sugars are structurally related to glycerol, being polyhydroxyl compounds as well, so that they are very soluble and should not cause significant changes in the chemistry involved in the production of the FAB spectrum. For all these reasons, su-

crose was chosen as a suitable additive to increase the viscosity of the sample solutions used.

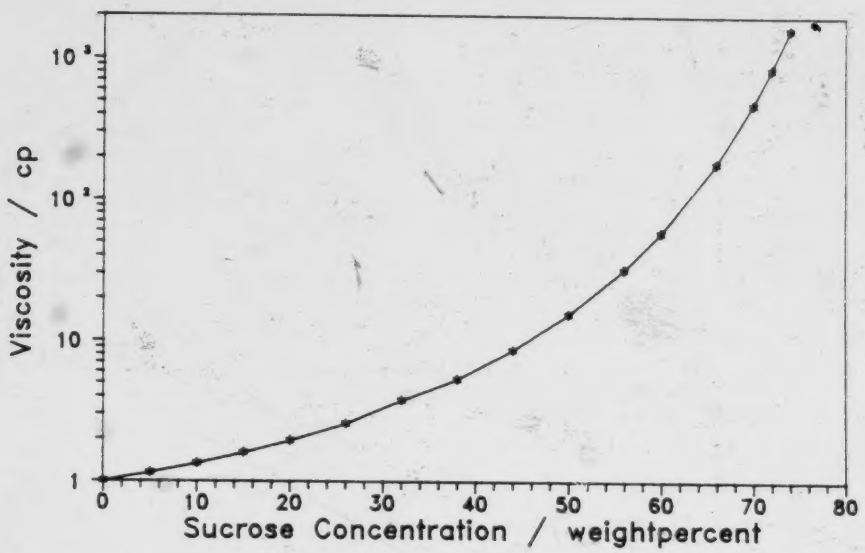

Figure 7.13. Viscosity of Aqueous Solution of Sucrose vs. Sucrose Concentration

The concentration of sucrose was increased from 0 to 80 weightpercent in all the cases. The solution viscosities were not measured, but they are assumed to change by three orders of magnitude as well, from about 10^3 cp for neat glycerol at room temperature, to over 10^6 cp for maximum concentrations of sucrose. In parallel experiments by Sunner,[231] with glucose as viscosity enhancing additive, the viscosity of the glycerol solutions were observed to change from 10^3 cp to 10^6 cp, as the glucose

concentration was increased from 0 to 70 weightpercent. As for diethanolamine, it is also a viscous liquid by itself, although less than glycerol, and its viscosity changes with the temperature in a similar way to that of glycerol.[231] It was assumed for the present experiments that the addition of sucrose would have a similar effect in all the sample solutions.

Figures 7.14 and 7.15 show examples of the kind of spectrum obtained, in these cases for glycerol and diethanolamine respectively, with 0, 20, 40 and 60 weightpercent of added sucrose. The changes observed in the ion intensities as a function of the sucrose concentration for each of the sample solutions used, are shown in Figures 7.16 (glycerol), 7.17 (diethanolamine), 7.18 (2 molepercent solution of diethanolamine in glycerol) and 7.19 (10 molepercent solution of diethanolamine in glycerol), as functions of the sucrose concentration. In all the cases, degradation of the spectra occurs when sucrose is increasingly added to the sample solution. The results are similar to the changes observed when decreasing the sample temperature. The intensity of glycerol and diethanolamine protonated molecular ions and clusters decrease with increasing viscosity. The change is stronger for diethanolamine peaks, while the fragment ion intensity variation is weak for both compounds. The noise ion intensity strongly increases for all the samples,as the viscosity increases when more sucrose is added. As expected, the peaks of sucrose are weak, although some in-

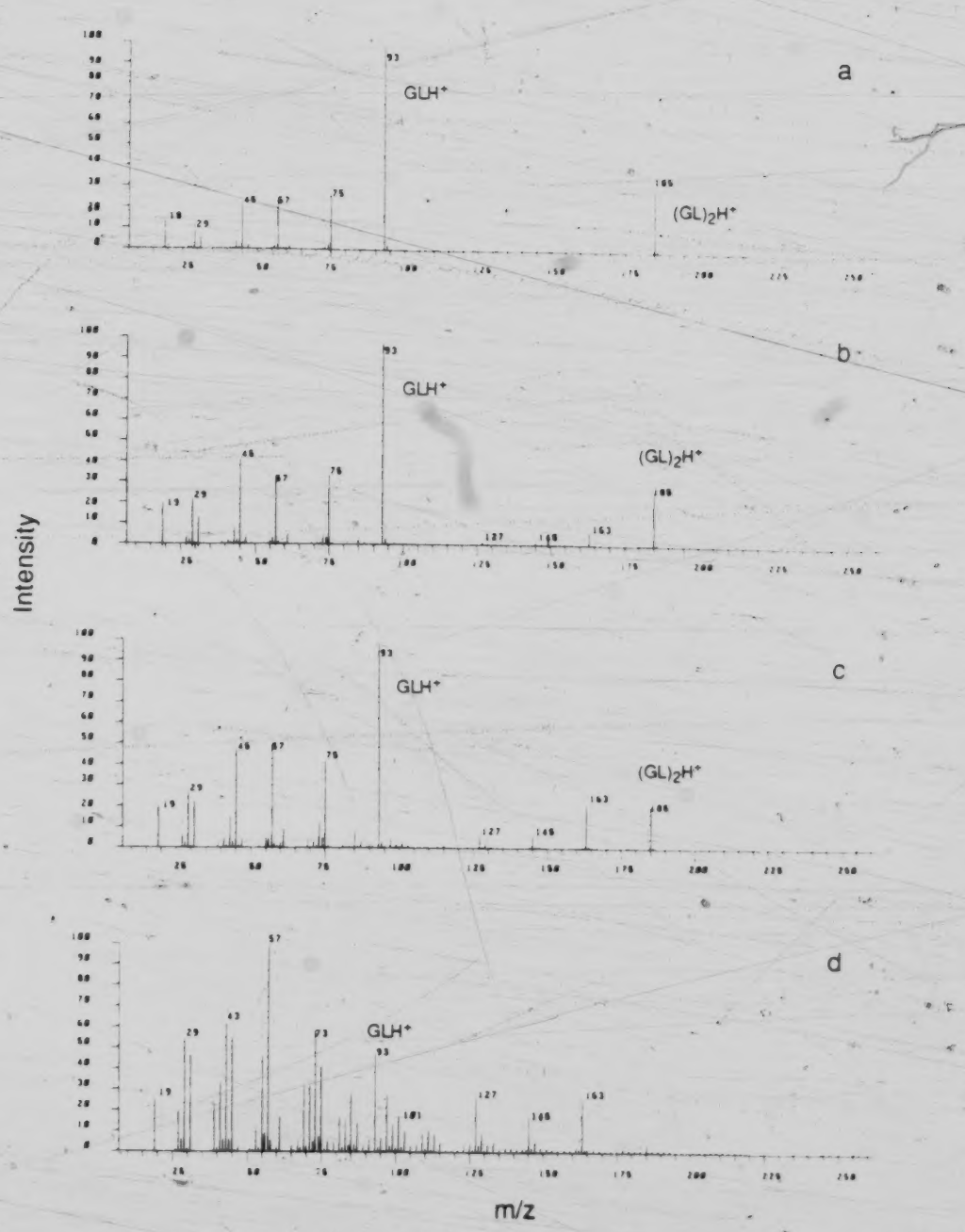

Figure 7.14. FAB Spectra of Glycerol with Increasing Concentrations of Sucrose Added to Increase the Viscosity. a- Neat Glycerol, b- 20 % Sucrose, c- 40 % Sucrose, d- 60 % Sucrose

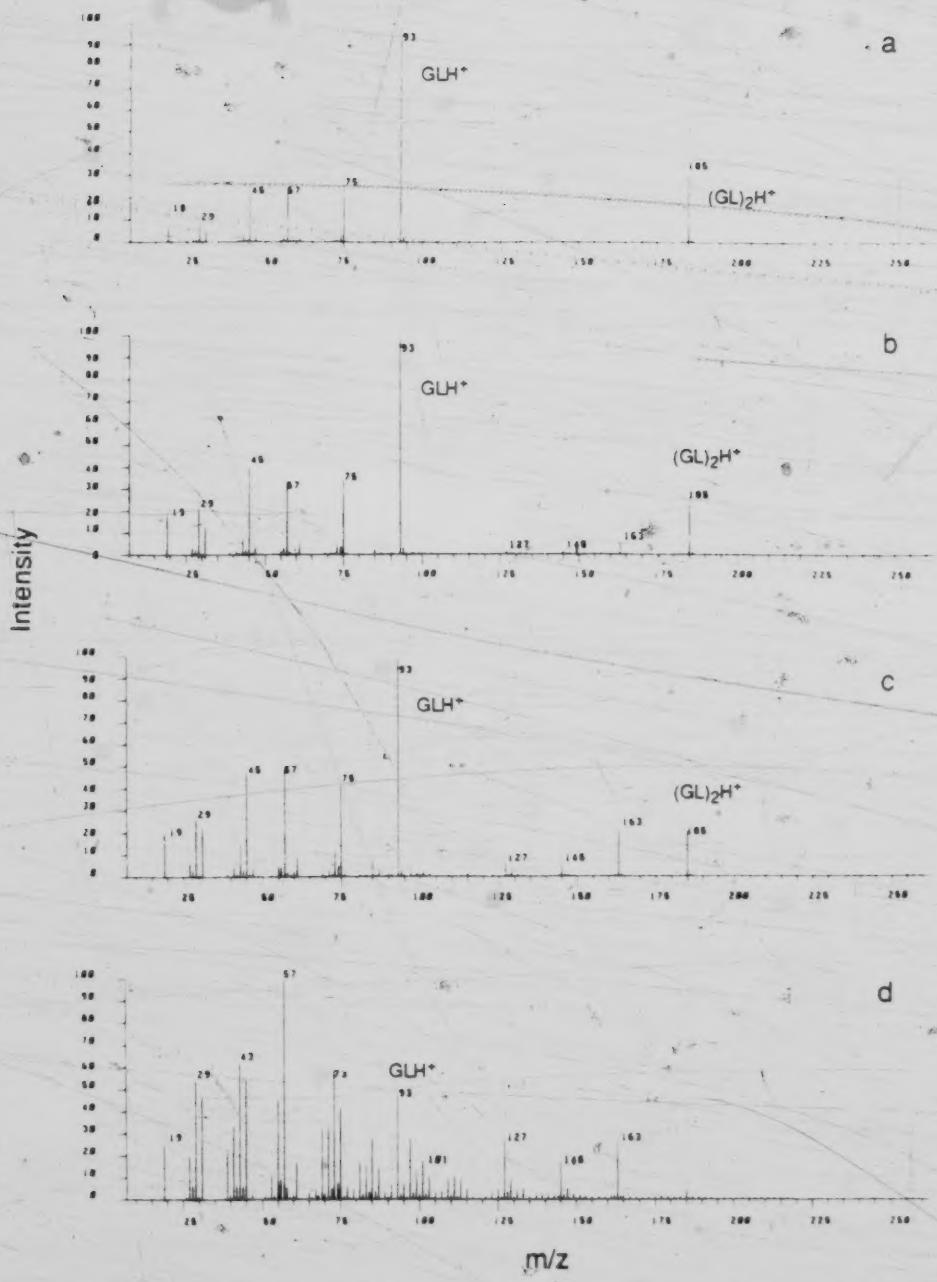

Figure 7.14. FAB Spectra of Glycerol with Increasing Concentrations of Sucrose Added to Increase the Viscosity. a- Neat Glycerol, b- 20 % Sucrose, c- 40 % Sucrose, d- 60 % Sucrose

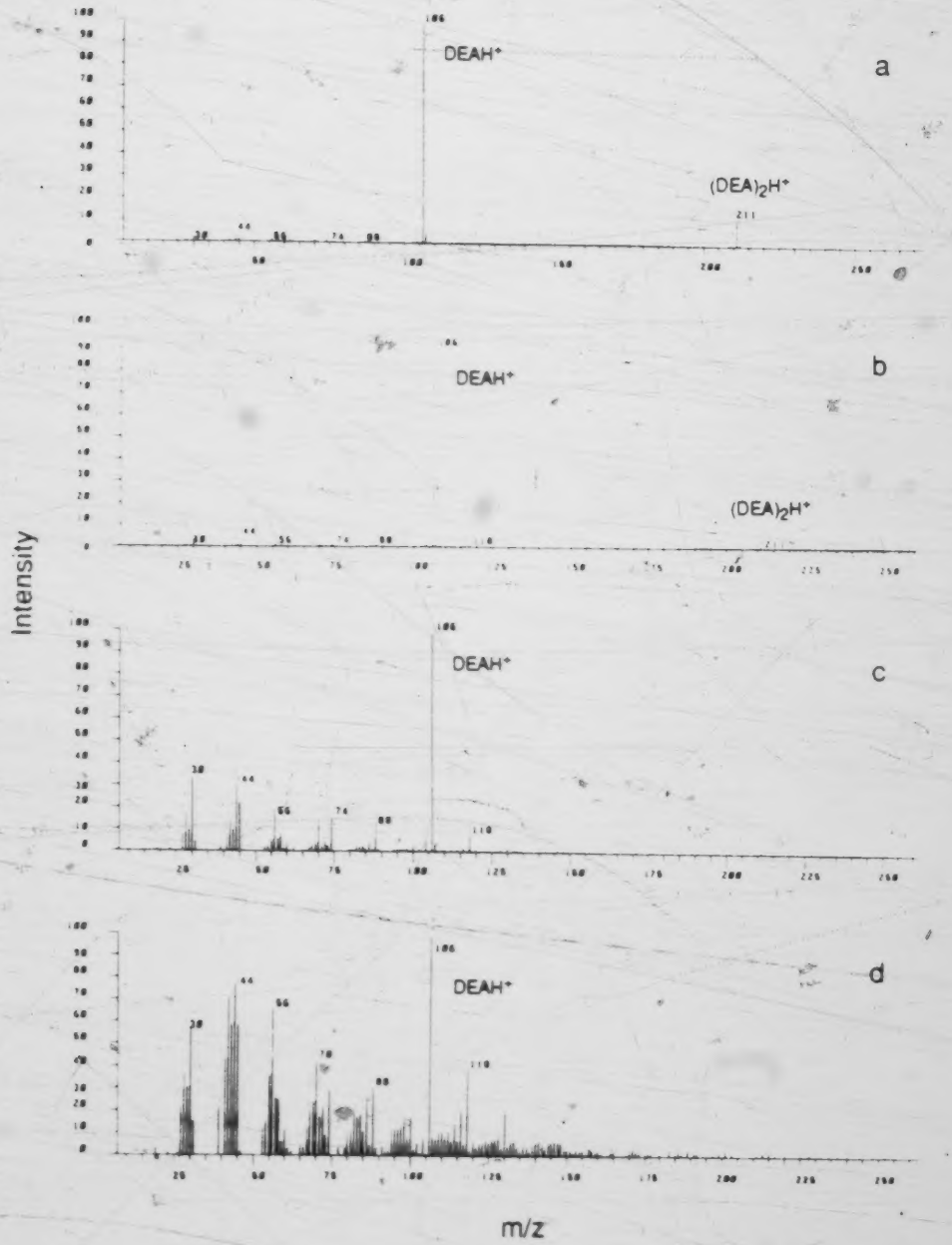

Figure 7.15. FAB Spectra of Diethanolamine with Increasing Concentrations of Sucrose Added to Increase the Viscosity. a- Neat Diethanolamine, b- 20 % Sucrose, c- 40 % Sucrose, d- 60 % Sucrose

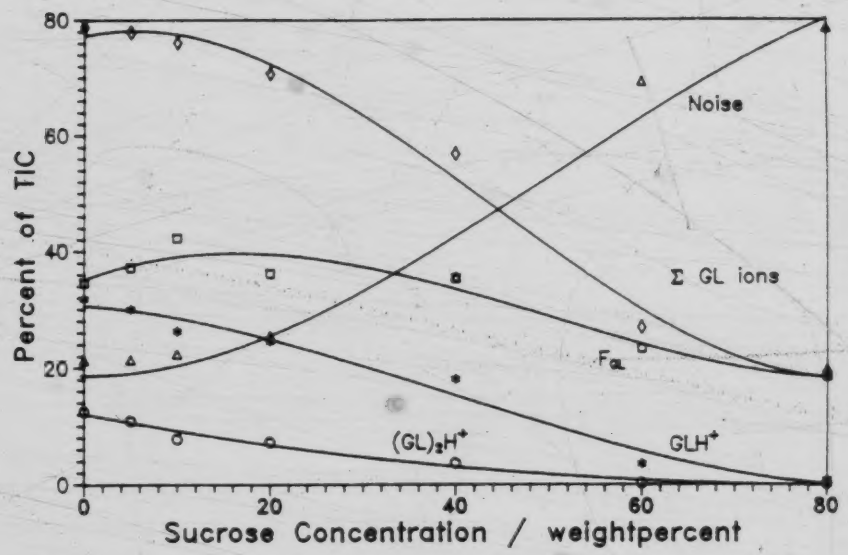

Figure 7.16. Intensity of Glycerol-Derived Ions vs. Sucrose Concentration Added to Increase the Viscosity, from FAB Spectra of Sucrose-Glycerol Solutions

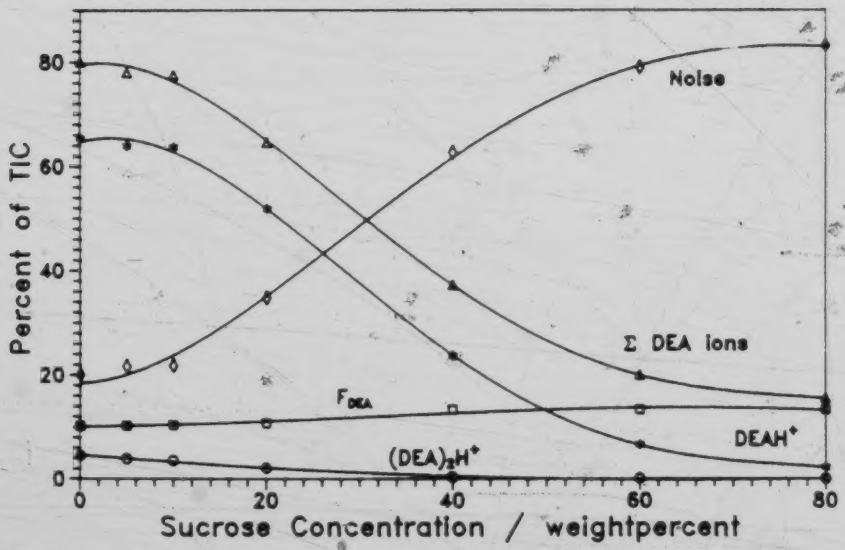

Figure 7.17. Intensity of Diethanolamine-Derived Ions vs. Sucrose Concentration Added to Increase the Viscosity, from FAB Spectra of Sucrose-Diethanolamine Solutions

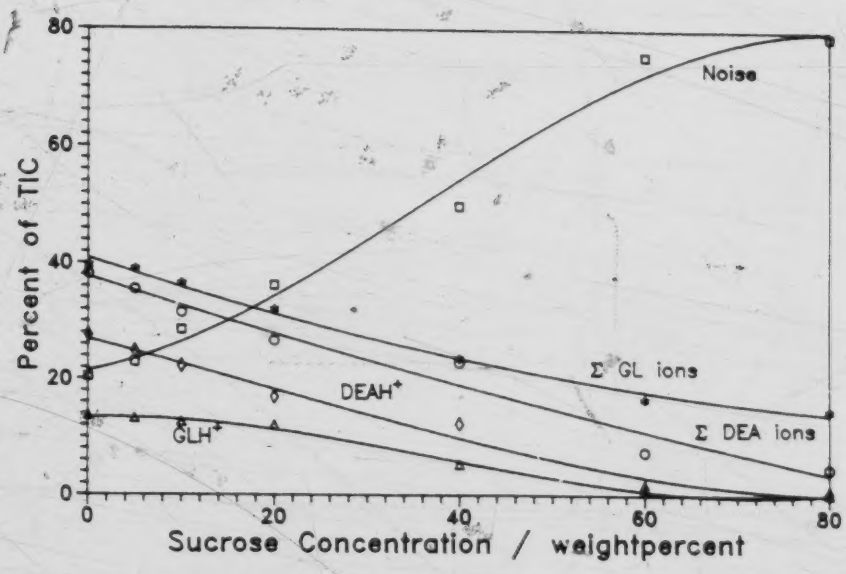

Figure 7.18. Intensity of Major Ions vs. Sucrose Concentration Added to Increase the Viscosity, from FAB Spectra of Sucrose-2 molepercent Diethanolamine in Glycerol Solutions

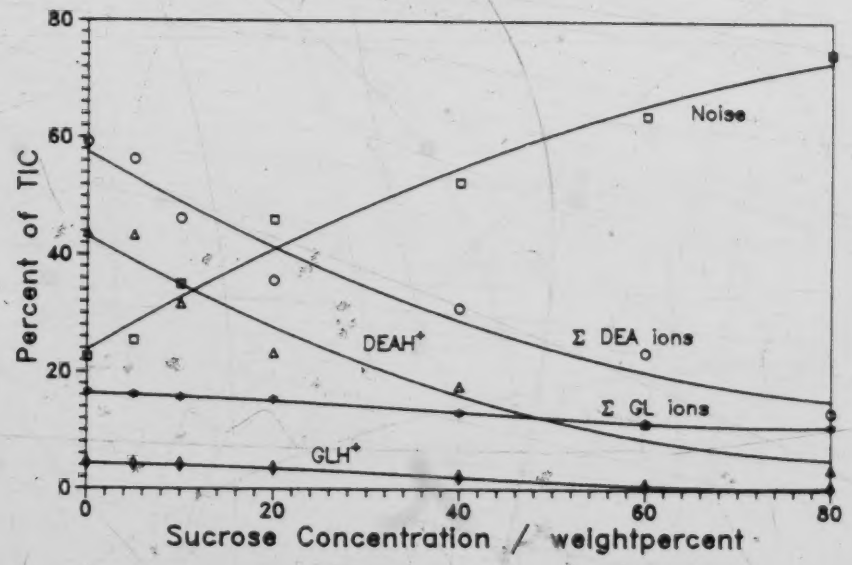

Figure 7.19. Intensity of Major Ions vs. Sucrose Concentration Added to Increase the Viscosity, from FAB Spectra of Sucrose-10 molepercent Diethanolamine in Glycerol Solutions

crease in their intensities is observed with increasing concentration, up to the middle range. At higher concentrations, the degradation also influences the sucrose signals.

The presented results bring strong support to the previous explanation given for the temperature dependence of the FAB spectrum. The viscosity seems to be the property that determines the quality of the spectrum, and the sample solution temperature by itself is not significant. Variation either of the sample solution temperature, which causes viscosity changes, or of the solution viscosity by other means, produce similar experimental results. As discussed earlier in this Chapter, these results can be successfully reproduced by a kinetic calculation based on gas phase reactions. The importance of the viscosity, or indirectly of the sample temperature, lies in the fact that the time available for those reactions is determined by the life-time of the cavity.

CHAPTER 8

CALCULATION OF IONIZATION CROSS SECTIONS IN GAS PHASE FAB

The ability of fast atoms such as Xe, accelerated to kinetic energies of ~ 6-7 KeV, as produced from a FAB gun, to ionize isolated, i.e. gas phase, molecules is of interest from the standpoint of the mechanism responsible for the formation of FAB spectra from analytes dissolved in a liquid matrix.

Much attention was paid in early work on FAB mechanisms on the presence of preformed analyte ions in the matrix.[137] One of the major points of the present research on the FAB mechanism has been the assumption that, due to the large excess of matrix molecules M relative to analyte molecules A, the presence of preformed AH^+ ions is not essential, since the fast atom impact produces ample ionization of the matrix molecules. These then react with other neutral matrix molecules and ultimately with analyte molecules. Protonation of the analyte A to AH^+ is often the end result of such a sequence of reactions when the basicity of the analyte is higher than that of the matrix molecules.

The measurement of the number of ions produced from liquid matrix molecules per impacting fast atom, which is central to the argument that the fast atom produces ample ionization, is experi-

mentally difficult. However, the ionization probability of gaseous molecules is relatively easy to determine, and such ionization cross sections could be related to ionization in solution.

Ionization probabilities, i.e. ionization cross sections, of gas phase molecules due to electrons of photons represent a well established research area,[4-6] and abundant data on such cross sections are available. Surprisingly, practically no measurement of ionization cross sections of molecules with relatively heavy atoms like Ar, Kr or Xe in the KeV range seem to be available in the literature. Considering the velocities of electrons or protons used for ionization, the above particles are relatively very slow and the ionization mechanism is expected to be of a different nature. Judging from the popularity of the Precursor Model[137] of SIMS/FAB spectra, it seems clear that many workers made the tacit assumption that the ionization cross sections for such "slow" particles are very low.

The possibility for abundant ionization by colliding neutrals has been already considered.[81,158,176] Bojesen and Møller[81] reported the formation of molecular ions in gas phase FAB experiments, and observed that the abundance of the ions decreased drastically with the beam energy. They suggested that collision between fast atoms and slow molecules could lead to ionization and that the ionization cross section would increase with the energy of the beam. On the basis of experimental gas phase data from the lit-

erature, involving collision center of mass energies in the hundreds of volts, Michl[158] was able to conclude that ionization is expected to occur with significant probability whenever such fast internuclear motion occurs. By contrast, Field,[176] based on adiabatic principle calculations by Wolfgang,[179] considered that argon atoms with an energy of several KeV cannot be regarded as ionizing radiation.

In order to have actual ionization cross sections for FABMS systems, experimental measurements of ionization cross section for Xe atoms with energies in the 6-7 KeV were performed for toluene, glycerol and 3-nitrobenzyl alcohol, as described in the Experimental Section. In addition to the ionization cross sections, ionic fragmentation patterns, i.e. FAB mass spectra, involving gaseous molecules were also obtained for the same compounds. These spectra are of interest from the standpoint of the mechanism of FAB of analytes in liquid matrices, since they can be an indication of the nature of the ions resulting from impact of the fast atoms on molecules of the liquid solution.

Figure 8.1 shows plots of the positive ion current observed vs. the uncorrected ion gauge reading for toluene gas. The plot in Fig. 8.1a was obtained with the secondary electron suppressor at -500 V. The plot in Figure 8.1b is for the suppressor at 0 V. The results are very close, which suggests that very few secondary electrons enter the ion source and lead to ionization, even in the absence

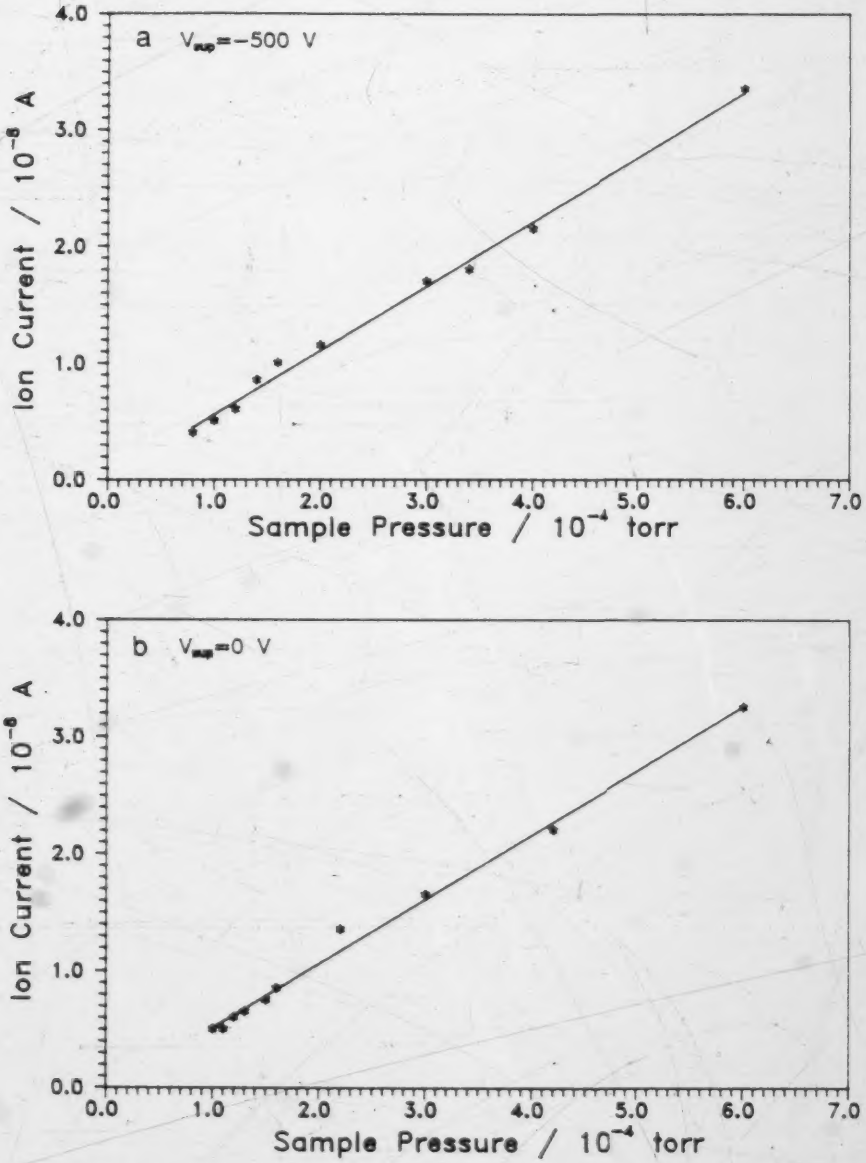

Figure 8.1. **Positive Ion Current vs. Uncorrected Ion Source Pressure for Gaseous Toluene Ionized by the Xe Fast Atom Beam**

of a suppressor. Similar results were obtained for glycerol and 3-nitrobenzyl alcohol. The analogous plots for these compounds are shown in Figures 8.2 and 8.3. The slope in Figure 8.1 (toluene) is 5.3×10^{-5} A/torr for the uncorrected reading. The sensitivity correction of the ion gauge for toluene is 6, and the pressure correction ion gauge to ion source is 1.24, as shown in the Experimental Section. Thus, the corrected slope is:

$$\frac{i_+}{P} = \frac{5.3 \times 10^{-5} \times 6}{1.24} = 2.6 \times 10^{-4} \text{ A/torr} \qquad (8.1)$$

Taking a temperature of ~ 100° C for the ion source, the number density of toluene per torr is evaluated with equation 4.2:

$$\rho_M = 2.6 \times 10^{16} \text{ molecules cm}^{-3} \text{ torr}^{-1} \qquad (8.2)$$

Substituting d = 1 cm and $f_{Xe} = 4 \times 10^{13}$ atoms/s (see Experimental Section) into equation 4.1 the cross section σ is obtained:

$$\sigma = \frac{i_+}{q_e \, d \, \rho_M \, f_{Xe}} = \frac{2.6 \times 10^{-4}}{1.6 \times 10^{-19} \times 1 \times 2.6 \times 10^{16} \times 4 \times 10^{13}} \qquad (8.3)$$

$$\sigma = 16 \times 10^{-16} \text{ cm}^2 \text{ (toluene)}$$

The cross section is estimated to be accurate to within a factor of two, i.e. it should be between 8×10^{-16} to 32×10^{-16} cm^2. The large

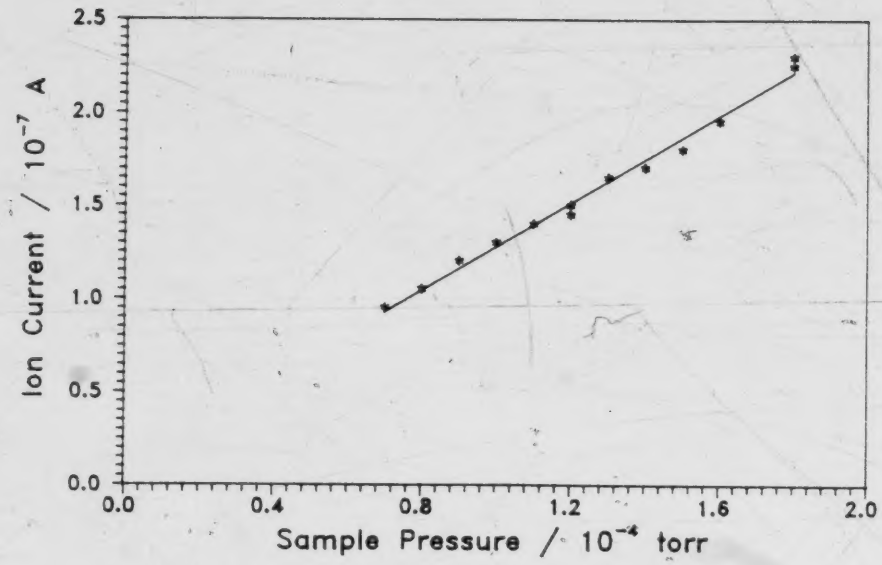

Figure 8.2. Positive Ion Current vs. Uncorrected Ion Source Pressure for Gaseous Glycerol Ionized by the Xe Fast Atom Beam

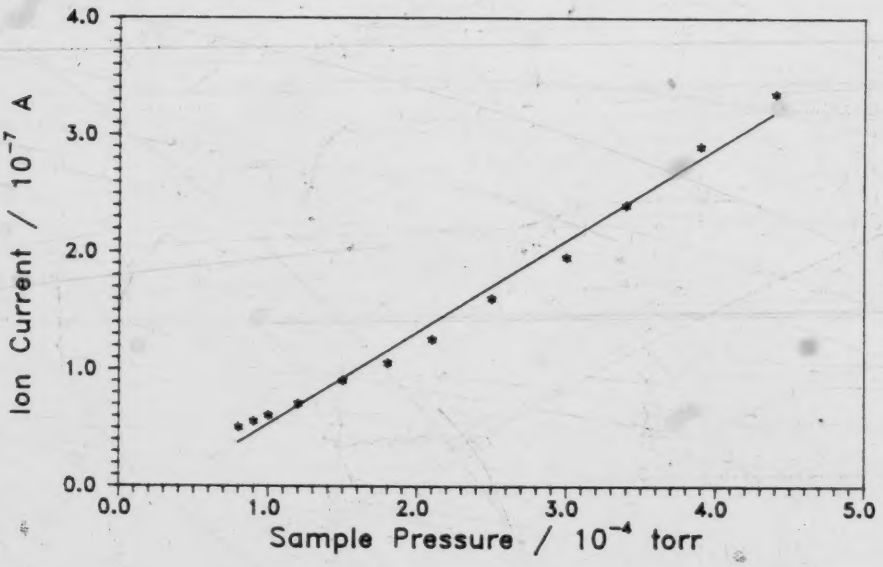

Figure 8.3. Positive Ion Current vs. Uncorrected Ion Source Pressure for Gaseous 3-Nitrobenzyl Alcohol Ionized by the Xe Fast Atom Beam

error assumed is based on the difficulty in determining the neutral Xe beam intensity[200] and the necessity to estimate the effective length d in equation 4.1.

The results in Figures 8.2 and 8.3, which give the ion currents vs. pressure measured for glycerol and 3-nitrobenzyl alcohol vapors, lead to cross sections which are roughly twice as large as that for toluene. Since the pressure determination for these two compounds was much less reliable, as explained in the Experimental Section, actual cross section values will not be quoted .

The cross sections determined above, which are between 20×10^{-16} and 40×10^{-16} cm^2, are quite large. They are of a magnitude similar to kinetic collision cross sections and cross sections for ionization by electron impact with 50-75 eV electrons, i.e. at electron energies where the electron ionization cross section is at its maximum. The 6 KeV Xe atoms are thus a very efficient ionizing medium.

The ionization cross sections in the liquids, i.e. liquid toluene, glycerol, etc., may be somewhat smaller, but are probably of similar magnitude to the gas phase ionization cross sections. This indicates that ample ionization is produced by the fast atom bombardment of the liquid matrix.

A very rough estimate of the ionization in the liquid can be obtained by assuming that an energy of 35 eV is dissipated per ion pair produced.[235] An atom of 6 KeV, assumed to be able to lead to ionization until it has been slowed down to 2.5 KeV, will produce 3500/35 = 100 ions. Assuming that such an atom "desorbs" some 1000 glycerol molecules[174] containing 5 molepercent of a preionized analyte, some 50 preformed ions will be also produced. These very rough estimates support the assumption of the previous discussion that ample ionization is produced by the fast atom impact and that the presence of preformed ions is not essential. In conclusion, abundant analyte ions may be expected on the basis of ion-molecule reactions between matrix ions, produced by the Xe impact, and neutral analyte molecules.

Mass Spectra of Gaseous Molecules Obtained with ~ 6-7 KeV Xe atoms

The FAB spectra for gaseous toluene, glycerol and 3-nitrobenzyl alcohol, obtained with ionization by the Xe fast atom beam, are shown in Figures 8.4, 8.5 and 8.6, respectively. Also included in the same figures, for comparison, are the corresponding EI mass spectra. There are considerable differences between the FAB and the EI spectra. In general, the FAB spectra show more fragmentation. For example, for toluene, the EI spectrum is dominated by the molecular ion $M^{+\cdot}$ at m/z 92 and the $(M-H)^+$ ion at m/z 91.

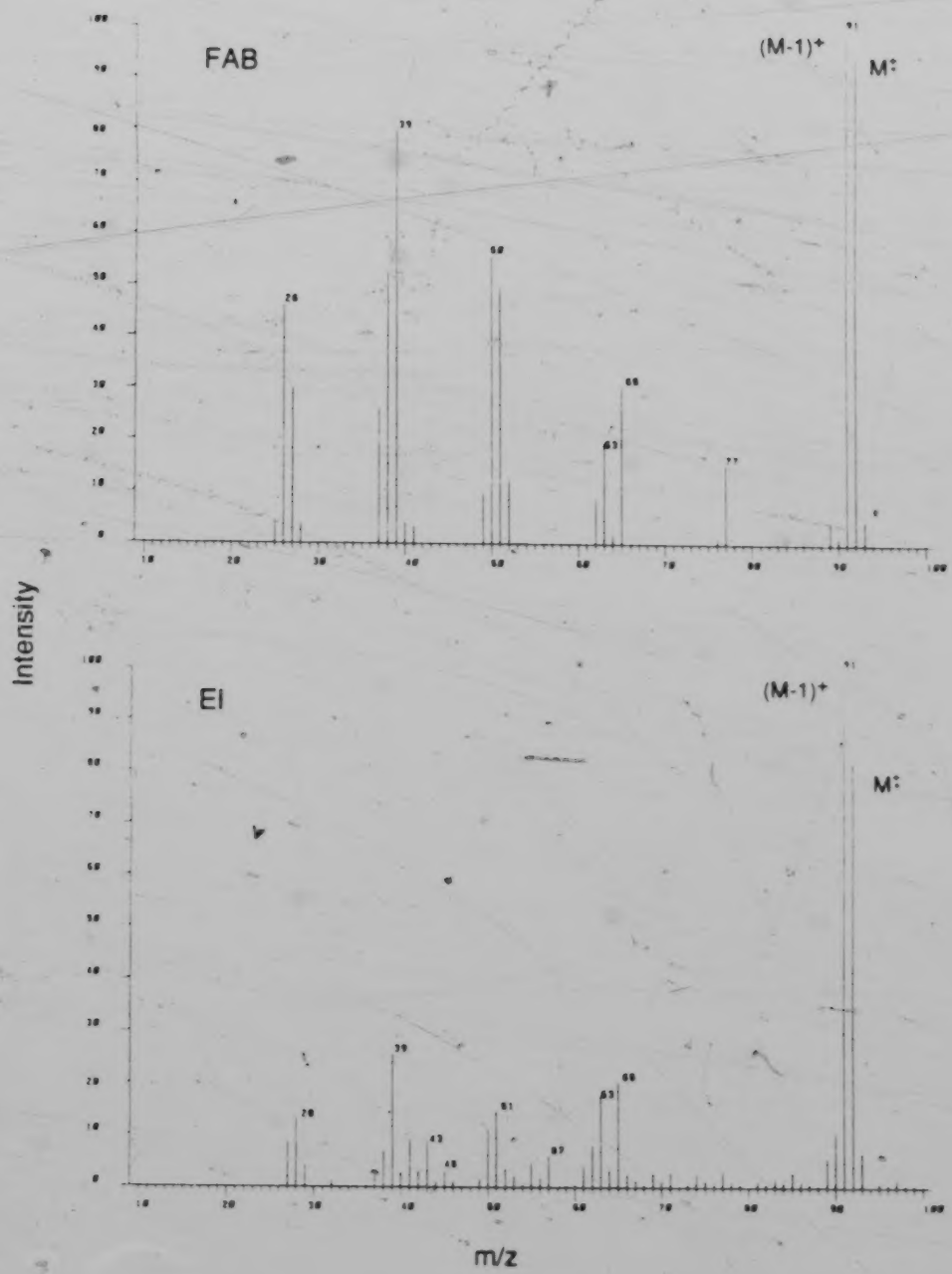

Figure 8.4. Gas-Phase FAB Spectrum (6 KeV Xe atoms) and EI Spectrum (70 eV electrons) of Toluene

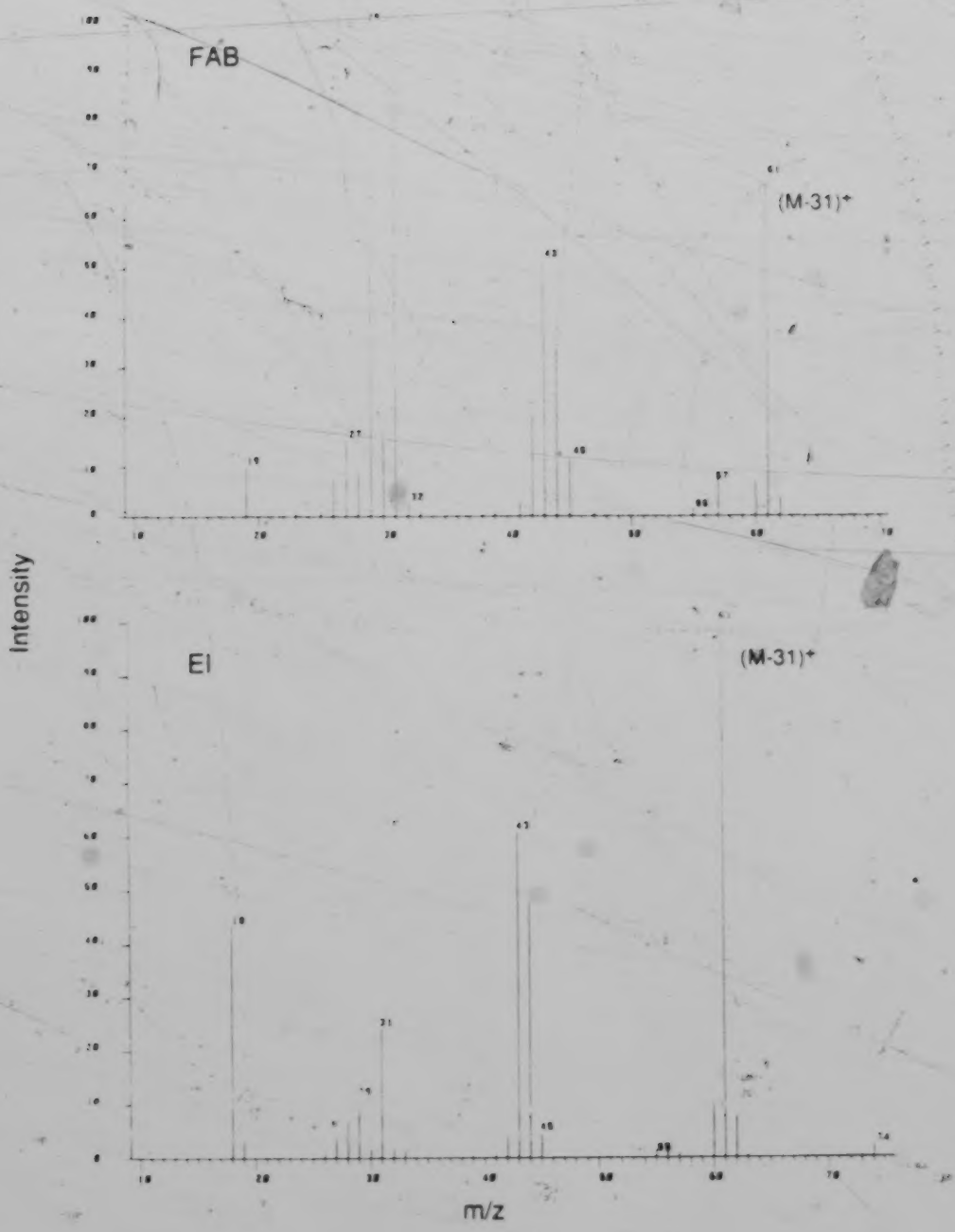

Figure 8.5. Gas-Phase FAB Spectrum (6 KeV Xe atoms) and EI Spectrum (70 eV electrons) of Glycerol

Figure 8.6. Gas-Phase FAB Spectrum (6 KeV Xe atoms) and EI Spectrum (70 eV electrons) of 3-Nitrobenzyl Alcohol

The FAB spectrum also shows abundant lower mass fragments, such as those at m/z 77, 65, 63, 51, 50, 39, 38, 27 and 26. Most of these fragments are also present in the EI spectrum, but at much lower intensities.

While the EI and the FAB spectra have distinctive features, the similarities should not be overlooked, as these are probably of significance. The EI spectra are known to result largely from the rapid ($t < 10^{-5}$ s) dissociation of the excited molecular ion. Most of the dissociation is attributed to vibrational excitation of the electronic ground state of the molecular ion.[236] The similarity of the EI and the FAB spectra suggests that the FAB spectra also originate, to a considerable extent, from the decomposition of excited molecular ions. Ionization of matrix molecules in the liquid matrix by a Xe fast atom beam, may lead to significantly different fragment ions, because collisional quenching of the molecular ion excitation is expected to be quite efficient. This may lead to more abundant molecular ions and, at the same time, relatively more abundant fragment ions, i.e. fragment ions formed within very short decomposition times, due to simple cleavages of the molecular ion.

CONCLUSIONS

The analytical use of FAB is based on the ability of the method to desorb and ionize large, thermally labile molecules for mass spectrometric analysis. However, it is not basically understood how such molecules survive the desorption process. This topic has been subject of great controversy, due to its complexity, and is still actively debated. The work presented here has attempted to bring some light to the elucidation of the DI mechanism and to lead to a basis for more rational choices for the optimization of analytical FAB experiments.

It was shown in this study that the basicity of the analyte in the gas phase, rather than its basicity in solution, determines the direction of the proton transfer reactions responsible for the formation of the protonated molecular ions.[237] Many spectral features of FAB could be explained on the basis of well known gas phase ionic processes, and experimental data were modelled by using a kinetic scheme for ion-molecule reactions in a high density gas,[238] in accordance with the Gas Collision Model proposed on the basis of previous results in our group.[189,190] A time dependence of the FAB spectrum was obtained from this kinetic modelling,[238] which was also applied to the experimental results of the study of the temperature dependence of the FAB spectrum.[239,240] It was found that the reaction time available for the ions in the high density gas is

strongly dependent on the temperature of the sample solution. This was explained on the basis of marked changes in the viscosity of the sample solution, that influence the formation of the gas bubble at the impact point. The behavior of the system was illustrated using a thermodynamic PVT surface.[239] Parallel results by Sunner[231] on the effect of the sample viscosity on the FAB spectrum, as well as SIMS experiments with alcohols in our group,[241] support this view of the phenomenon in the proposed Gas Phase Explosion Model.[238-241]

Even if the assumptions and proposals made so far seem to be in agreement with the experimental observations and with some aspects of work developed by other groups,[151,161,169,242-245] there is discrepancy with some authors on several points, such as the dominance of the basicity in the gaseous or liquid media,[74,246] or about where and when (liquid phase before desorption or gas phase during sputtering) the ionization takes place,[137,247,248] or else about the possibility of a different ionization mechanism operating at low and high temperatures[249] and for volatile or non-volatile samples,[81] etc. There is a substantial body of evidence in support of the widely accepted Precursor Model.[122,137] Many studies[71,74,80,94,102,250] indicate that the charge of the emitted ions correspond to the charge of preformed ions in solution. On the contrary, other results show no relationship between the observed signal and the concentration of ions in solution.[245,251]

The large values of ionization cross sections obtained from the gas phase FAB experiments in this work,[252] indicate that ionization is produced by the fast atom beam[81,158,176,179,253] and support the mechanisms where the ionization of the analyte is assumed to occur by reactions of the analyte molecules and matrix-derived ions, which are produced by the atom impact. The gas phase FAB spectra obtained,[252] although different from the EI spectra, have some common features with those, which indicates that decomposition of excited molecular ions is involved.[81,253]

In addition, there may be other variables related to the DI mechanism. Radiation damage caused by the sputtering is a generally accepted explanation for the degeneration of the spectrum,[174,176,178] but some authors give more importance to other factors in this matter, such as sample depletion and evaporation of the liquid matrix,[254] or formation of a polymeric film on the surface of the solution.[249] The renewal of the surface to expose fresh sample solution to the atom impact has been explained by removal of layers of sample solution during the sputtering,[174] by surface activity effects,[93,242,255] by diffusion,[69,256] etc. As a matter of fact, transport mechanisms governed by surface tension, convection or diffusion, are influenced by the viscosity of the medium. Therefore, the pronounced effect observed in the FAB experiments with varying viscosity could be associated to changes in transport processes. The DI mechanism might not be the same for all condi-

tions, but rather be dependent on the initial properties of the sample solution.[231,253] Experiments in which properties such as surface tension and diffusion were carefully observed would be very valuable.

FAB is a remarkable method for the mass spectrometric analysis of polar, non-volatile and thermally labile compounds, but the phenomena involved in the production of the spectra are complex and still not well understood. Although the results presented here were reasonably reproducible and could be explained on the basis of well established theoretical foundations,[237-240,252] this kind of study is difficult to accomplish, due to the large number of variables, already considered or still hidden, that may play an important role in the production of the spectrum.

REFERENCES

1- A. L. Burlingame, A. Dell and D. H. Russell, *Anal. Chem.*, **54**, (1982) 363R.

2- A. L. Burlingame, J. O. Whitney and D. H. Russell, *Anal. Chem.*, **56** (1984) 417R.

3- A. L. Burlingame, T. A. Baillie and P. J. Derrick, *Anal. Chem.*, **58** (1986) 165R.

4- M. S. B. Munson and F. H. Field, *J. Am. Chem. Soc.*, **88** (1966) 2621

5- B. Munson, *Anal. Chem.*, **49** (1977) 772A.

6- R. I. Reed, *J. Chem. Soc.*, (1981) 3432.

7- A. Dell, D. H. Williams, H. R. Morris, G. A. Smith, J. Feeney and G. C. K. Roberts, *J. Am. Chem. Soc.*, **97** (1975) 2497.

8- M. A. Baldwin and F. W. McLafferty, *Org. Mass Spectrom.*, **7** (1973) 1353.

9- G. D. Daves, *Acc. Chem. Res.*, **12** (1970) 359.

10- R. J. Cotter, *Anal. Chem.*, **52** (1980) 1589A.

11- U. Rapp, G. Dielmann, D. E. Games, J. L. Gower and E. Lewis, *Adv. Mass Spectrom.*, **8** (1980) 1660.

12- G. R. Waller and O. C. Dermer (eds.), "*Biochemical Applications of Mass Spectrometry*", Wiley, New York, 1980.

13- H. R. Morris (ed.), "*Soft Ionization Biological Mass Spectrometry*", Heyden and Son, London, 1981.

14- M. E. Rose and R. A. W. Johnstone, *"Mass Spectrometry for Chemists and Biochemists"*, Cambridge University Press, Cambridge, 1982.

15- H. D. Beckey and D. Schuelte, *Z. Instrum.*, **68** (1960) 302.

16- H. D. Beckey, *"Field Ionization Mass Spectrometry"*, Pergamon Press, Oxford, 1971.

17- H. D. Beckey, *Int. J. Mass Spectrom. Ion Phys.*, **2** (1969) 500.

18- H. D. Beckey and H. R. Schulten, *Angew. Chem.*, **87** (1975) 425.

19- H. D. Beckey, *"Principles of Field Ionization and Field Desorption Mass Spectrometry"*, Pergamon Press, Oxford, 1977.

20- D. F. Torgerson, R. P. Skrowronski and R. D. Macfarlane, *Biochem. Biophys. Res. Commun.*, **60** (1974) 616.

21- R. D. Macfarlane and D. F. Torgerson, *Int. J. Mass Spectrom. Ion Phys.*, **21** (1976) 81.

22- O. Becker, N. Fürstenau, F. R. Krueger, G. Weiss and K. Wien, *Nucl. Instrum. Methods*, **139** (1976) 195.

23- M. A. Posthumus, P. G. Kistemaker, H. L. C. Meuzelaar and M. C. Ten Noever de Brauw, *Anal. Chem.*, **50** (1978) 985.

24- R. Stoll and F. W. Rölgen, *Org. Mass Spectrom.*, **14** (1979) 642.

25- R. Cotter, *Anal. Chem.*, **53** (1981) 1306.

26- M. L. Vestal, in *"Ion Formation from Organic Solids"*, Springer Ser. in Chem. Phys., Vol. 25, A. Benninghoven (ed.), Springer-Verlag, Berlin, 1983, Chapter 5.1.

27- M. Dole, L. L. Mach, R. L. Hines, R. C. Mobley, L. D. Ferguson and M. B. Alice, *J. Chem. Phys.*, **49** (1968) 2240.

28- D. S. Simons, R. N. Colby and C. A. Evans, *Int. J. Mass Spectrom. Ion Phys.*, **15** (1974) 291.

29- B. A. Thomson and J. V. Iribane, *J. Chem. Phys.*, **71** (1979) 4451.

30- C. R. Blakley, J. J. Carmody and M. L. Vestal, *J. Am. Chem. Soc.*, **102** (1980) 5931.

31- R. E. Honig, *Adv. Mass Spectrom.*, **2** (1962) 25.

32- A. F. Dillon, R. S. Lehrle and J. C. Robb, *Adv. Mass Spectrom.*, **4** (1968) 477.

33- A. Benninghoven, *Z. Naturforsch.*, **24A** (1969) 859.

34- A. Benninghoven, D. Jaspers and W. Sichtermann, *Appl. Phys.*, **11** (1976) 35.

35- A. Benninghoven and W. Sichtermann, *Org. Mass Spectrom.*, **12** (1977) 595.

36- A. Benninghoven and W. Sichtermann, *Anal. Chem.*, **50** (1978) 1180.

37- R. J. Colton, J. S. Murday, J. R. Wyatt and J. J. DeCorpo, *Surf. Sci.*, **84** (1979) 235.

38- R. J. Day, S. E. Unger and R. G. Cooks, *Anal. Chem.*, **52** (1980) 557A.

39- W. R. Groves, *Philos. Mag.*, **5** (1853) 203.

40- J. J. Thomson, *Philos. Mag.*, **20** (1910) 752.

41- G. K. Wenher, *Phys. Rev.*, **102** (1956) 690.

42- R. E. Honig, *J. Appl. Phys.*, **29** (1958) 549.

43- M. W. Thompson and R. S. Nelson, *Philos. Mag. Ser. 8*, **7** (1962) 2015.

44- G. Carter and J. S. Colligon, *"Ion Bombardment of Solids"*, Heinemann Ltd., London, 1968.

45- H. H. Andersen and H. L. Bay, *J. Appl. Phys.*, **45** (1974) 953.

46- P. Sigmund, in *"Sputtering by Ion Bombardment I"*, Topics in Applied Chemistry, Vol 47, R. Behrich (ed.), Springer-Verlag, Berlin, 1981, Chapter 2.

47- A. Benninghoven and A. Müller, *Phys. Lett. A*, **40** (1972) 169.

48- G. H. Morrison and G. Slodzian, *Anal. Chem.*, **47** (1975) 932A.

49- J. A. Mc Hugh, in *"Methods of Surface Analysis"*, A. W. Czanderna (ed.), Elsevier, New York, 1975, p. 223 ss.

50- H. Oechsner, *Appl. Phys.*, **8** (1975) 185.

51- G. K. Wehner, in *"Methods of Surface Analysis"*, A. W. Czanderna (ed.), Elsevier, New York, 1975, p. 5 ss.

52- A. Benninghoven, *Surf. Sci.*, **35** (1973) 427.

53- A. Benninghoven, *Surf. Sci.*, **53** (1975) 596.

54- M. Barber and J. C. Vickerman, *Surf. Defect. Prop. Solids*, **5** (1976) 162.

55- H. Grade, N. Winograd and R. G. Cooks, *J. Am. Chem. Soc.*, **99** (1977) 7725.

56- D. M. Heyes, M. Barber and J. H. R. Clarke, *Surf. Sci.*, **105** (1981) 225.

57- N. H. Turner, B. I. Dunlap and R. J. Colton, *Anal. Chem.*, **56** (1984) 373R.

58- S. J. Pachuta and R. G. Cooks, in *"Desorption Mass Spectrometry. Are SIMS and FAB the Same?"*. P.A. Lyon (ed.), Am. Chem. Soc., Washington, D.C., 1985, Chapter 1.

59- M. L. E. Oliphant, *Proc. R. Soc. London A*, **124** (1929) 228.

60- F. M. Devienne and G. Grandclement, *C. R. Acad. Sci. Paris*, **262** (1966) 696.

61- F. M. Devienne, *Entropie*, **18** (1967) 61.

62- F. M. Devienne and A. Roustan, *Entropie*, **20** (1968) 9.

63- F. M. Devienne and J. C. Roustan, *C. R. Acad. Sci. Paris*, **276** (1973) 923.

64- F. M. Devienne and A. Diebold, *C. R. Acad. Sci. Paris C*, **278** (1974) 1219.

65- M. Barber, R. S. Bordoli, R. D. Sedgwick and A. N. Tyler, *J. Chem. Soc. Chem. Commun.*, (1981) 325.

66- D. J. Surman and J. C. Vickerman, *J. Chem. Soc. Chem. Commun.*, (1981) 324.

67- M. Barber, R. S. Bordoli, R. D. Sedgwick and A. N. Tyler, *Nature*, **293** (1981) 270.

68- M. Barber, R. S. Bordoli and R. D. Sedgwick, in *"Soft Ionization Biological Mass Spectrometry"*, H. R. Morris (ed.), Heyden, London, 1981, p. 137 ss.

69- M. Barber, R. S. Bordoli, G. J. Elliott, R. D. Sedgwick and A. N. Tyler, *Anal. Chem.*, **54** (1982) 645A.

70- D. H. Williams, C. Bradley, G. Bojensen, S. Santikarn and L. C. E. Taylor, *J. Am. Chem. Soc.*, **103** (1981) 5700.

71- S. A. Martin, C. E. Costello and K. Biemann, *Anal. Chem.*, **54** (1982) 2362.

72- R. Stoll, U. Schade and F. W. Röllgen, *Int. J. Mass Spectrom. Ion Phys.*, **43** (1982) 227.

73- M. Barber, R. S. Bordoli, R. D. Sedgwick, A. N. Tyler, B. N. Green, V. C. Parr and J. L. Gower, *Biomed. Mass Spectrom.*, **9** (1982) 11.

74- R. M. Caprioli, *Anal. Chem.*, **55** (1983) 2387.

75- H. R. Morris, M. Panico and N. J. Haskins, *Int. J. Mass Spectrom. Ion Phys.*, **46** (1983) 363.

76- G. Puzo and J.-C. Prome, *Org. Mass Spectrom.*, **19** (1984) 448.

77- M. E. Hemling, R. K. Yu, R. D. Sedgwick and K. L. Rinehart, *Biochemistry*, **23** (1984) 5706.

78- W. D. Lehmann, M. Kessler and W. A. Konig, *Biomed. Mass Spectrom.*, **11** (1984) 217.

79- R. M. Caprioli, in *"Desorption Mass Spectrometry. Are SIMS and FAB the Same?"*. P.A. Lyon (ed.), Am. Chem. Soc., Washington, D.C., 1985, Chapter 12.

80- B. D. Musselman, J. T. Watson and C. K. Chang, *Org. Mass Spectrom.*, **21** (1986) 215.

81- G. Bojesen and J. Møller, *Int. J. Mass Spectrom. Ion Processes*, **68** (1986) 239.

82- D. H. Williams, A. F. Findeis, S. Naylor and B. W. Gibson, *J. Am. Chem. Soc.*, **109** (1987) 1980.

83- G. J. Gallegos, *J. Chromatog. Sci.*, **25** (1987) 296.

84- H. Nakazawa, *Chem. Pharm. Bull.*, **36** (1988) 988.

85- K. Isa and Y. Takeuchi, *Org. Mass Spectrom.*, **24** (1989) 153.

86- K. L. Rinehart, *Science*, **218** (1982) 254.

87- C. J. McNeal, *Anal. Chem.*, **54** (1982) 43A.

88- K. L. Busch and R. G. Cooks, *Science*, **218** (1982) 247.

89- C. Fenselau, in *"Ion Formation from Organic Solids"*, Springer Ser. in Chem. Phys., Vol. 25, A. Benninghoven (ed.), Springer-Verlag, Berlin, 1983, Chapter 3.2.

90- M. Przybylski, *Fresenius Z. Anal Chem.*, **315** (1983) 402.

91- J. M. Miller, *Adv. Inorg. Chem. Radiochem. Rev.*, **28** (1984) 1.

92- J. L. Gower, *Biomed. Mass Spectrom.*, **12** (1985) 191.

93- E. DePauw, *Mass Spectrom. Rev.*, **5** (1986) 191.

94- C. Fenselau and R. J. Cotter, *Chem. Rev.*, **87** (1987) 501.

95- R. M. Caprioli, *Biochemistry*, **27** (1988) 513.

96- H. Oechsner, *Appl. Phys.*, **8** (1975) 185.

97- G. M. McCracken, *Rep. Prog. Phys.*, **38** (1975) 241.

98- F. Bernhardt, H. Oechsner and E. Stumpe, *Nucl. Instrum. Methods*, **132** (1976) 329.

99- G. Blaise and A. Nourtier, *Surf. Sci.*, **90** (1979) 495.

100- P. Williams, *Surf. Sci.*, **90** (1979) 588.

101- A. Benninghoven, F. G. Rüdenauer and H. W. Werner, "*Secondary Ion Mass Spectrometry. Basic Concepts, Instrumental Aspects, Applications and Trends*", Chemical Analysis Ser., Vol 86, Wiley-Interscience, New York, 1987.

102- S. J. Pachuta ans R. G. Cooks, *Chem. Rev.*, **87** (1987) 647.

103- R. Kelly, *Radiat. Eff.*, **32** (1977) 91.

104- P. Sigmund and C. Claussen, *J. Appl. Phys.*, **52** (1981) 990.

105- C. W. Magee, *Int. J. Mass Spectrom. Ion Phys.*, **49** (1983) 211.

106- J. A. Schultz, R. Kumar and J. W. Rabalais, *Chem. Phys. Lett.*, **100** (1983) 214.

107- J. W. Rabalais and J.-N. Chen, *J. Chem. Phys.*, **85** (1986) 3615.

108- M. W. Thompson, *Philos. Mag.*, **18** (1968) 377.

109- P. Sigmund, *Phys. Rev.*, **184** (1969) 383.

110- B. J. Garrison and N. Winograd, *Science*, **216** (1982) 805.

111- R. T. Poole, J. G. Jenkin, J. Liesegand and R. C. G. Leckey, *Phys. Rev. B: Solid State*, **11** (1975) 5179.

112- G. Slodzian, *Surf. Sci.*, **48** (1975) 161.

113- H. Gnaser, *Int. J. Mass Spectrom. Ion Processes*, **61** (1984) 81.

114- W. F. van der Weg and D. J. Bierman, *Physica*, **44** (1969) 206.

115- R. Kelly and C. B. Kerkdijk, *Surf. Sci.*, **46** (1974) 537.

116- P. T. Murray and J. W. Rabalais, *J. Am. Chem. Soc.*, **103** (1981) 1007.

117- C. A. Andersen and J. R. Hinthrone, *Anal. Chem.*, **45** (1973) 1421.

118- P. Williams and C. A. Evans, *Surf. Sci.*, **78** (1978) 324.

119- J. K. Nørskov and B. I. Lundsqvist, *Phys. Rev. B: Condens. Matter*, **19** (1979) 5661.

120- M. L. Yu, *Phys. Rev. Lett.*, **47** (1981) 1325.

121- F. W. Röllgen, U. Giessmann and R. Stoll, *Nucl. Instrum. Methods*, **198** (1982) 93.

122- A. Benninghoven, in *"Ion Formation from Organic Solids"*, Springer Ser. in Chem. Phys., Vol. 25, A. Benninghoven (ed.), Springer-Verlag, Berlin, 1983, Chapter 3.1.

123- R. E. Honig, *Int. J. Mass Spectrom. Ion Processes*, **66** (1985) 31.

124- R. D. Macfarlane, in *"Desorption Mass Spectrometry. Are SIMS and FAB the Same?"*. P.A. Lyon (ed.), Am. Chem. Soc., Washington, D.C., 1985, Chapter 3.

125- D. W. Brenner and B. J. Garrison, in *"Secondary Ion Mass Spectrometry, SIMS V"*, Springer Ser. Chem. Phys., Vol. 44, A. Benninghoven, R. J. Colton, D. S. Simons and H. W. Werner (eds.), Springer-Verlag, Berlin, 1986, p. 462 ss.

126- R. E. Johnson, *Int. J. Mass Spectrom. Ion Processes*, **78** (1987) 357.

127- R. J. Beuhler and L. Friedman, *Int. J. Mass Spectrom. Ion Processes*, **78** (1987) 1.

128- B. V. King, I. S. Tsong and S. H. Lin, *Int. J. Mass Spectrom. Ion Processes*, **78** (1987) 341.

129- R. E. Johnson and W. L. Brown, *Nucl. Instrum. Methods*, **198** (1982) 103.

130- J. Kissel and F. R. Krueger, *Appl. Phys. A*, **42** (1987) 69.

131- L. E. Seiberling, J. E. Griffth and T. A. Tombrello, *Radiat. Eff.*, **52** (1980) 201.

132- R. R. Lucchese, *J. Chem. Phys.*, **86** (1986) 443.

133- C. C. Watson and T. A. Tombrello, *Radiat. Eff.*, **89** (1985) 263.

134- P. J. Derrick, *Frezenius Z. Anal. Chem.*, **324** (1986) 486.

135- M. F. Jarrold, A. J. Illies and M. T. Bowers, *J. Chem. Phys.*, **81** (1984) 222.

136- A. Hedin, P. Håkansson, I. Kamenski, M. Salehpour, B. Sundqvist and S. Widdiyasekera, *Radiat. Eff.*, **80** (1984) 141.

137- A. Benninghoven, *Int. J. Mass Spectrom. Ion Phys.*, **46** (1983) 459.

138- T. Ishitani and R. Shimizu, *Phys. Lett.*, **46A** (1974) 487.

139- J. P. Biersak and L. G. Haggmark, *Nucl. Instrum. Methods*, **174** (1980) 257.

140- B. J. Garrison, *J. Am. Chem. Soc.*, **104** (1982) 6211.

141- B. J. Garrison, *Int. J. Mass Spectrom. Ion Phys.*, **53** (1983) 243.

142- B. J. Garrison, in *"Desorption Mass Spectrometry. Are SIMS and FAB the Same?"*. P.A. Lyon (ed.), Am. Chem. Soc., Washington, D.C., 1985, Chapter 2.

143- D. E. Harrison and C. B. Delaplain, *J. Appl. Phys.*, **47** (1976) 2252.

144- D. E. Harrison, P. W. Kelly, B. J. Garrison and N. Winograd *Surf. Sci.*, **76** (1978) 311.

145- M. Hautala, *Phys. Rev. B*, **30** (1984) 5010.

146- H. J. Whitlow and M. Hautala, *Nucl. Instrum. Methods B*, **18** (1987) 370.

147- H. J. Whitlow, M. Hautala and B. U. R. Sundqvist, *Int. J. Mass Spectrom. Ion Processes*, **78** (1987) 329.

148- R. D. Macfarlane, *Nucl. Instrum. Methods*, **198** (1982) 75.

149- R. D. Macfarlane, *Acc. Chem. Res.*, **15** (1982) 268.

150- F. Honda, G. M. Lancaster, Y. Fukuda and J. W. Rabalais, *J. Chem. Phys.*, **69** (1978) 4931.

151- G. M. Lancaster, F. Honda, Y. Fukuda and J. W. Rabalais, *J. Am. Chem. Soc.*, **101** (1979) 1951.

152- H. T. Jonkman and J. Michl, *J. Chem. Soc. Chem. Commun.*, (1978) 751.

153- H. T. Jonkman, J. Michl, R. N. King and J. D. Andrade, *Anal. Chem.*, **50** (1978) 2078.

154- H. T. Jonkman and J. Michl, *J. Am. Chem. Soc.*, **103** (1981) 733.

155- R. G. Orth, H. T. Jonkman and J. Michl, *J. Am. Chem. Soc.*, **103** (1981) 6026.

156- R. G. Orth, H. T. Jonkman and J. Michl, *J. Am. Chem. Soc.*, **104** (1982) 1834.

157- R. G. Orth, H. T. Jonkman and J. Michl, *Int. J. Mass Spectrom. Ion Phys.*, **43** (1982) 41.

158- J. Michl, *Int. J. Mass Spectrom. Ion Phys.*, **53** (1983) 255.

159- D. Stulik, R. G. Orth, H. T. Jonkman and J. Michl, *Int. J. Mass Spectrom. Ion Phys.*, **53** (1983) 341.

160- T. F. Magnera, D. E. David, R. Tian, D. Stulik and J. Michl *J. Am. Chem. Soc.*, **106** (1984) 5040.

161- D. E. David, T. F. Magnera, R. Tian, D. Stulik and J. Michl, *Nucl. Instrum. Methods Phys. Res. B*, **14** (1986) 378.

162- D. E. David, T. F. Magnera, R. Tian and J. Michl, *Radiat. Eff.*, **99** (1986) 247.

163- T. F. Magnera, D. E. David and J. Michl, *Chem. Phys. Lett.*, **123** (1986) 327.

164- R. J. Day, S. E. Unger and R. G. Cooks, *J. Am. Chem. Soc.*, **101** (1979) 501.

165- L. K. Liu, K. L. Busch and R. G. Cooks, *Anal. Chem.*, **53** (1981) 109.

166- D. Zakett, A. E. Schoen, R. G. Cooks and P. H. Hemberger, *J. Am. Chem. Soc.*, **103** (1981) 1295.

167- S. E. Unger, R. J. Day and R. G. Cooks, *Int. J. Mass Spectrom. Ion Phys.*, **39** (1981) 231.

168- K. L. Busch, B. H. Hsu, Y.-X. Xie and R. G. Cooks, *Anal. Chem.*, **55** (1983) 157.

169- R. G. Cooks and K. L. Busch, *Int. J. Mass Spectrom. Ion Phys.*, **53** (1983) 111.

170- K. L. Busch, B. H. Hsu, Y.-X. Xie and R. G. Cooks, in "*Ion Formation from Organic Solids*", Springer Ser. in Chem. Phys., Vol. 25, A. Benninghoven (ed.), Springer-Verlag, Berlin, 1983, p. 138 ss.

171- B. H. Hsu and R. G. Cooks, *Anal. Chem.*, **57** (1985) 2925.

172- W. V. Ligon, *Int. J. Mass Spectrom. Ion Phys.*, **52** (1983) 183.

173- W. V. Ligon, *Int. J. Mass Spectrom. Ion Phys.*, **52** (1983) 189.

174- S. S. Wong, F. W. Röllgen, I. Manz and M. Przybylski, *Biomed. Mass Spectrom.*, **12** (1985) 43.

175- S. S. Wong and F. W. Röllgen, *Nucl. Instrum. Methods Phys. Res. B*, **14** (1986) 436.

176- F. H. Field, *J. Phys. Chem.* **86** (1982) 5115.

177- F. H. Field, in *"Ion Formation from Organic Solids"*, Springer Ser. in Chem. Phys., Vol. 25, A. Benninghoven (ed.), Springer-Verlag, Berlin, 1983, p. 172 ss.

178- T. Keough, F. S. Ezra, A. F. Russell and J. D. Pryne, *Org. Mass Spectrom.*, **22** (1987) 241.

179- R. Wolfgang, *Prog. React. Kinet.*, **3** (1965) 97.

180- H. S. W. Massey, *Rep. Prog. Phys.*, **12** (1949) 248.

181- G. Dube, *Org. Mass Spectrom.*, **19** (1984) 242.

182- R. Cooper and S. Unger, *J. Antibiot.*, **38** (1985) 24.

183- E. Schröder, H. Münster and H. Budzikiewicz, *Org. Mass Spectrom.*, **21** (1986) 707.

184- H. Münster, F. Theobald and H. Budzikiewicz, *Int. J. Mass Spectrom. Ion Processes*, **79** (1987) 73.

185- R. B. Freas, M. M. Ross and J. E. Campana, *J. Am. Chem. Soc.*, **107** (1985) 6195.

186- K. Harada, M. Suzuki and H. Kimbara, *Org. Mass Spectrom.*, **17** (1982) 386.

187- Y. Tondeur, A. J. Clifford and L. DeLuca, *Org. Mass Spectrom.*, **20** (1985) 157.

188- R. Kulatunga, M.Sc. Thesis, University of Alberta, 1986.

189- J. A. Sunner, R. Kulatunga and P. Kebarle, *Anal. Chem.*, **58** (1986) 1312.

190- J. A. Sunner, R. Kulatunga and P. Kebarle, *Anal. Chem.*, **58** (1986) 2009.

191- A. M. Hogg, *Int. J. Mass Spectrom. Ion Phys.*, **49** (1983) 25.

192- A. H. Mc Ilraith, *Nature*, **212** (1966) 1422.

193- A. H. Mc Ilraith, *J. Vac. Sci. Technol.*, **9** (1971) 209.

194- J. Franks and A. M. Ghander, *Vacuum*, **24** (1974) 489.

195- F. M. Devienne and J. C. Roustan, *C. R. Acad. Sci. Paris*, **283** (1976) 397.

196- H. Lew, in "*Methods of Experimental Physics*", Vol. 4A, V. W. Hudghes and H. L. Schultz (eds.), Academic Press, New York, 1967.

197- O. Beeck, *Ann. Physik*, **19** (1934) 121.

198- R. A. McDowell and H. R. Morris, *Int. J. Mass Spectrom. Ion Phys.*, **46** (1983) 443.

199- J. Franks, *Int. J. Mass Spectrom. Ion Phys.*, **46** (1983) 343.

200- A. J. Alexander and A. M. Hogg, *Int. J. Mass Spectrom. Ion Processes*, **69** (1986) 297.

201- D.D. Perrin and W. L. F. Armarego, "*Purification of Laboratory Chemicals*", 2nd ed., Pergamon Press, Oxford, 1980, p. 208.

202- S. G. Lias, J. F. Liebman and R. D. Levin, *J. Phys. Chem. Ref. Data*, **13** (1984) 695.

203- J. A. Sunner, R. Kulatunga and P. Kebarle, *Anal. Chem.*, **58** (1986) 1312.

204- D.D. Perrin, "*Dissociation Constants of Organic Bases in Aqueous Solution*", Butterworths, London, 1965. Supplement, Butterworths, London, 1972.

205- R. C. Weast, Ed., *"Handbook of Chemistry and Physics"*, 64th ed., CRC Press, Boca Ratón, Florida, 1983-1984.

206- R. F. Cookson, *Chem. Rev.*, **74** (1974) 5.

207- R. G. Bates, *Pure Appl. Chem.*, **18** (1969) 421.

208- A. Albert and E. Serjeant, *"The Determination Of Ionization Constants of Acids and Bases"*, 2nd ed., Chapman and Hall, London, 1971, Chapter 3.

209- L. Z. Benet and J. E. Goyan, *J. Pharm. Sci.*, **56** (1967) 665.

210- W. D. Johnson and J. E. Sherwood, *Aust. J. Chem.*, **25** (1972) 81.

211- S. Dushman, *"Scientific Foundations of Vacuum Technique"*, Wiley and Sons, New York, 1958.

212- J. W. Otvos and P. P. Stevenson *J. Chem. Phys.*, **78** (1956) 546.

213- A. M. Hogg, personal communication.

214- B. T. Chait and F. H. Field, *Int. J. Mass Spectrom. Ion Phys.*, **41**, (1981) 17.

215- W. V. Ligon and S. B. Dorn, *Int. J. Mass Spectrom. Ion Processes*, **63**, (1985) 315.

216- R. W. Taft, in *"Kinetics of Ion-molecule Reactions"*, P. Ausloos (ed.), Plenum, New York, 1979, p. 27.

217- P. Kebarle, G. Caldwell, T. Magnera and J. Sunner, *J. Pure Appl. Chem.*, **57** (1985) 339.

218- W. Gibbs, *"The Scientific Papers"*, Vol. 1, Dover, New York, 1961.

219- V. P. Skripov, "*Metastable Liquids*", Wiley, New York, 1974.

220- P. Kebarle, in "*Techniques for the Study of Gas Phase Ion-Molecule Reactions*", W. H. Saunders and J. M. Farrar (eds.), Wiley, New York, 1988.

221- A. M. Hogg and P. Kebarle, *J. Chem. Phys.*, **43** (1965) 449.

222- A. M. Hogg, R. M. Haynes and P. Kebarle, *J. Am. Chem. Soc.*, **88** (1966) 28.

223- R. N. Katz, T. Chaudhary and F. H. Field, *J. Am. Chem. Soc.*, **108** (1986) 3897.

224- R. N. Katz, T. Chaudhary and F. H. Field, *J Int. J. Mass Spectrom. Ion Processes*, **78** (1987) 85.

225- C. T. Avedisian, *J. Chem. Phys. Ref. Data*, **14** (1985) 695.

226- Ya. Zeldovich and O. M. Todes, *Zh. Eksp. Teor. Fiz.*, **10** (1940) 1441.

227- M. Volmer and A. Weber, *Z. Phys. Chem.*, **11** (1926) 277.

228- W. Doring, *Z. Phys. Chem.*, **36** (1937) 37.

229- W. Doring, *Z. Phys. Chem.*, **37** (1938) 292.

230- Yu. Kagan, *Zh. Fiz. Khim*, **34** (1960) 92.

231- J. Sunner, personal communication.

232- H. S. W. Massey and E. H. S. Burhop "*Electronic and Ionic Impact Phenomena*" Oxford Univ. Press,Oxford, 1956.

233- F. H. Field and J. L. Franklin "*Electron Impact Phenomena*" Academic Press, New York, 1957.

234- J. Berkovitz "*Photoabsorption, Photoionization and Photoelectron Spectroscopy*", Academic Press, New York, 1979.

235- G. Friedlander and J. W. Kennedy, "*Nuclear and Radiation Chemistry*", Wiley and Sons, New York, 1960.

236- K. Levsen, "*Fundamental Aspects of Organic Mass Spectrometry*", Progress in Mass Spectrometry, Vol. 4, H. Budzikiewicz (ed.), Verlag Chemie, Weinheim, 1978.

237- J. Sunner, A. Morales and P. Kebarle, *Anal. Chem.*, **59** (1987) 1378.

238- J. Sunner, A. Morales and P. Kebarle, *Anal. Chem.*, **60** (1988) 98.

239- J. Sunner, A. Morales and P. Kebarle, *Int. J. Mass Spectrom. Ion Processes*, **86** (1988) 169.

240- J. Sunner, A. Morales and P. Kebarle, *Int. J. Mass Spectrom. Ion Processes*, **87** (1989) 287.

241- J. Sunner, M. Ikonomou and P. Kebarle, *Int. J. Mass Spectrom. Ion Processes*, **82** (1988) 221.

242- M. P. Lacey and T. Keough, *Rapid Commun. Mass Spectrom.*, **3** (1989) 46.

243- C. W. Kazakoff, R. T. B. Rye and O. S. Tee, *Can. J. Chem.*, **67** (1989) 413.

244 J. M. Miller, K. Balasanmugam and A. Fulcher, *Org. Mass Spectrom.*, **24** (1989) 497.

245- T. R. Sharp and J. H. Futrel, *Int. J. Mass Spectrom. Ion Processes*, **90** (1989) 39.

246- Xiao Yu, unpubllished results.

247- P. J. Todd, unpublished results.

248- L. Yan, Y. Fang, M. Fang, L. Zhu, S. Dekang and L. Xiyun, *Org. Mass Spectrom.*, **24** (1989) 303.

249- R. A. W. Johnstone and A. H. Wilby, *Int. J. Mass Spectrom. Ion Processes*, **89** (1989) 249.

250- J. H. Clark, N. D. S. Owen, C. V. A. Duke and J. M. Miller, *J. Fluorine Chem.*, **44** (1989) 413.

251- M. J. Connolly and R. G. Orth, *Anal Chem.* **59** (1987) 903.

252- A. Morales, A. M. Hogg and P. Kebarle, *Int. J. Mass Spectrom. Ion Processes*, submitted for publication.

253- M. Takayama, T. Fukai and T. Nomura, *Int. J. Mass Spectrom. Ion Processes*, **89** (1989) R1.

254- P. J. Todd and G. S. Groenewold, *Anal. Chem.*, **58** (1986) 895.

255- W. V. Ligon and S. B. Dorn, , *Int. J. Mass Spectrom. Ion Processes*, **78** (1987) 99.

256- P. J. Todd, *Org Mass. Spectrom.* **23** (1988) 419.